UNIVERSITY OF LONDON

Imperial College of Science and Technology

Department of Physics

Optics Section

SURFACE COORDINATE MEASUREMENT OF ROUGH DIAMONDS

Laurence John Robinson

Thesis submitted for the degree of Doctor of Philosophy

of the University of London (1983).

To My Father.

Abstract

This thesis describes a non-contacting method for measuring and storing the cylindrical coordinates characterizing the surface of a small object less than 10 mm in size. Particular reference is made to the surface properties of rough diamonds in the discussion of the operation of the system. The object illuminating optics, the viewing optics, electronic signal processing and data storage are described, and discussion of the various parameters affecting their performance is given. Mechanical and optical tolerances are calculated and the methods of aligning components shown. Experimental results on the ability of the system to measure surface points with varying orientations are given and theoretical explanations attempted. The production of a random speckle component in the images, due to coherent illumination, is discussed and the reduction of the speckle contrast using the defocussed beam of a TV camera explained. The response of the electronics is calculated and possible errors estimated. Tests on linearity and performance are reported; the latter involved measurements on a steel ball.

AKNOWLEDGEMENTS

I would like to thank my supervisor, Professor W.T.Welford for his help and constant availability during the last three years. I am also indebted to Fred Reavell for giving much advice to a new postgraduate and to the old members of Room 611 for their long suffering. I am very grateful to Tony Canas for his help in preparing this thesis. I would like to aknowledge the financial support of the Diamond Trading Co throughout this work.

Finally, my thanks to those who suffered most, Marcia Wallace and Karen Dudmesh.

CONTENTS

CHAPTER 1.

CHAPTER 1. INTRODUCTION

1.1 The Aim.

Diamonds are highly valued as decorative ornaments because of their "sparkle" and "fire" and rarity. Due to the regular structure of diamond, rough stones can be cleaved along the crystal planes to form planar facets. This, combined with the high refractive index of diamond ($\approx$2.4) can cause incident light on a polished stone to suffer many internal reflections before exiting. The shape or cut of a stone will determine how light is refracted by a stone and thus its sparkle and fire. The decision on how to cut a particular rough stone is affected by several factors. The effect of internal defects in the stone will be minimised in the cut stone or stones. The shape of a stone will suggest a particular cut so as to allow the maximum possible proportion to be included in the final product. The value of a gem varies with its purity, cut and weight. For a given cut and purity the value may vary exponentially with the weight.

Consideration of all these variables in the decision on how to cut a rough stone is a highly skilled and time consuming task. For example a stone of about 6.5 mm in diameter can be worth as much as £20,000 (DODSON[1]) and take a diamond cleaver a week to cut. An incorrect attempt to cleave a stone can leave a pile of relatively worthless dust.

The aim of the work described in this thesis was to construct a

machine capable of measuring and storing the coordinates describing the surface of a rough diamond. Stones of up to 10 mm in size were to be measured with an accuracy of the order of 25 μm. This data should be collected within minutes and stored for further manipulation. With the knowledge of the external shape of the stone it is hoped that complex computer algorithms will enable determination of the best possible cleavage of a rough stone faster than at present. Though the surface properties of diamonds are considered in this thesis, they do not determine significantly the design of the system. Within certain limitations placed on the roughness of the object surface, the system can be used to measure the surface shape of any object.

1.2 Present Methods of 3-Dimensional Measurement.

Methods for obtaining information on a point in 3-dimensional space can be separated into two categories. In one category the information is presented in a 2-dimensional form and the third coordinate is measured indirectly. In the second category all three coordinates are measured directly. Examples of the direct measurement methods are radar and three degrees of freedom instrumented arms. In radar the direction of a transmitted beam of radiation identifies two of the coordinates whilst the two-way travel time of the radiation reflected from the object supplies the third. At the present time radar sytems do not have the necessary resolution for measuring objects as small as 10 mm.

The three degrees of freedom instrumented arm is becoming a

common feature in factories. With the advent of microcomputers, robot arms with an attached proximity detector can be used to map out the surface of an object. Such instruments are used mainly with large objects ($\approx$metres) as the servo mechanisms for the arm require high tolerances more easily built into large machines. A smaller version of such instruments is the "Talysurf" used to measure the surface profiles of roughly flat objects. This is accomplished by passing a needle-like scribe over the suface of the object and measuring the out of plane movement of the scribe as it remains in contact. Both these methods are slow due to the mechanical processes involved.

The measuring methods that present the third coordinate indirectly appear most commonly as stereophotogrammetry and interferometry. Stereophotogrammetry consists of viewing an object from two different directions. Consideration of a point on the object as it appears in two different two-dimensional planes supplies the third coordinate describing that point. This method has been extended to the case when one viewing direction is used to project a grid onto the object[2]. Viewing this grid from a second direction supplies the 3 coordinates. This method, known as raster stereophotogrammetry is shown in figure 1.1. In interferometry the object is illuminated with a wavefront of known shape and the reflected wavefront is compared with another wavefront of known shape by coherent addition. Contours of constant object "height" appear as fringes in the viewed image.

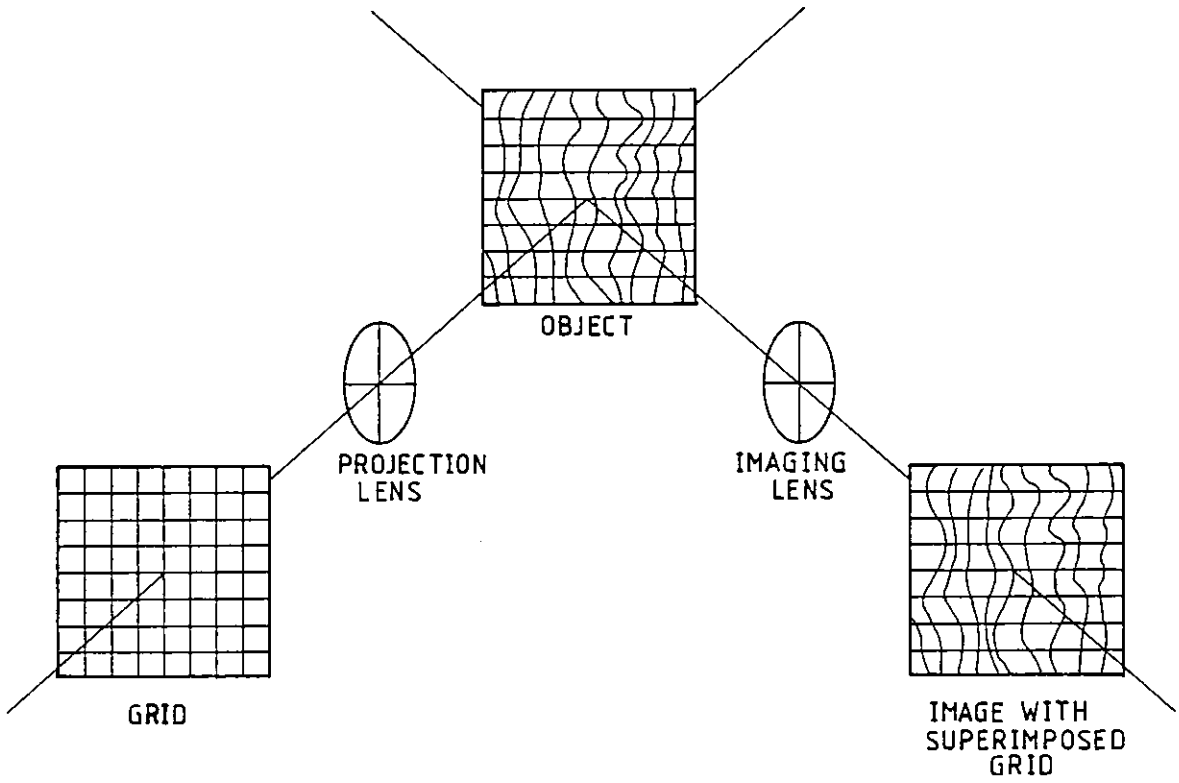

Figure 1.1 The basic method of raster stereophotogrammetry.

To enable fast data aquisition times, the images of both the above two methods must be processed electronically. If this is done with a TV camera then ambiguities can occur. Figure 1.2a shows an image which is to be scanned by a camera. As the camera scans a grid the resultant TV image will only have data on the grid lines. This is shown in figure 1.2b. Clearly there are many possible images that can be fitted to these data points. Even if a fringe counting technique is employed for each line, obscured fringes will cause errors. These ambiguities can be overcome if a single illumination line is used on the object. This method was used in the SCHMALZ profile microscope which was evaluated by the Institute of Production Engineers in 1942 (SCHLESSINGER[3]). The basic method is shown in figure 1.3. The surface to be measured is illuminated by a focussed plane of light. A viewing microscope, whose optical axis is normal to the plane of illumination, is focussed on one edge of the illuminating beam. With the illuminating and viewing directions orthogonal, the illuminated surface will always lie in the focal plane of the microscope. Variations in depth of the surface will appear as deviations of the image line from a straight line. It is upon this basic method that a system was designed to measure surface shapes. The remainder of this thesis describes the design of the system and results obtained from it.

The work described in this thesis is entirely due to the author based upon an original idea of the Diamond Trading Co Ltd.

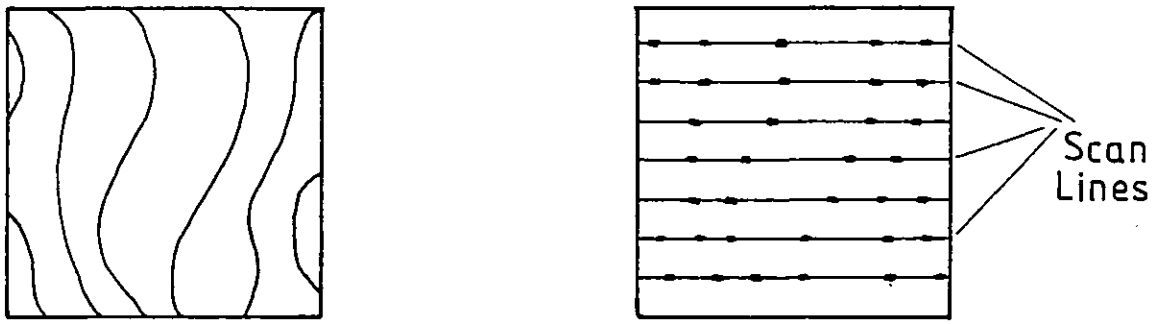

a b

Figure 1.2 a. An image showing fringes whose position are to be measured.

b. The image after scanning by a TV camera.

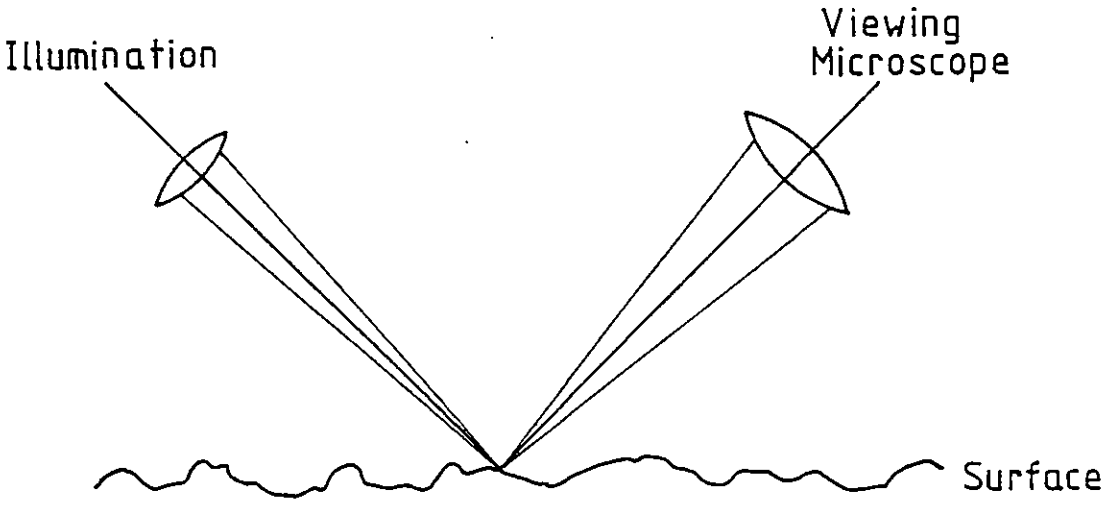

Figure 1.3 The principle of the SCHMALZ profile microscope.

CHAPTER 2.

CHAPTER 2 - GENERAL DESIGN OF THE SYSTEM

2.1 Introduction

In this chapter the general principle and design of the system is given, showing the method of obtaining information from the surface of the stone. Calculations of parameters governing the ability of the system to record the surface co-ordinates are given.

2.2 Principle of System

Referring to figure 2.1, A is a point on the z axis about which the stone can be rotated. The stone is illuminated by a plane of light which passes through the axis z. Viewing the stone at an angle θ from the plane of illumination the point B on the surface will appear to be a distance $r' = r \sin\theta$ from A. The surface as viewed will therefore be a segment of the surface whose r coordinate is magnified by a factor $\sin\theta$. The z co-ordinate which is orthogonal to the plane containing the illuminating and viewing directions will be unchanged. Figure 2.2 shows a series of a viewed surface with various values of θ.

Information is now available about a segment of the surface and the r and z co-ordinates can be extracted. The degree to which the data can be extracted will depend on several factors. Firstly, whether every point on the surface is illuminated, and if so, whether the reflected light in the viewing direction is above a certain critical value. The first requirement must be that the stone is coated with some matt reflecting substance to provide a

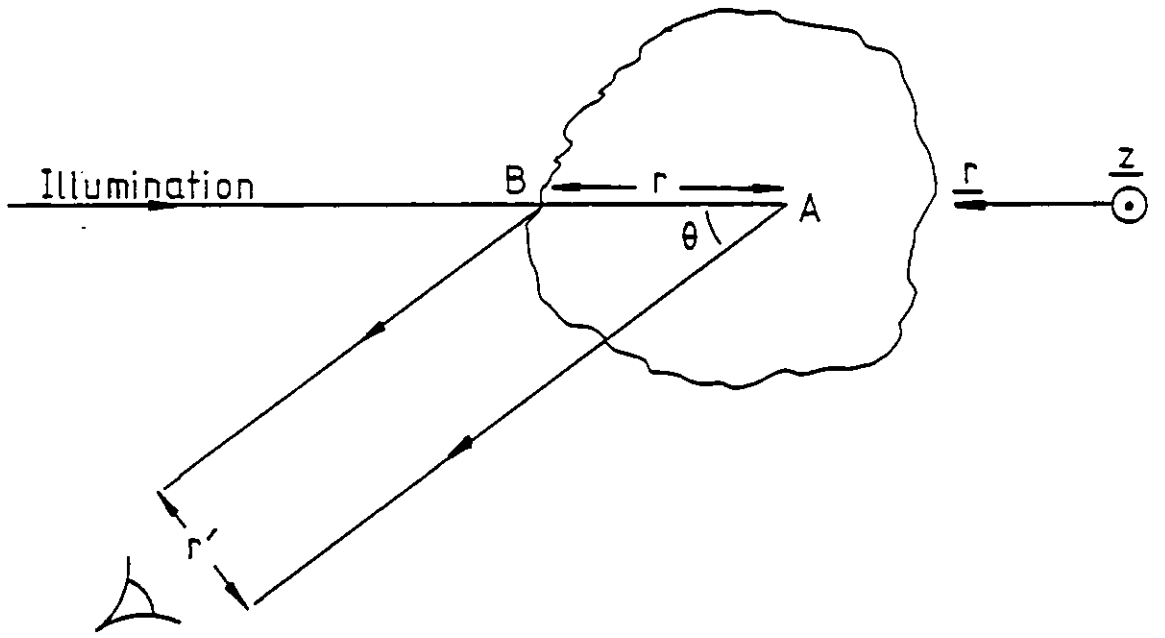

Figure 2.1

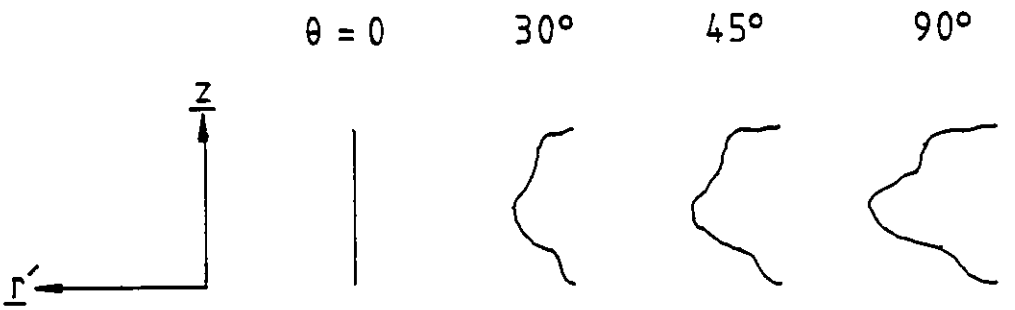

Figure 2.2 Object viewed at different angles.

non-specular reflection. This coating must also be of such thickness so that the surface co-ordinates remain the same to within the resolution limits that are hoped to be achieved. The substance used was a liquid corrector as used for typing errors. The basic liquid "Slick"* was thinned with an equal volume of "Slick" thinners to provide a reasonable coating for the stones. In Chapter 6 the reflection properties of "Slick" are discussed.

To achieve the illumination of surfaces tilted about an axis orthogonal to the $\underline{r}$ and $\underline{z}$ axes, a three-beam illumination system was used as shown in figure 2.3. The three beams of light, coplanar in the area of the stone, will now increase the probability that a point on the surface will reflect light in the viewing direction above the critical value, for a larger range of orientations of the surface at that point. Theoretical and experimental results on the viewed illuminations are given in Chapter 6. Another problem with the above system would be that any point on the illuminated surface which lies as in Figure 2.4, would not be visible due to the point C obscuring the illuminated point B. This is overcome in part by the introduction of a second viewing direction as in figure 2.5. If θ_1 and θ_2 are equal, then the two images may be added and the resulting image will have some information about B. Even so, a concavity as in figure 2.6 will be invisible to both viewing directions. It would seem that a reduction in θ would reduce the likely occurences of such situations, but as will be shown in section 2.4 this introduces other problems.

* Slick is a registered trademark.

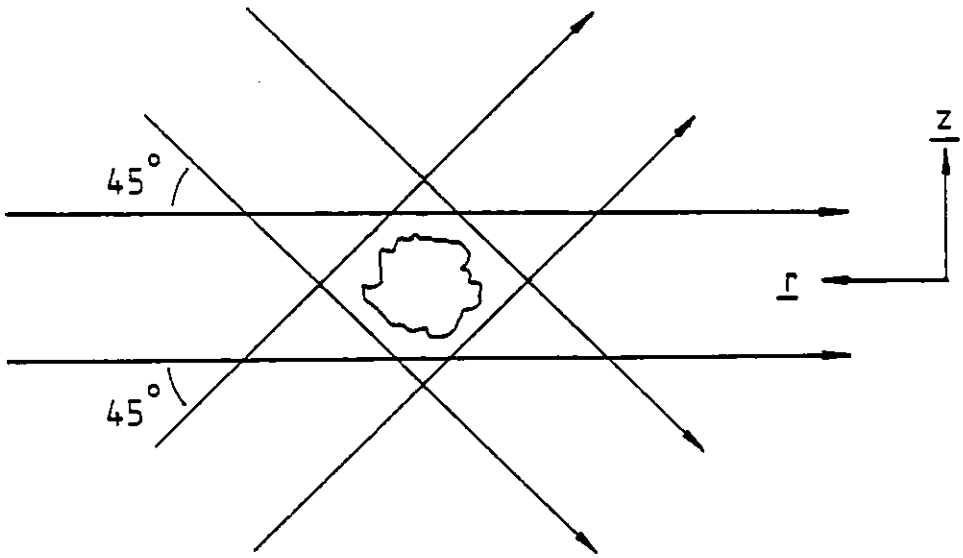

Figure 2.3 Three beam illumination.

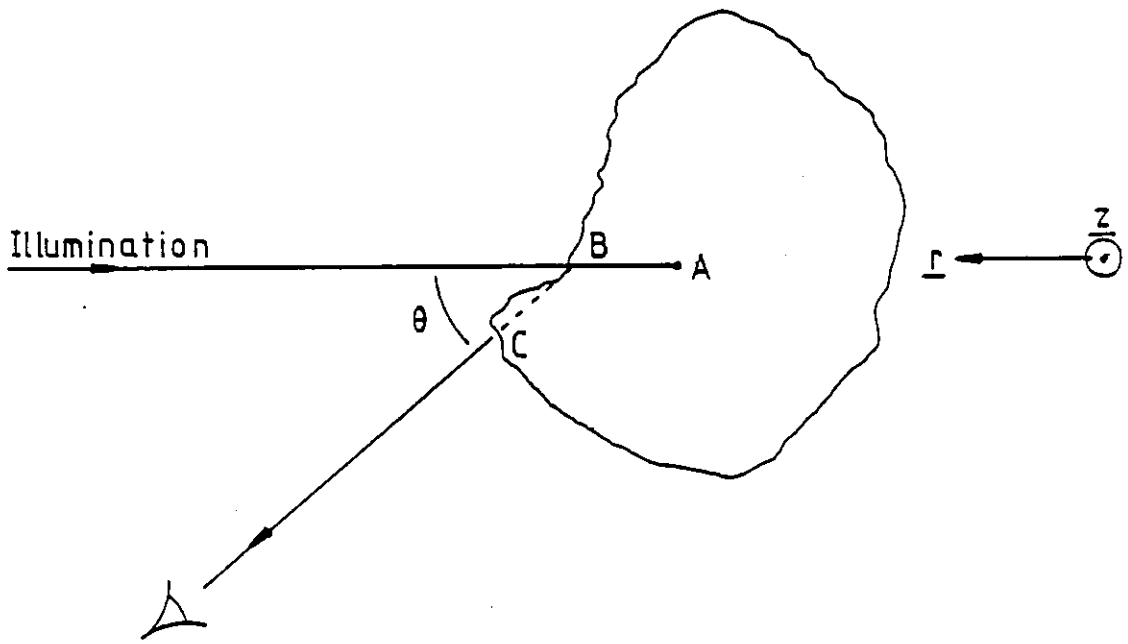

Figure 2.4 Example of a hidden point.

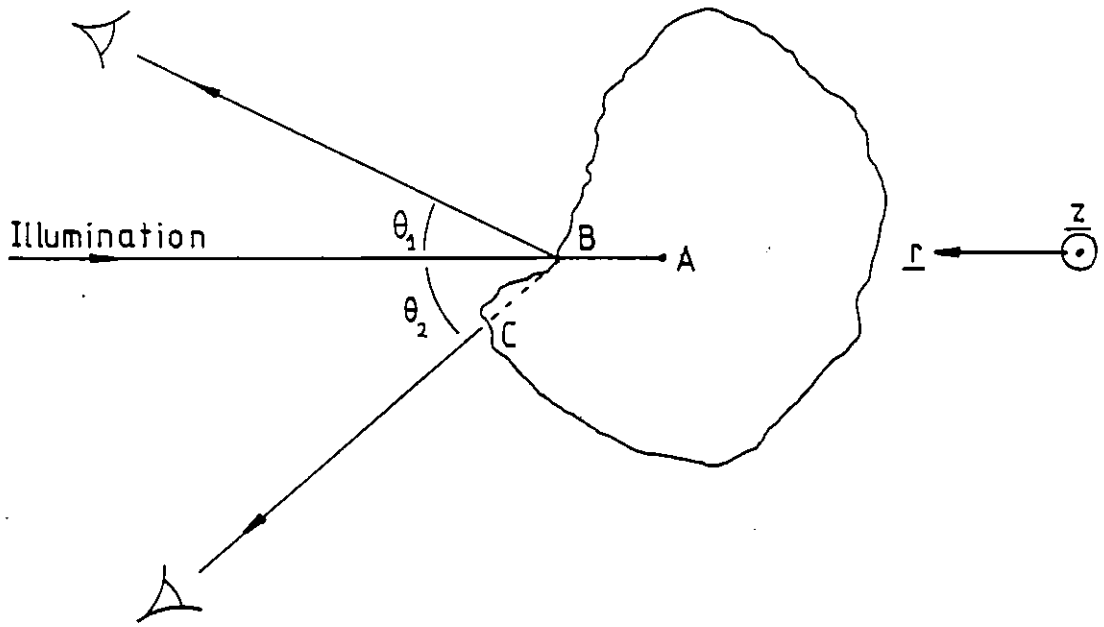

Figure 2.5 Two viewing directions.

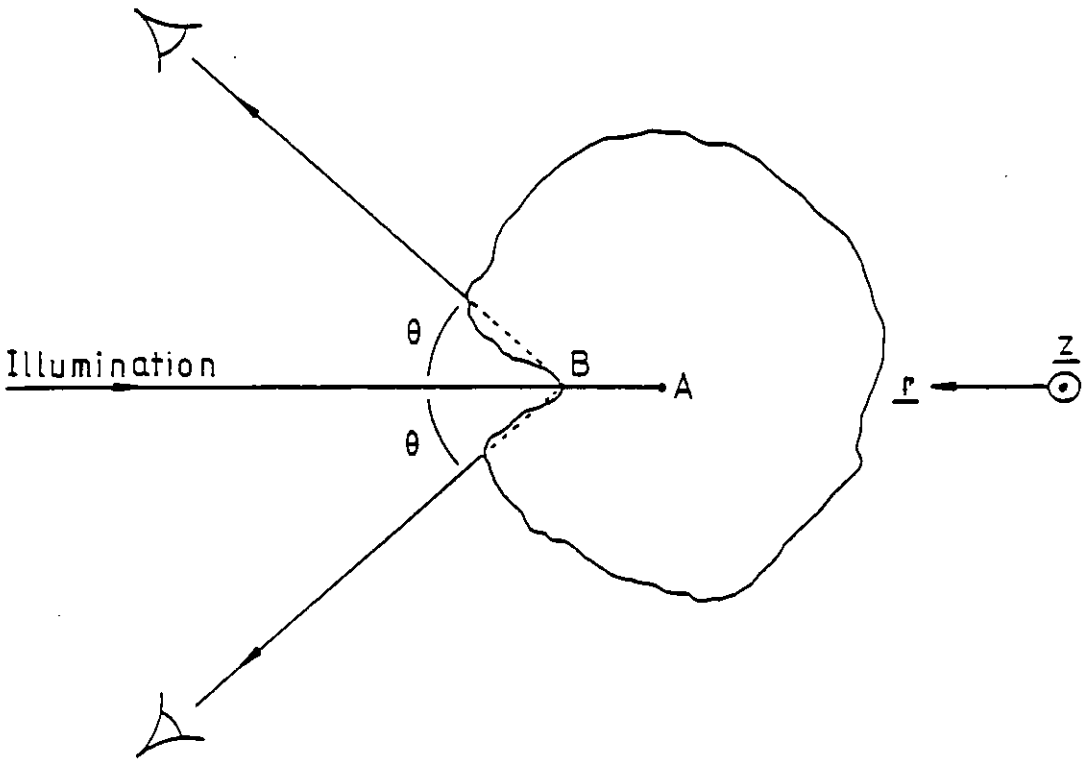

Figure 2.6 An hidden concavity.

2.3 Illuminating Beam Width

With the high resolution required of the system, it is desirable to minimize all factors that could lead to image degradation and with any optical system, monochromatic light if possible is an obvious first step. A laser not only supplies this (a good approximation), but also supplies a collimated beam of small diameter which facilitates alignment of optical components.

In the following discussion of the propagation of the laser beam, the work of Kogelnik and Li [4] is followed, but instead of assuming a circularly symmetrical solution, e.g. $\Psi(x^2 + y^2)$, we use a solution $\Psi(\frac{x^2}{a} + \frac{y^2}{b})$ to find the propagation of a laser beam focussed with a cylindrical lens.

The complex amplitude u of the coherent light satisfies the scalar wave equation

$$\nabla^2 u + k^2 u = 0 \qquad (2.1)$$

where $k = \frac{2\pi}{\lambda}$ is the propagation constant in the medium.

Assuming for light traveling in the z direction,

$$u = \Psi(x,y,z)e^{-ikz} \qquad (2.2)$$

Inserting (2.2) into (2.1), one obtains

$$\frac{\partial^2 \Psi}{\partial x^2} + \frac{\partial^2 \Psi}{\partial y^2} - 2ik\frac{\partial \Psi}{\partial z} = 0 \qquad (2.3)$$

where we assume Ψ varies so slowly with z that $\frac{\partial^2 \Psi}{\partial z^2}$ can be ignored.

We now differ from Kogelnik and Li by assuming

$$\Psi = \exp\left[-i\left(P(z) + \frac{k}{2}\left(\frac{x^2}{a(z)} + \frac{y^2}{b(z)}\right)\right)\right] \qquad (2.4)$$

where P, a, b represent complex beam parameters and imply a non-circularly symmetric solution. After substitution of (2.4) into (2.3) and comparing terms of equal power in x^2 and y^2, one obtains the relations,

$$\frac{da}{dz} = 1 \quad : \quad \frac{db}{dz} = 1 \quad : \quad \frac{dP}{dz} = -\frac{i}{2}\left[\frac{1}{a(z)} + \frac{1}{b(z)}\right]$$

giving $a = z + a_o$ (2.5)

and $b = z + b_o$ (2.6)

For convenience, one introduces four real beam parameters, R_1, R_2, w_1 and w_2 related to a and b by:

$$\frac{1}{a} = \frac{1}{R_1} - \frac{i\lambda}{\pi w_1^2} \qquad (2.7)$$

$$\frac{1}{b} = \frac{1}{R_2} - \frac{i\lambda}{\pi w_2^2} \tag{2.8}$$

On substituting (2.7) and (2.8) into (2.4), one obtains,

$$\Psi = \exp\left\{-i\left[P(z) + \frac{k}{2}\left(\frac{x^2}{R_1} + \frac{y^2}{R_2}\right)\right]\right\}\exp\left\{-\left[\frac{x^2}{w_1^2} + \frac{y^2}{w_2^2}\right]\right\} \tag{2.9}$$

As one would expect from the form of (2.4), the beam widths in the x and y directions are independent and the solution for the beam width w_x will follow Kogelnik and Li.

$$w_x^2(z) = w_o^2\left[1 + \left(\frac{\lambda z}{\pi w_o^2}\right)^2\right] \tag{2.10}$$

where w_o is the beam waist, i.e. where the beam amplitude is 1/e of the value at x = 0.

Clearly the narrower the illuminating beam at the stone, the higher the resolution on the stones surface. As stated in Chapter 1, it is desired to be able to measure stones of up to 10 mm in size and it is therefore the value of w_o that gives the minimum value of $w_x(z)$ at $z = \pm 5$ mm that is desired. On differentiating (2.10) one obtains

$$2w_x\frac{dw_x}{dw_o} = 2w_o - \frac{2}{w_o^3}\left(\frac{\lambda z}{\pi}\right)^2$$

Setting $\frac{dw}{dw_o} = 0$ leads to $w_o^2 = \frac{\lambda z}{\pi}$

giving $w_x^2 (\pm 5) = 2w_o^2$

for a Helium Neon Laser $\lambda = 6.32 \times 10^{-4}$ mm.

This gives a beam waist diameter of approximately 60 um with a diameter of 85 um at ± 5 mm. The inclusion of the three beam illuminating system shows that beam diameters greater than this exist inside the 10 mm square which is our object field. Figure 2.7 shows the 10 mm square ABCD. The points A,B,C,D are each illuminated by beams, 5 mm, $5\sqrt{2}$ mm and 0 mm from the beam waists, giving beam widths of

$$w_o \ , \ \sqrt{2}w_o \ , \ \text{and} \ \sqrt{3}w_o$$

The $1/e^2$ beam width will for the purposes of image formation therefore be assumed to be 80 um as a reasonable average over the object field.

2.4 Decision on the Viewing Angle

Figure 2.8 shows a flat surface AC illuminated perpendicularly with an 80 μm wide beam and viewed at an angle θ. The image of AC as seen in the object field will be AB = $\frac{80}{\tan\theta}$ and it will be this profile of the illuminating beam that the system will use to find the co-ordinate r of the mid-point of AC.

The specifications for the system are for a $\pm$ 25 μm accuracy and it is clear that either $\frac{80}{\tan\theta}$ must be of the order of

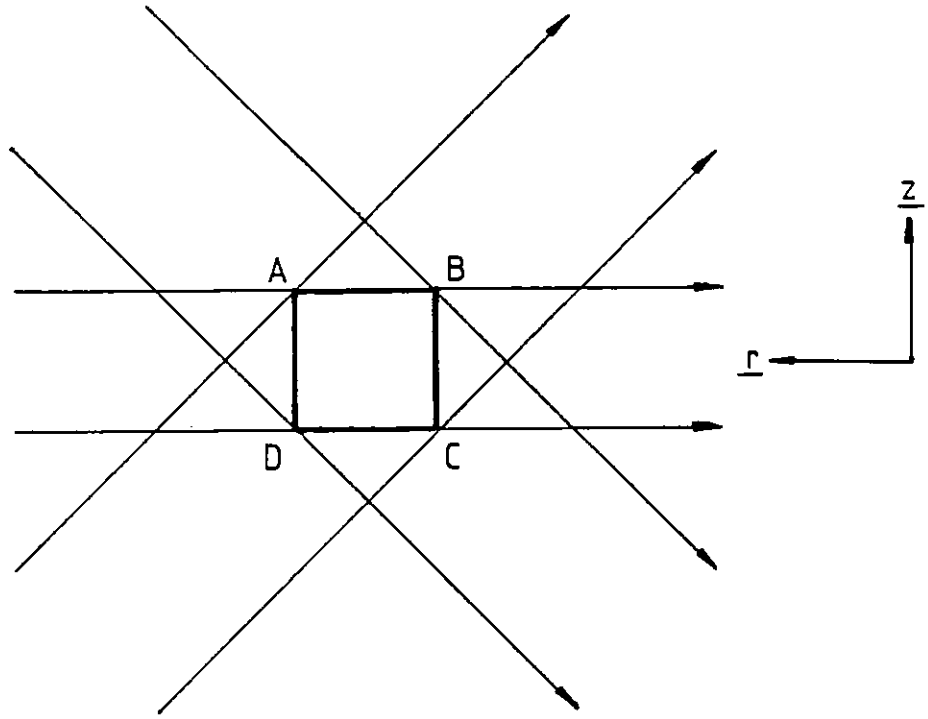

Figure 2.7 Three different beam widths in the object field ABCD.

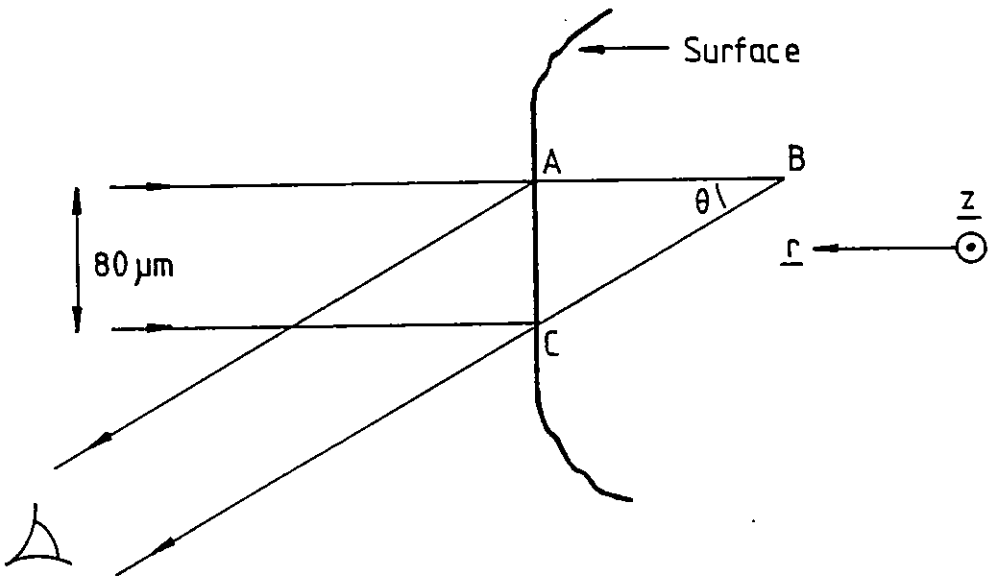

Figure 2.8 Image line width.

50 μm or some processing of the viewed gaussian profile will have to be carried out to find the centre of a profile much wider than 50 μm. Rotation of the surface about the $\underline{z}$ axis does not change the problem as shown in figure 2.9. Whilst the profile viewed by (1) increases in width, the profile at (2) decreases so that there is always an image less than $\frac{80}{\tan\theta}$ in width. The particular forms of these profiles are discussed in Chapter 6.

The decision on the angle θ thus depends on two factors, the image profile width and the ability of the system to detect the centre to 25 μm and the inclusions in the surface of the stone which could be undetectable to either viewing direction. Figure 2.10 shows a graph of the profile width of a perpendicularly illuminated surface and of the internal angle of an inclusion when undetectable against θ.It would be reasonable to expect that the centre of a gaussian of variance a^2 could be found to within $\pm a$ or better, i.e. one quarter of the image width plotted in Fig. 2.10, which for a 100 μm image width would be a viewing angle of 40°. This would leave the possibility that many points on a rough stone would be undetected and an angle of between 20 and 30 degrees would be more desirable but would require the ability to obtain the 25 μm accuracy on a profile between 130 and 220 μm in width and would leave no allowance for other errors in the system.

The value finally used in the system was 32° giving a profile as in figure 2.11. The over-riding factor in the decision was

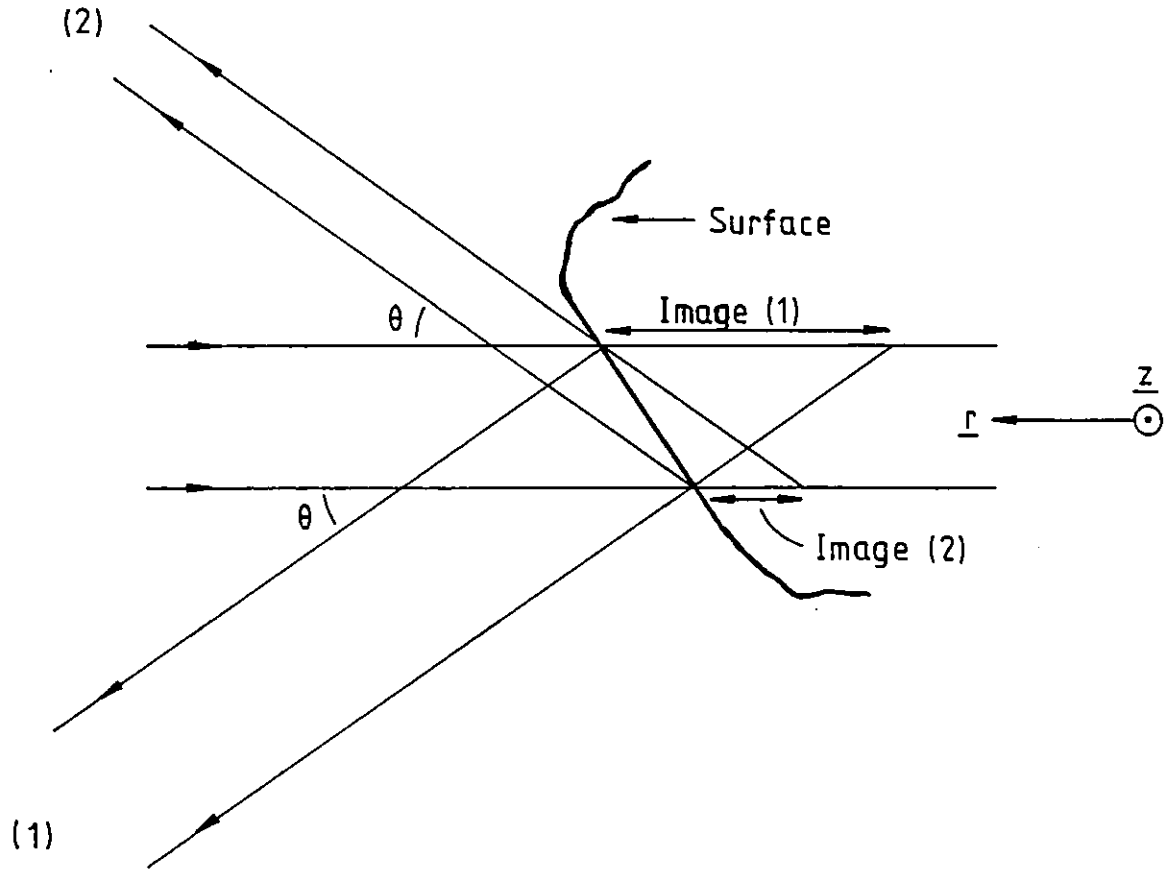

Figure 2.9 The variation of image line widths as the object orientation changes.

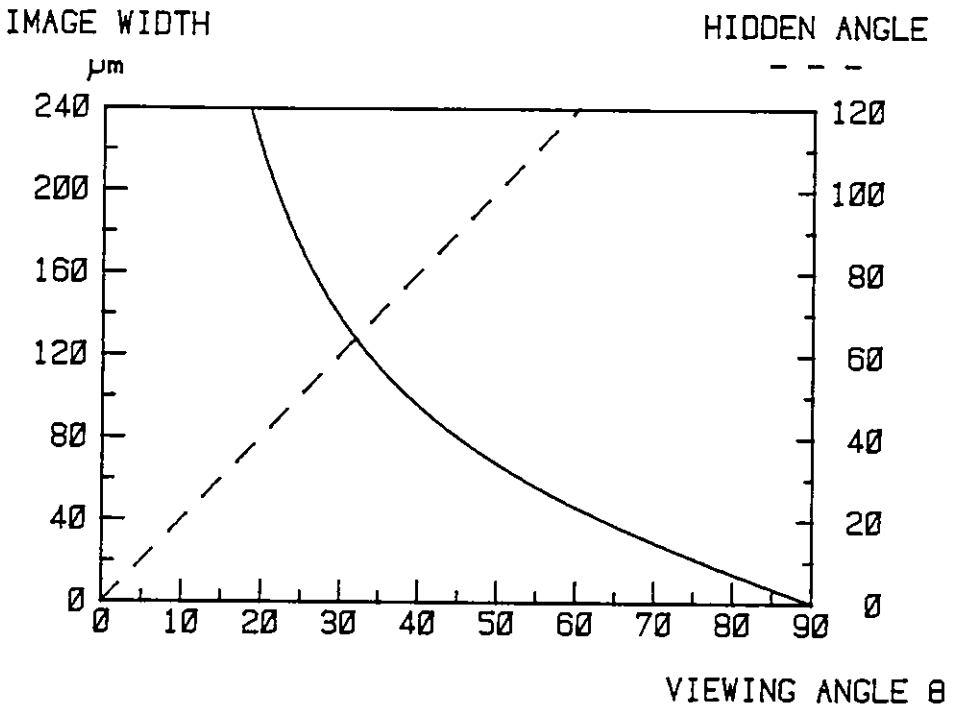

Figure 2.10 The variation of image line width and hidden concavity angle against viewing angle.

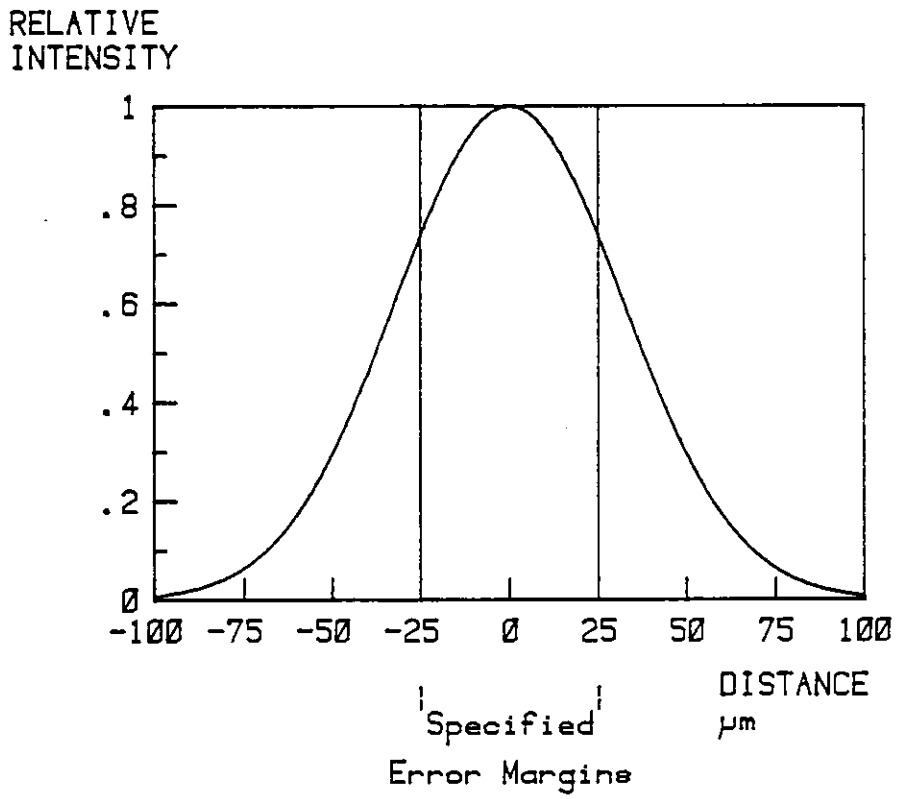

Figure 2.11 The image profile with a viewing angle of 32°.

the mechanical mounting of the detectors which could not accomodate angles of less than 32° for the viewing direction. Results given in Chapter 8 show that at 32° the system is close to achieving a 25 μm accuracy.

2.5 Data Acquisition from the Whole Surface

It has been shown in this chapter how the shape from one segment of the stone can be acquired. To cover the whole surface requires two additional actions. Firstly the stone is rotated about the z axis to a new position where the co-ordinates of a new section are measured. This process would then repeat until the stone has been rotated through 360°. To achieve a 25 μm resolution on the circumference of a 10 mm diameter stone, a step angle of approximately 0.25° is required. A stepping motor of step angle 0.9° is used with a 2:1 belt driven step down giving a final step angle of 0.45°. Though not as high a resolution, this gives a sampling interval of 40 μm on a surface 5 mm from the centre of rotation. A smaller stepping angle would produce more data on the stone which it is not possible to store with the present storage system, as described in Chapter 7.

The second action is necessitated by the fact that the stone has to be mounted on some shaft by which it is rotated. For information on this point the stone would have to be rotated such that the z axis is changed. This process will also help to acquire information on any parts of the surface that lie such that they are

invisible to any viewing direction in the planes parallel to the r axis. Figure 2.12 shows such a situation, and the effect of changing the axis of rotation of the stone.

Besides obvious concavities, surfaces that are nearly parallel to the r axis will obviously be more susceptible to errors in co-ordinate measurement and may not even reflect light above the critical value of the detection system. The changing of the axis of rotation will thus give a much lower probability of a point being undetected.

The possibility of rough diamonds of the alluvial type having concavities as in figure 2.13, is very low due to the form of abrasion the stones have undergone. The "roof" hiding the surface at X is a weak point and would be expected to be eroded away by the constant contact with other materials, during the life of the stone whilst in its natural environment.

The compression of the two sets of data on the stone's surface is a problem beyond the scope of this thesis, but it can be seen that with an accurate rotation of the stone through 90^{o} for the second set of data, the problem is one of autocorrelating two very high order 2 dimensional matrices which though time consuming is a reasonable problem for a large computer.Referring to figure 2.14, the point X is characterised by r,θ,z. If the axes are now rotated about the y axis by 90^{o} the new co-ordinates r',θ', z' are given by the following equations,

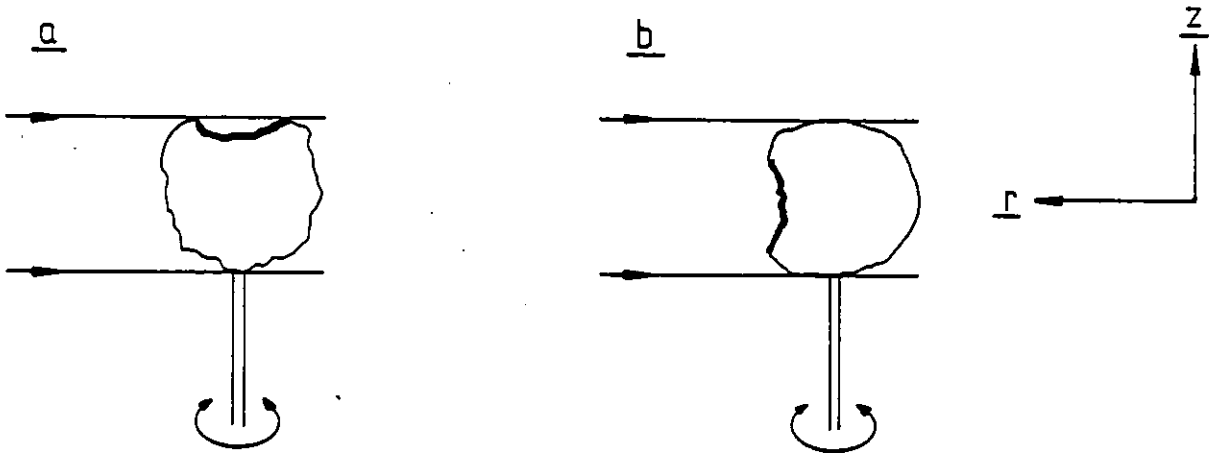

Figure 2.12 Rotation of the object revealing previously hidden areas at the poles.

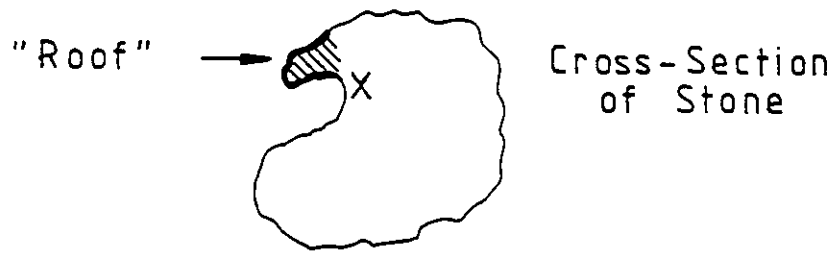

Figure 2.13 An example of an improbable concavity.

$$r' = (z^2 + r^2 \sin^2\theta)^{1/2}$$

$$\theta' = \tan^{-1}\frac{(r \sin\theta)}{z}$$

$$z' = -r \cos\theta$$

Extending this to the case when the axis of rotation intersects the r,z plane at r_o, z_o the transfer equations become;

$$r' = ((z-z_o)^2 + r^2\sin^2\theta)^{1/2}$$

$$\theta' = \tan^{-1}\left(\frac{r \sin\theta}{z - z_o}\right)$$

$$z' = -r \cos\theta - r_o$$

These operations on the matrix describing the second set of data $R_2(\theta,z)$ would yield $R_2'(\theta',z')$. Defining a function P as a measure of the correlation between R_1, the first data set, and R_2' by the equation

$$P(r_o, z_o) = \sum_{ij}(r_{ij}(\theta,z) - r'_{ij}(\theta,z))^2$$

where r_{ij} is an element of $R_1(\theta,z)$ and r'_{ij} an element of $R_2(\theta',z')$. This assumes that the rotation of the stone is done accurately by 90^o in the r,z plane and without any lateral movement out of this plane. The minimum value of $P(r_o,z_o)$ would give the values of r_o,z_o, thus enabling the addition of the two data sets to a single one.

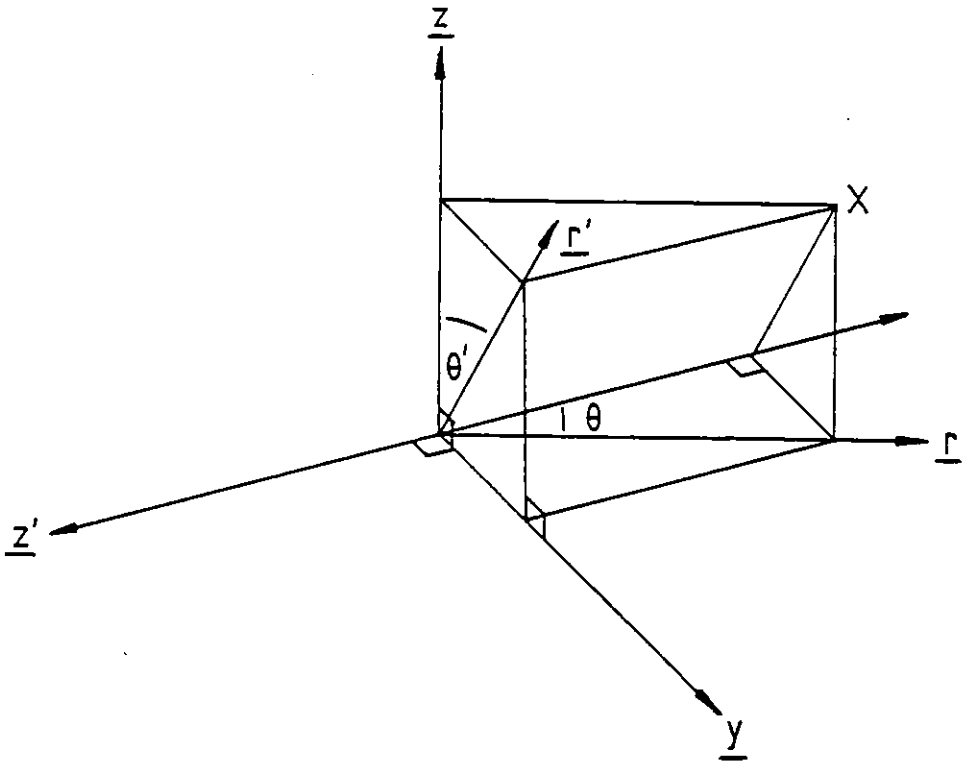

Figure 2.14 Rotation of the coordinate axes by 90 degrees about the y axis.

CHAPTER 3.

CHAPTER 3 - LINE PRODUCING OPTICS

3.1 Introduction

It was shown in section 2.3 that for an object field of 10 mm the optimum line beam waist was 60 μm diameter. In this chapter the method for producing this line is given and the parameters governing the performance of the optics calculated. The system which then produces the 3-beam illumination is described and the method of aligning the optical components given.

3.2 Primary Line Forming Optics

The optical arrangement is shown in figure 3.1 and consists of a 2 milliwatt HeNe laser, a microscope objective and spatial filter and a cylindrical lens. Due to the precision required of the complete line producing system and the fact that the machine is to be designed so as to be used in an industrial environment, the minimum number of optical components has been a criterion in the design. Cylindrical lenses have to be able to be rotated about their optical axes and this requires a more complex mount than one that provides translational movements only. For these reasons a second cylindrical lens was not introduced at A in figure 3.1 to collimate the beam.

The conjugates of the system were governed mainly by the overall system set up as described in Chapter 5 and the object, image distance of the cylindrical lens had to be of the order of

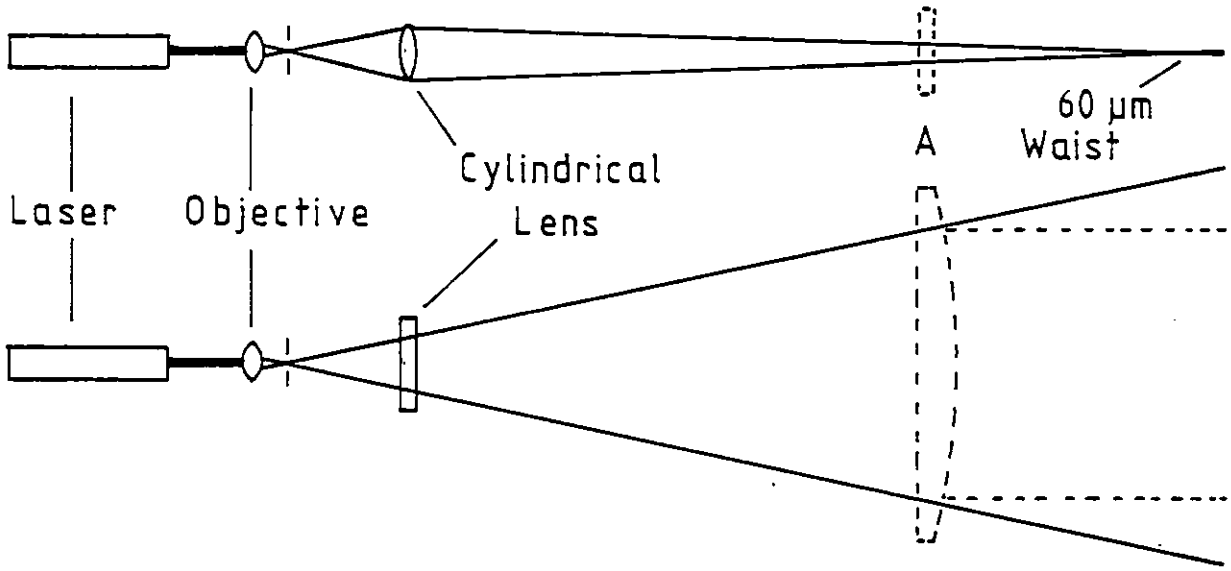

Figure 3.1 Illumination line producing system.

one metre. The focal length of the cylindrical lens is 80 mm and a 10:1 conjugate ratio is used. Considering geometrical optics only, this would require a 6 μm beam diameter produced by the microscope objective. The cylindrical lens is a 30 x 30 mm bi-convex lens manufactured to a specification of no inclusions with a laser quality finish. A biconvex lens was specified rather than a plano-convex lens which would give a better performance at the conjugates used in order to increase the radius of curvature of the faces to ease problems in manufacture. The low numerical aperture of approximately 0.017 should render any spherical aberrations negligible with respect to the 60 μm image size.

3.3 Diffraction Considerations

With a cylindrical lens width D, image distance V and coherent illumination wavelength λ, the line spread function will be of the form

$$I(x) \propto \mathrm{sinc}^2(2\pi ax)$$

where $a = \frac{D}{2\lambda V}$

The width of the central maximum is given by

$$W = \frac{1}{a} = \frac{2\lambda V}{D} \qquad (3.1)$$

Substituting in (3.1) the following values

$V = 880$ mm

$D = 30$ mm

$\lambda = 6.3 \times 10^{-4}$ mm

one obtains the width of the line spread function

$W = 37$ μm

This function is obviously going to broaden the image line and a reduction in W would seem to be a worthwhile aim. Unfortunately, an increase in the width D of the lens would not achieve this as the pupil illumination is controlled not only by the laser beam, objective combination, but by the aperture of the mechanical mount of the spatial filter. The clear aperture available is such that an increase in D would not achieve any appreciable decrease in W. As it was found that the image line produced was of an acceptable profile with the arrangement so far described, the commercially available spatial filter mount was not replaced by a specially designed unit. Such considerations are important when the system is to used in an industrial environment where replacement of components should be as easy as possible.

For the reasons given above, a lens was not included between the laser and the objective so as to fill the aperture of the objective. If a system such as this, but requiring less than the 10 mm field size was designed, a different filter mount would be a necessity with an increased cylindrical lens aperture.

The laser beam diameter is 0.6 mm and a X40 microscope

objective is used. Writing equation (2.10)

$$w = w_o\left[1 + \left(\frac{\lambda z}{\pi w_o^2}\right)^2\right]^{0.5}$$

where w is the beam radius at a distance z from the beam waist, whose radius is w_o, the far field diffraction approximates to

$$w = \frac{\lambda z}{\pi w_o}$$

Using

$w_o = 0.3$ mm

$\lambda = 0.63 \times 10^{-3}$ mm and

$z = 4$ mm (i.e. the objectives focal length)

one obtains

$w = 2.7$ μm

This gives a geometrical beam width at the image of 54 μm. The observed beam profile is shown in figure 3.2. This is a purely qualitative measurement in intensity observed through a microscope focussed in the image plane of the cylindrical lens. The side lobes have been estimated by eye to be less than 10% of the peak intensity and are probably of the order of 1%. The width of the central maximum measured throughout the 10 mm image field is shown in figure 3.3. This graph is intended to show only the general form of the image and is not meant to give an accurate description.

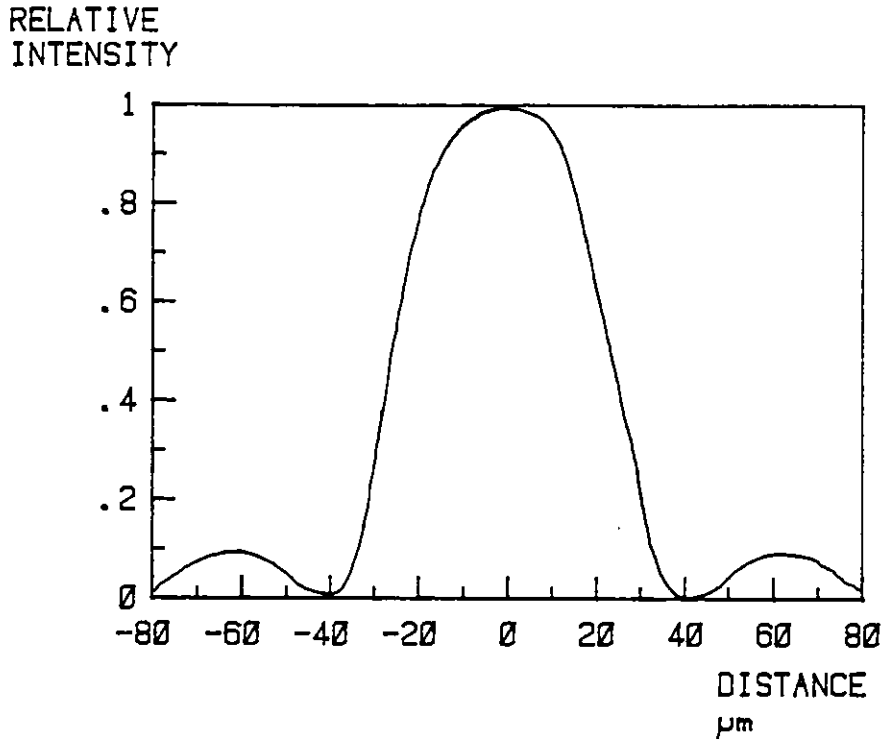

Figure 3.2 The profile of the illumination line in the centre of the object field.

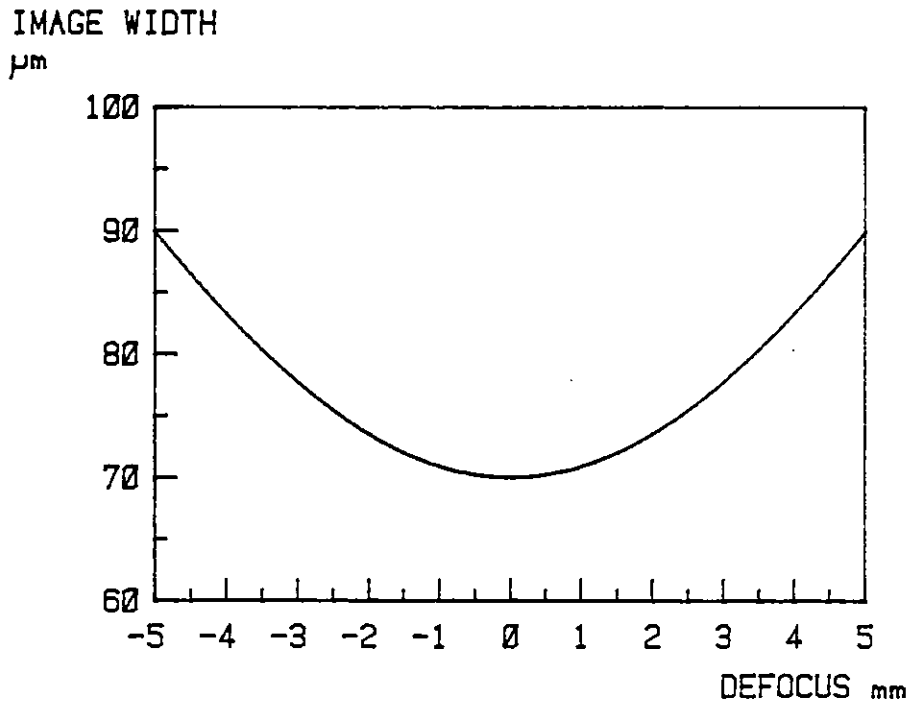

Figure 3.3 The variation of the illuminating line width with z.

In section 2.3 it was stated that with the addition of three 60 μm beams, an average beam width of 80 μm over the object field could be used. With the inclusion of diffraction and using the observed beam width of figure 3.3, an average beam width of 90 μm would be a more realistic value, giving a beam width viewed at 32^{o} of approximately 140 μm. This line width will be further modified by the imaging optical system, as described in Chapters 4 and 6.

3.4 3 Beam Producing Optics

For the rest of this thesis, the horizontal reference plane for this system will be the table upon which the system is mounted, and which is parallel to the r axis of Chapter 2 with the z axis orthogonal to the table surface.

The 3-beam producing prism system is shown in Figure 3.4 with ray paths indicated. The rays are shown for a collimated beam for simplicity but as explained in section 3.2, the beam is in fact diverging. Only the paraxial rays are shown for ease of explanation. The beam enters the 45^{o} prism from the primary line forming optics, is reflected internally through 90^{o} and enters the composite beam-splitting prism. This prism is constructed from three 45^{o} prisms, as shown by the dashed line. The individual prisms are ground and polished on the 10 mm faces to a flatness of one fringe of mercury green light across any 10 mm face. The individual prisms are then adhesed by bringing them

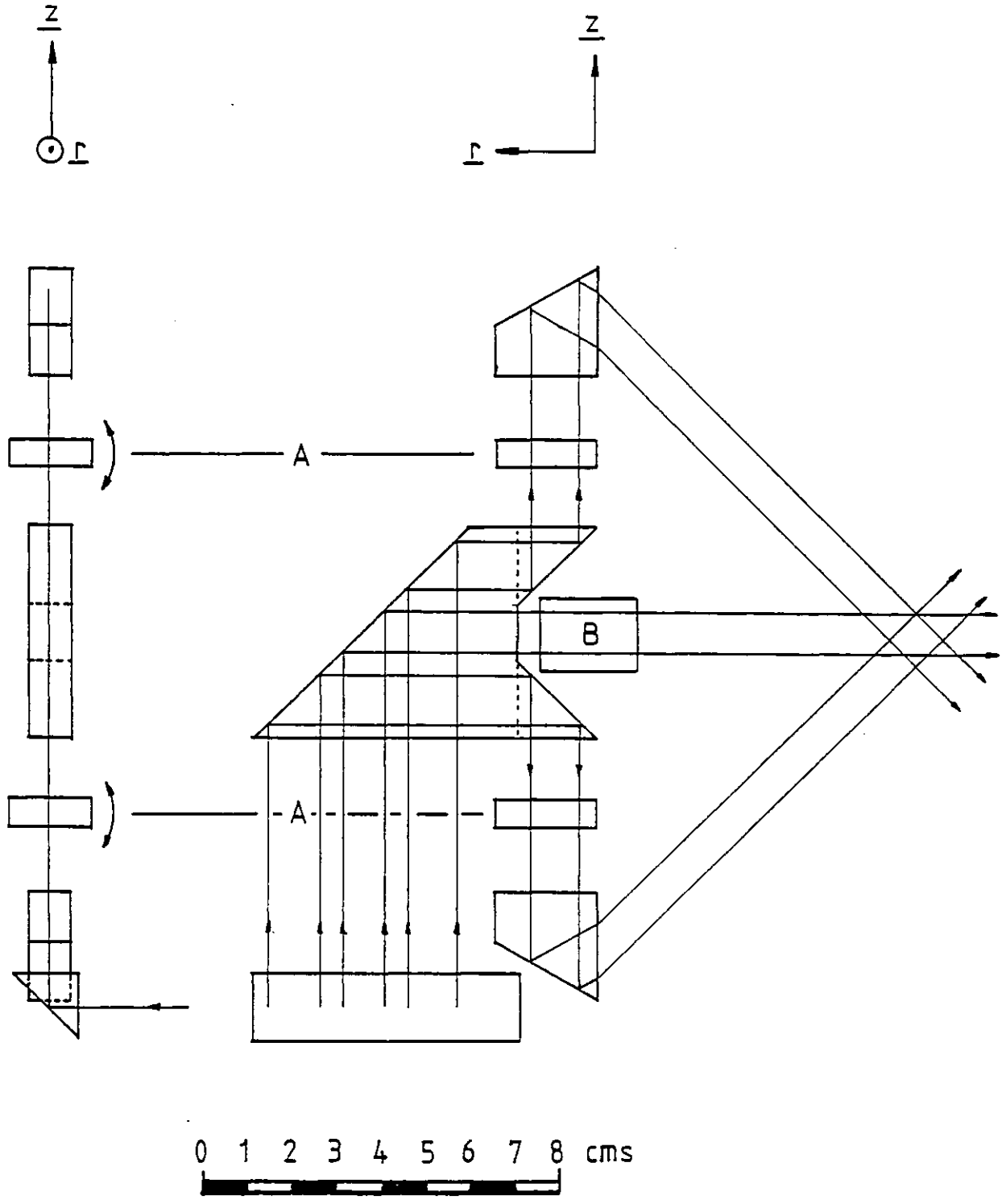

Figure 3.4 The three-beam producing prism system.

into contact, heating them and causing the surfaces to fuse. For optical purposes, the prism is now a single unit with no discontinuities across the fused boundaries. The entire prism has pyramidal errors of less than 1' of arc. The beam is divided into three; one 12 mm central beam and two vertical beams. The vertical beams pass through plates of parallel faced float glass A which can be rotated. These allow a lateral movement of the beams to be performed so as to assist in alignment of the beams in the object field. The aluminium coated 30^{o} prisms internally reflect the beams which emerge after refraction at an angle of approximately 45^{o} to the central beam.

Due to the difference in path length between the central and vertical beams, a refocussing system is introduced at B for the central beam. The design of this is discussed in section 3.6. All prisms are antireflection coated with magnesium fluoride.

3.5 Mechanical Adjustment of Prism System

Each prism is attached to a brass backplate as shown in figure 3.5. The acetate sheet spacers allow an even coating of adhesive to be formed between the prism and its mount. The mounts themselves have a three point positioning system which allow them to be adjusted in position with respect to the main prism support. The z and r axes are the same as used in Chapter 2.

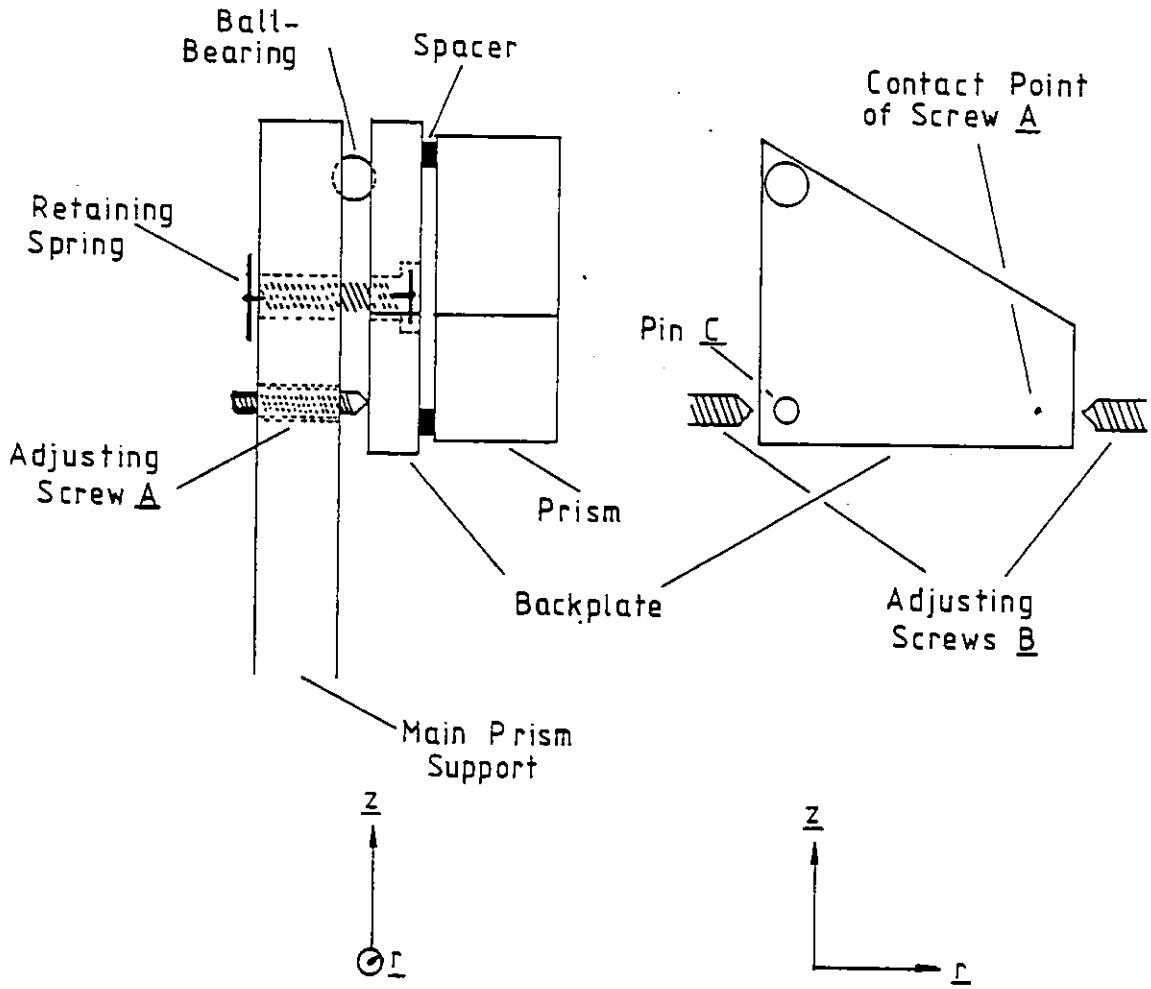

Figure 3.5 The method of mounting the prisms with their adjustments.

The backplates and main prism support are constructed from brass, a material easy to machine with a low linear coefficient of expansion of $2 \times 10^{-5}\ ^{o}K^{-1}$. The difference in expansion between the backplates and the prism whose coefficient is $7 \times 10^{-6}\ ^{o}K^{-1}$ is taken up by the adhesive which is very elastic. The adjustments are shown in figures 3.5 and 3.6. Their effective axes of rotation of the output beams are:

Adjustment	Axes
Screws A, pins C	z and r
Screws B	x
Screw D	r

Adjustments to screw B clearly cause a change of beam angle in the object plane and do not affect out of plane alignment of the 3 beam system, and are therefore non critical.

Alignment of the prism with respect to rotations about the z and r axes is accomplished by removal of the primary line forming optics described in section 3.2. Figure 3.7 shows the positions of the optical elements. The rectangular glass block causes the laser beam to shift in position across the prism mount. In this way reflections from the 45^{o} prism, the composite prism and either of the two 30^{o} prisms can be obtained. The prisms are then adjusted so that the reflection coincides with the laser beam at the laser. This adjustment is carried out by removing metal

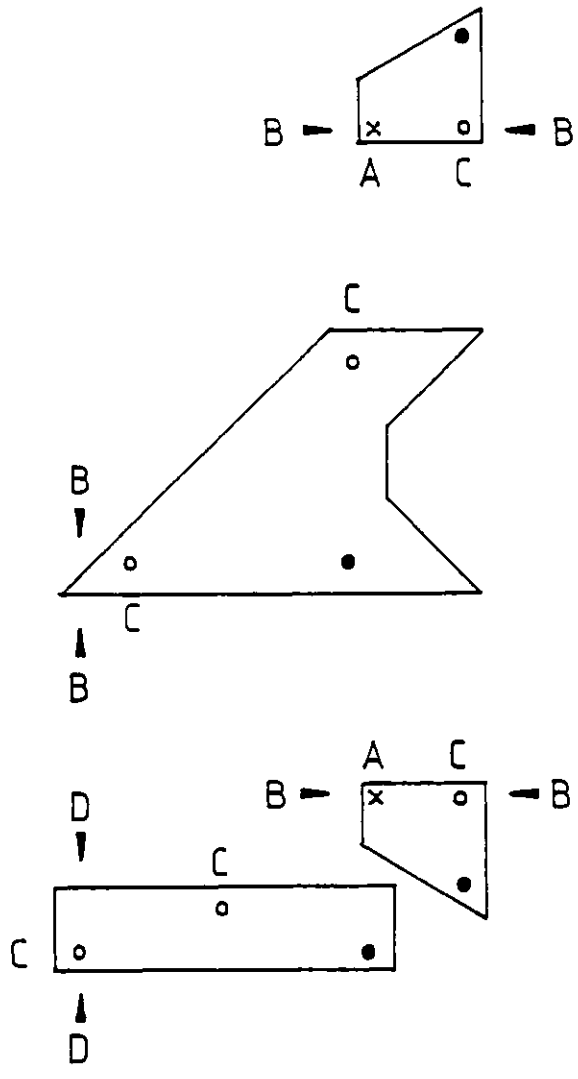

- Ball Bearing
- Pin
- Screw Adjustment // to Paper
- × Screw Adjustment ⊥ to Paper

Figure 3.6 The prisms and their adjustments.

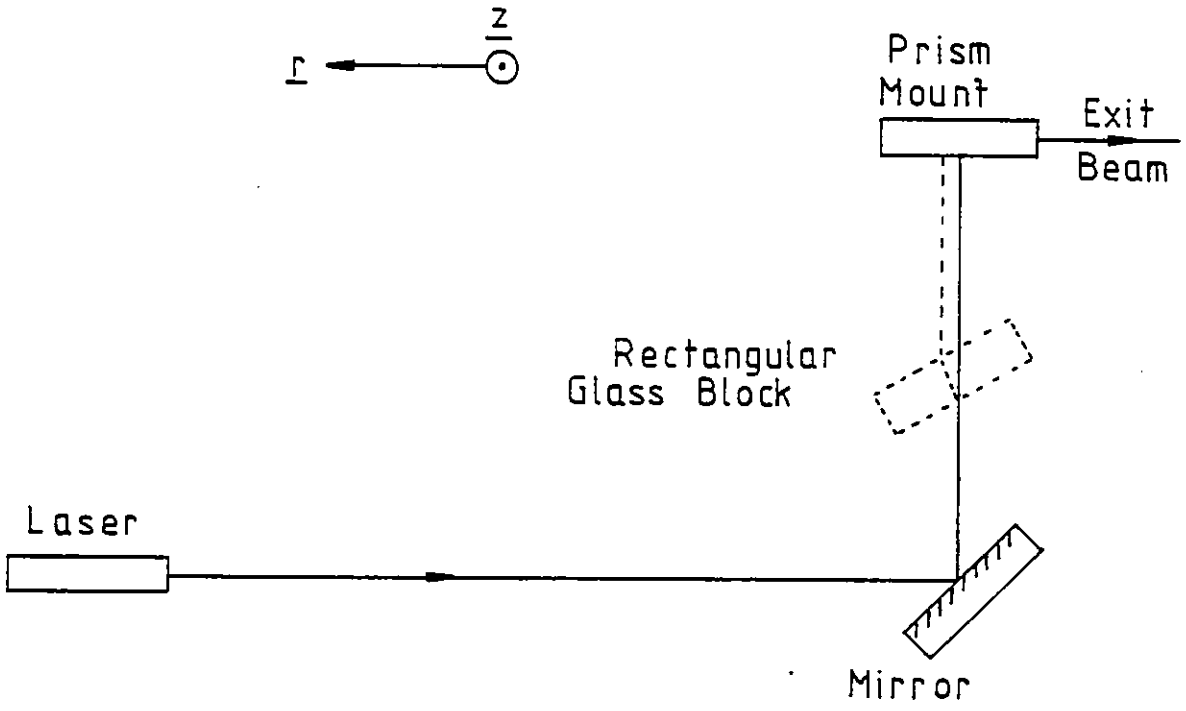

Figure 3.7 The positions of the optical components for the alignment of the prisms.

from the pins C in figures 3.5 and 3.6. The reflected beam can be measured to within 1 mm where the total travel length of the beam is approximately 2 metres. The faces of the prisms are now perpendicular to the beam to within one thousandth of a radian. This adjustment is not done with screws as part of the policy that the fewer adjustments that exist, the less chance in an industrial environment of someone incorrectly adjusting them.

The composite prism is now considered to be in correct alignment. If the primary optics are now replaced, the central line through this prism can be viewed with a travelling microscope in the object field. If the viewed line is not vertical, then adjustment of screw D in figure 3.5 will correct this without introducing any other beam errors. Adjustment of screw A for the 30^{o} prisms will now be used to produce vertical beams. Any lateral discrepancy in their beam positions with respect to the central beam, can be allowed for by rotation of the float glass plates A in figure 3.4. The screw adjustment B is an M3 x 0.5 mm grub screw.

The present system which includes the refocussing lenses, as described in Section 3.6 has achieved registration of the three beams to within $\pm$ 5 μm without it being necessary to include the glass plates.

3.6 Central Beam Refocussing System

Due to the difference in path lengths of the central and 45^{o} beams to the object plane, it is necessary to introduce a system to refocus the central beam when the 45^{o} beams focus correctly in the object plane. A single lens could accomplish this, but would obviously cause magnification of the image. With the prism system as described in section 3.5, the required object plane is 82.5 mm from the composite prism whereas the beam waist is situated 165 mm from the prism. A single lens would thus give a demagnified beam of 30 μm waist in the object plane. A three lens system as shown in figure 3.8 would be ideal in that it allows movement of the final lens and correspondingly of the image without change in image size.

This consideration is important in the prototype system as it allows for changes in the object plane to occur without the need for new lenses. The system in figure 3.8 is unsuitable as the three lenses and their separations have to be included in a small distance, and the alignment of three cylindrical lenses would be very complex. This distance is governed by the viewing optics as shown in figure 3.9. The distance x is governed by the lens system and the angle and aperture of the viewing system. To allow for possible improvement in the overall system, x was designed to be at least 50 mm which with the small lenses used in the refocussing optics, could accommodate a 20^{o} viewing angle with an f/6 aperture. The lens system must therefore be less than 30 mm overall in length and this is accomplished with a two lens

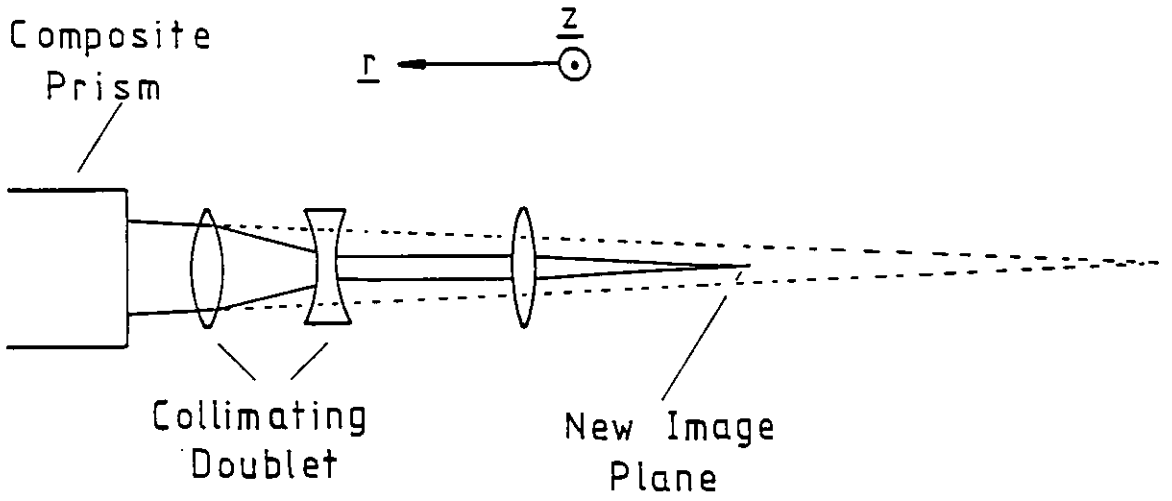

Figure 3.8 A three lens refocussing system.

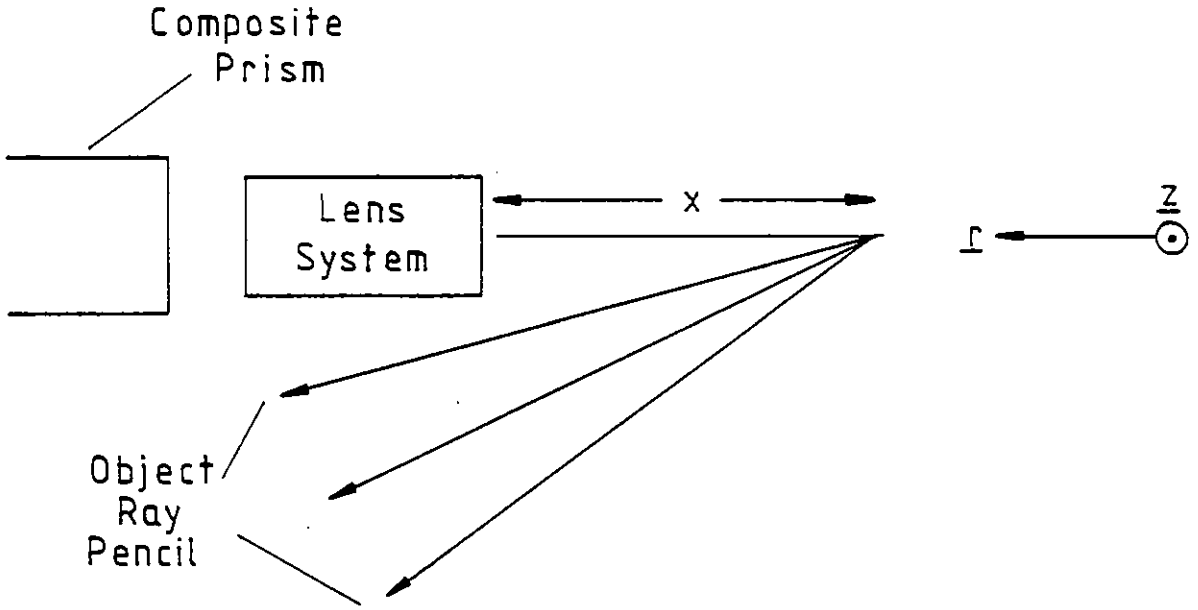

Figure 3.9 The effect of the imaging system angle and aperture on the lens spacing.

system, as shown in figure 3.10. The calculations use the thin lens formulae throughout.

Writing M_1 and M_2 as the magnifications due to f_1 and f_2 respectively, then

$$M_1 = \frac{f_1}{u - f_1}$$

$$M_2 = \frac{(v-d) - f_2}{f_2}$$

Setting $M_1 M_2 = 1$, and solving for f_2 and d in terms of f_1 it is easily shown that

$$d = f_1(1 + \frac{v}{u}) \qquad (3.2)$$

$$f_2 = \frac{f_1}{u^2}(uv - f_1(u+v)) \qquad (3.3)$$

Inserting approximate values for u and v of -160 and +80 respectively, in (3.2) and (3.3) one obtains,

$$d = \frac{f_1}{2} \qquad (3.4)$$

$$f_2 = \frac{-f_1}{320}(160 - f_1) \qquad (3.5)$$

The maximum value of d is 30 mm as stated above and the practical minimum 10 mm. This places limits on f_1 and f_2 of:

$$60 > f_1 > 20$$

and

$$-8.75 > f_2 > -18.75$$

The larger values of the focal length would be desirable for

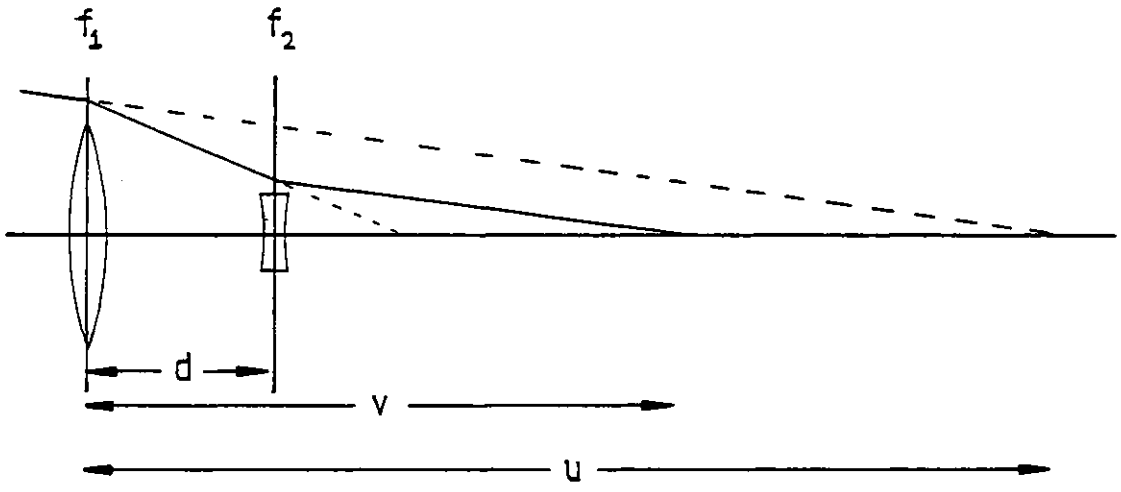

Figure 3.10 A two lens refocussing system.

the purpose of ease of manufacture but the effect of changing d in the system should be considered. For a change of d the Magnification M and Image distance v would change and the ratio $\frac{\Delta M}{\Delta v}$ should be considered in the decision on f_1.

Writing $$M = M_1 M_2 \tag{3.6}$$

we obtain $$\frac{dM}{dv} = M_1 \frac{dM_2}{dv} \tag{3.7}$$

but $$M_2 = \frac{(v-d) - f_2}{f_2}$$

differentiating produces

$$\frac{dM_2}{dv} = \frac{1}{f_2}\left[1 - \frac{dd}{dv}\right]$$

The object distance u' for f_2 is given by

$$u' = d - \frac{uf_1}{u-f_1}$$

giving $$\frac{du'}{dd} = 1$$

But $$\frac{d(v-d)}{du'} = \frac{dv}{dd} - 1 = -M_2^2 \tag{3.8}$$

Substituting (3.8) and (3.6) into (3.7) and setting M=1, one obtains,

$$\frac{dM}{dv} = \frac{M_1}{f_2(1-M_1^2)} \tag{3.9}$$

where

$$M_1 = \frac{f_1}{u-f_1}$$

with $f_1 < 60$, $M_1^2 << 1$ we approximate

$$\frac{dM}{dv} = \frac{M_1}{f_2}$$

Substituting for f_2 from equation (3.5), and using v = -160 we obtain

$$\frac{dM}{dv} = \frac{1}{80(1 - (f_1/160)^2)} \qquad (3.10)$$

It can be seen that for $60 > f_1 > 20$ this value will not vary significantly. The values for f_1 and f_2 were picked to allow ease of mechanical mounting by choosing a fairly large value of d. The values were

$f = 50$ mm

$f_2 = -16$ mm

$d = 25.9$ mm

These values give, $\frac{dM}{dv} = \frac{1}{70}$

Giving a change in the object plane of 7 mm for a 10% change in image size.

3.7 Alignment of Refocussing System

With the central and 45° beams registered in the same plane in the object field, but with the central beam defocussed, it is necessary to calculate the accuracy with which the two cylindrical

lenses have to be positioned in order to maintain the registration. Figure 3.11 shows a paraxial ray of the central beam entering the two lens system where the two lenses are off axis by distances a and b. It is assumed for the following argument that the axes of the two lenses are parallel and that the ray lies in the plane of the paper throughout the system. It is required to calculate the off axis distance of the emergent ray in the object field and its angle u' to the object plane. The relationship between the incident ray angle u, the emergent ray angle u', the lens power K and incident off axis height h can be written as,

$$u' = u - hK \tag{3.11}$$

Applying equation (3.11) to the situation in figure 3.11 produces,

$$u = -aK_1 \tag{3.12}$$

$$h' = b + ud \tag{3.13}$$

$$u' = u - h'K_2 \tag{3.14}$$

Substituting for u and h' in (3.14) gives,

$$u' = -aK_1(1- dK_2) - bK_2 \tag{3.15}$$

The off axis distance H of the ray after a distance x will then be given by

$$H = ud + u'x$$

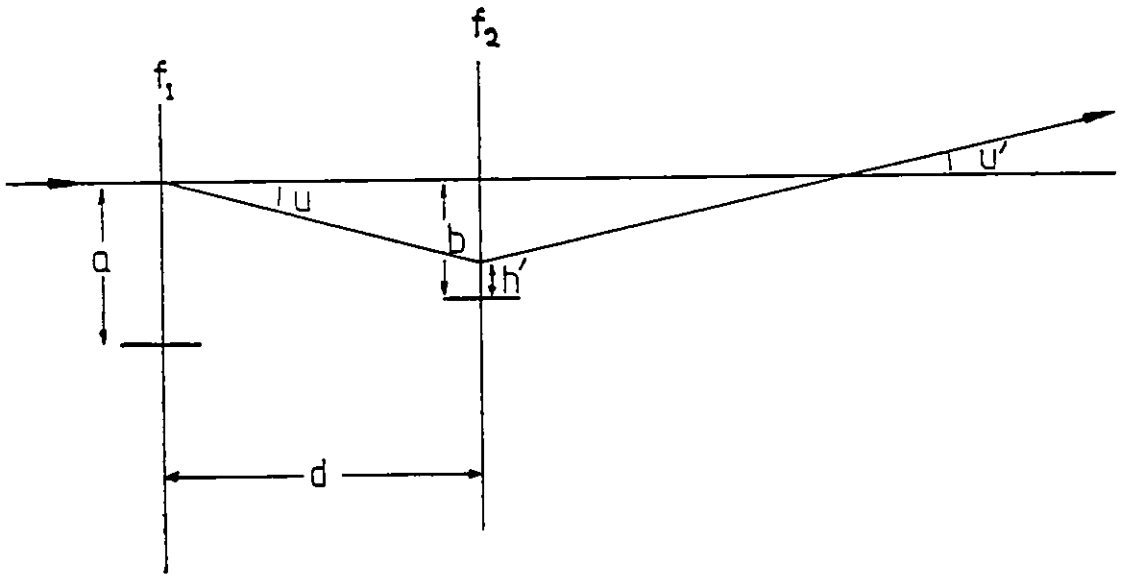

Figure 3.11 The effect of misalignment of the refocussing lenses.

Substituting for u, one obtains,

$$H = -aK_1 d + u'x \qquad (3.16)$$

Inserting the values for K_1, K_2, d and x of 0.02,-0.0167, 25.9 and 50 respectively in (3.15) and (3.16), we obtain to 3 significant figures,

$$u' = -.052a + .0625b \qquad (3.17)$$

$$H = -3.14a + 3.13b \qquad (3.18)$$

If it is required that the beam be on axis to within 5 μm, then from (3.18) it can be seen that a and b must be within approximately 2 μm of each other. If the beam angle is also to be small, such that within the 10 mm object field the beam diverges less than 5 μm, from (3.17), we obtain with a and b equal

$$u' = .01a < 5 \times 10^{-4}$$

$$a < .05 \text{ mm}$$

This is fairly simple to accomplish, whilst the restriction on (a-b) is far more difficult. It implies that the axes of the cylindrical lens must be parallel to within 5×10^{-4} radians.

The two lenses are mounted on a specially designed brass holder where they are held in position by pressure from two rubber pads. The adjustment of their axes was carried out by trial and

error involving aligning the 50 mm lens so as not to introduce any twist in the central beam as viewed through a travelling microscope and then introducing the -16 mm lens and adjusting that. The whole mount is then adjusted by the use of three M3 x 0.5 screws against which the mount is held by a spring. Despite the instability of such a mount good results have been obtained as discussed in section 3.8.

3.8 Conclusions

Although the intention was to construct a machine for an industrial environment and thus to limit as far as possible the number of adjustments in the system, the three-beam illuminating optics suffer from the high resolution required. The primary line forming optics are of no problem and the prism system can be aligned in a short time with practice, but the two lens refocussing system is difficult to adjust. At the time of writing this thesis, the optics had remained aligned for a period of three months in a laboratory environment where great care is taken not to disturb the equipment. In an industrial situation the machine could spend much time inoperative due to misalignment of components. With the conjugates used in this system it is possible to replace the cylindrical refocussing lenses with spherical ones and still maintain a 12mm line in the object field. This would remove the necessity for aligning the cylindrical lenses to the high tolerances required and is now possible due to proven success of the system, as described in Chapter 8.

CHAPTER 4

CHAPTER 4 - IMAGING SYSTEM

4.1 Theoretical Design Parameters of the Imaging Optics

In this section, all lenses are assumed to be aberration free thin lenses as a first step in designing the imaging system. Figure 4.1 shows the optical system viewed in the direction of the z axis. The object plane is at an angle θ to the optical axis and the image plane at an angle ϕ for the system with magnification m. Considering a ray from the object point described by r travelling in the direction of the r axis, and passing through the image point described by r' it can be seen that

$$\tan\theta = m\tan\phi \tag{4.1}$$

Considering the principal ray, the relationship between r' and r can be written as

$$\frac{r\sin\theta}{y_o - r\cos\theta} = \frac{r'\sin\phi}{my_o + r'\cos\phi} \tag{4.2}$$

After substitution of equation (4.1), and for y_o from the relationship,

$$y_o = \frac{(m+1)f}{m}$$

equation (4.2) yields

$$r' = \frac{m^2 r\cos\theta}{\cos\phi(1-mr\cos\theta/f)} \tag{4.3}$$

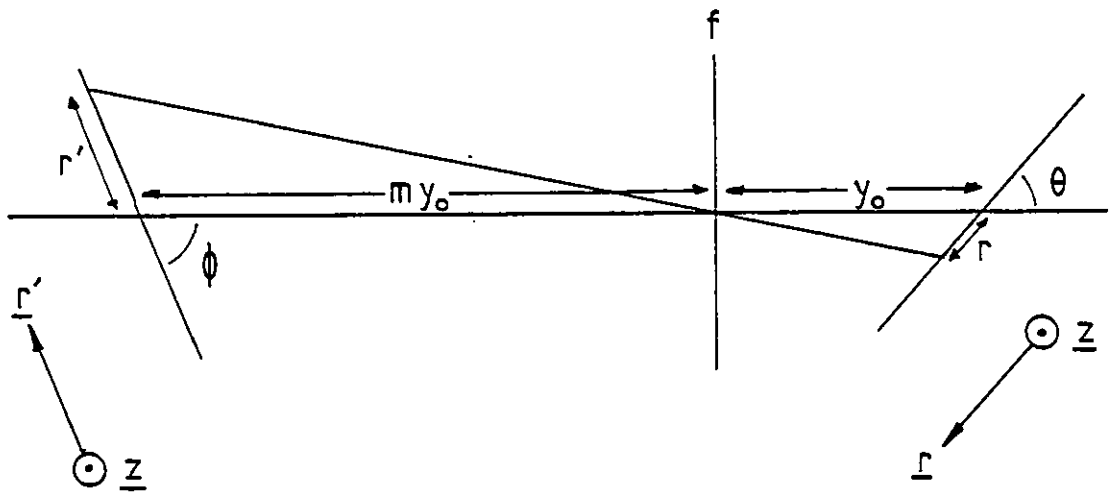

Figure 4.1 A single lens imaging system.

Assuming $\frac{mr}{f} << 1$, r' can be written as

$$r' = \frac{m^2 r\cos\theta}{\cos\phi}\left(1 + \frac{mr\cos\theta}{f}\right)$$

The term $mr\cos\theta/f$ causes a nonlinear relationship between the object and image coordinates. If this term is such that for an object distance of 5 mm an image error of 10 μm is caused, we have;

$$\frac{mr\cos\theta}{f} = 0.002$$

giving

$$f = 2.5\ m\cos\theta \quad \text{metres}$$

For $\theta = 32^{o}$

$$f \approx 2\ m \text{ metres} \qquad (4.4)$$

This implies a total object, image plane distance of $2(m+1)^2$ metres. Obviously a single lens system is going to require a highly corrected lens of large focal length to correct this nonlinearity in the system. Such a lens though would be expected to introduce aberrations of its own which are likely to be worse than the ones it would be trying to correct.

The preceding argument was for an unknown magnification which would depend on the size of the detector used. The detectors are

25mm Vidicon Tube cameras which normally have an image area of 9.5 x 12.5 mm to work with most TV systems which have a 3:4 aspect ratio. The tube drives were adjusted to give a square image area of side 10.5 mm. The cameras and associated electronics are discussed further in Chapters 7 and 8.

4.2 The Telecentric Lens System.

With the need for long focal length optics, the telecentric system was an obvious choice. The ability also to have object and image planes of similar dimensions allows unit magnification thereby producing a symmetrical system as shown in figure 4.2. The factors governing the performance of the system are the pupil and lens diameters, the maximum off axis object distance, the alignment of the components and the performance of the individual lenses.

The alignment of the lenses on a common optical axis was achieved by reflecting a laser beam off the two lenses individually and by observing the transmitted beam with either or both lenses in position. Experimentally all lenses had a maximum tilt of 0.001 radians to the axis. The effect of tilt is the same as having off axis object points and for the purposes of considering aberrations in the system the lens tilts are negligible.

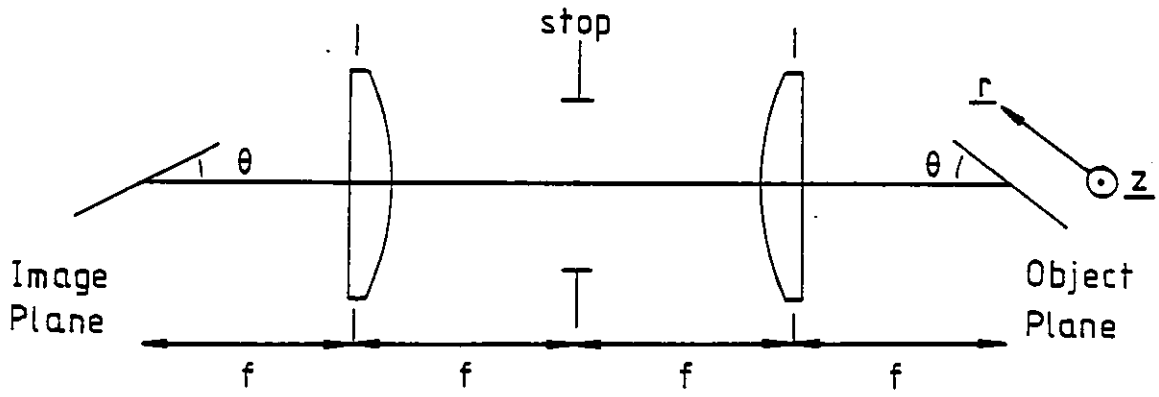

Figure 4.2 The telecentric lens system.

The separation of the two lenses was adjusted by forming a collimated beam of light from a laser, microscope objective and collimating lens. This beam was aligned along the viewing optical axis, and retroreflected after transmission through the two lenses. The separation of the two lenses was then adjusted so that the return beam produced a spot, similar to the laser exit spot, on the laser. The power K of two lenses focal length f, separated by 2f + d is given by

$$K = \frac{-d}{f^2}$$

The required power for reduction of image distortion as explained in section 4.1 was shown in equation (4.4) to be

$$K = \pm .5 \quad m^{-1}$$

giving

$$d = \pm .5 \, f^2 \quad \text{metres}$$

Due to constraints on the overall system design as given in Chapter 5, lenses of focal length 180 mm were used. This yields for d a value of ± 16 mm. The separation could be set to within this by simple measurement but the closer the system to a symmetrical one the less the aberrations that will be introduced. Using the above method the focal length of the combination was adjusted to be greater than 50 metres, giving d less than 0.5 mm.

For the purposes of imaging the gaussian profile onto the camera faceplate, the lens system is not required to have high resolution capabilities but to map faithfully from object to image

planes. This implies that the telecentric system with by definition the principal ray parallel to the optical axis in the object and image spaces, can be allowed to have any aberrations which are circularly symmetric about the principal ray. Thus any spherical aberration or defocus will not affect the performance of the system. With the object and image in the focal planes of the two lenses, the system is symmetrical and thus any coma which may be introduced in the space between the lenses by the object lens is cancelled by the image lens. Therefore the specifications for the lenses are only that with the maximum off axis object distance at the greatest distance from the focal plane of the object lens (i.e. when the system is non-symmetric) they should not introduce such aberrations in the object plane so as to cause an image shift greater than the desired resolution of the system.

The lenses used were 180 mm focal length cemented achromats. These were tested on a Twyman-Green interferometer and found to be very close to diffraction limited for on axis imaging. To check the aberrations caused by off axis objects and by objects not at the focal plane of the lens, for which the lenses were designed, a ray trace was carried out on the system for the object point defined by

$r = -5$ mm

$z = 5$ mm

The ray trace was carried out on a Hewlett Packard 9845 mini computer in the Optical Design Group of Imperial College. The

data on the lenses was not available from the manufacturer and therefore the ray trace was carried out on a computer optimised lens design. The criteria for the design was an 180 mm achromatic doublet with diffraction limited performance at infinite conjugates. The lens separation was such that the effective focal length was 50 metres. The pupil size was 28 mm which with lenses of 38 mm clear aperture ensure no vignetting. The ray trace showed an image distortion as described by equation 4.3. The maximum antisymmetry of the exit ray pencil was less than 0.2 micrometers. The greatest deviation of the principal ray from the gaussian image position was 0.5 μm. The f/6.4 system described creates an image intensity with a 2 mwatt laser that is capable of saturating the vidicon cameras, thereby ensuring adequate allowance for variations in the system.

4.3 Effects of the Camera Faceplate

The front of the camera tube is covered by a 2.5 mm thick sheet of glass protecting the photo-conductive layer of the tube. The image must therefore be focussed on the rear of this plate and with an incident angle of 58^{o} for the principal ray in air the aberrations caused by the passage through the glass should be considered. It must be remembered that the exit pencil of rays from the confocal telecentric system is identical for all object points and therefore the faceplate will not introduce any distortion of the image and therefore only affect the ability of the overall system to measure the position of an object point by

introducing some form of defocus causing broadening of the gaussian image. For completeness, an assessment of this defocus is made here. Figure 4.3 shows a principal ray and another ray focussed to a point A with incident angles i_o and i respectively. For the purposes of this exercise, rays only in the plane containing the object r axis and the imaging optical axis are considered though it is clear that the glass will introduce astigmatism. Describing the distance AB by P, the distance R is given by

$$R = P \frac{\sin(i_o - i)}{\cos i} + d(\tan r - \tan r_o) \tag{4.5}$$

To calculate P, the second term in equation (4.5) is approximated by,

$$(\tan r - \tan r_o) = \Delta r \frac{d(\tan r)}{dr} \tag{4.6}$$

Differentiating Snells law, the relationship

$$\frac{dr}{di} = \frac{\cos i_o}{n \cos r_o} \tag{4.7}$$

is obtained. Substituting this and equation (4.6) into equation (4.5), the relationship

$$R = (i - i_o)\left[\frac{P}{\cos i_o} - \frac{d \cos i_o}{n \cos^3 r_o}\right] \tag{4.8}$$

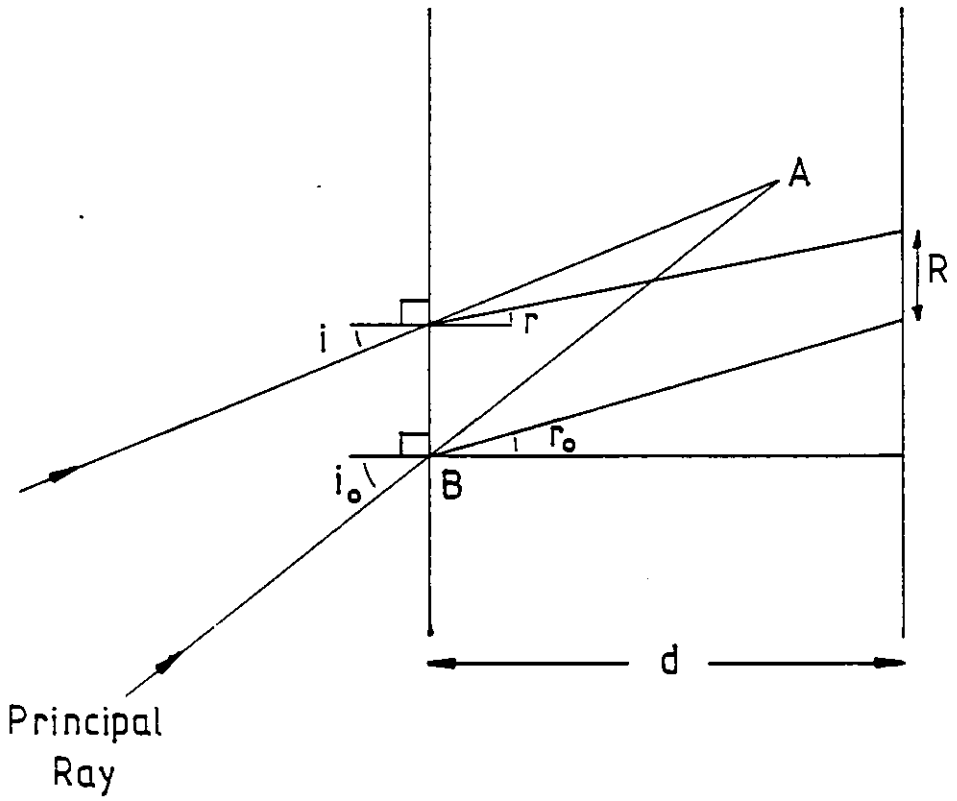

Figure 4.3 The effect of the camera faceplate.

is obtained where $(i_o - i)$ has been assumed to be small. Equation (4.8) suggests a value of P given by

$$P = \frac{d \cos^2 i_o}{n \cos^3 r_o}$$

which, on insertion into equation (4.5) gives

$$R = d\left[\tan r - \tan r_o + \frac{\sin(i_o - i) \cos^2 i_o}{n \cos i \cos^3 r_o}\right] \qquad (4.9)$$

Figure 4.4(a) shows a graph of this function for a value of i_o of 58^o for a glass plate 2.5 mm thick and refractive index 1.5. Figure 4.4(b) shows an approximate intensity distribution found by discrete differentiation of the curve in figure 4.4(a) for a field angle of 9^o. The curve shows a coma type aberration with a central spot diameter of approximately 4 μm.

4.4 Conclusions

It has been shown that a cheap and simple telecentric lens system will provide the necessary image qualities to ensure that distortion errors in the image are well below the resolution required of the whole system. Thus in calculating design parameters for a required resolution, the viewing system can be considered error free for resolutions down to a few micrometers.

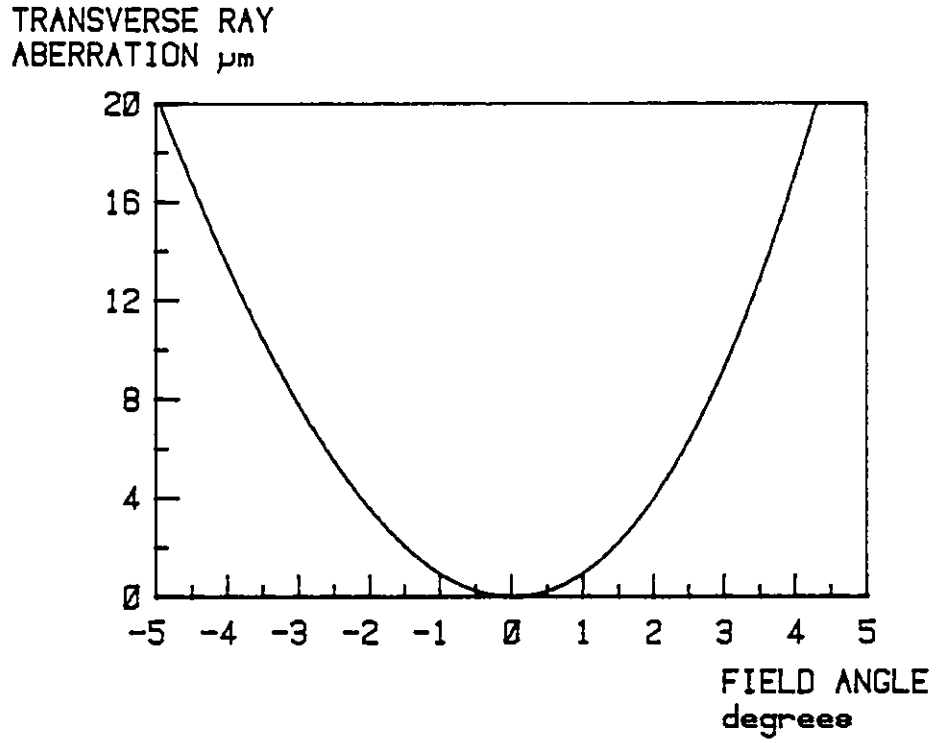

a

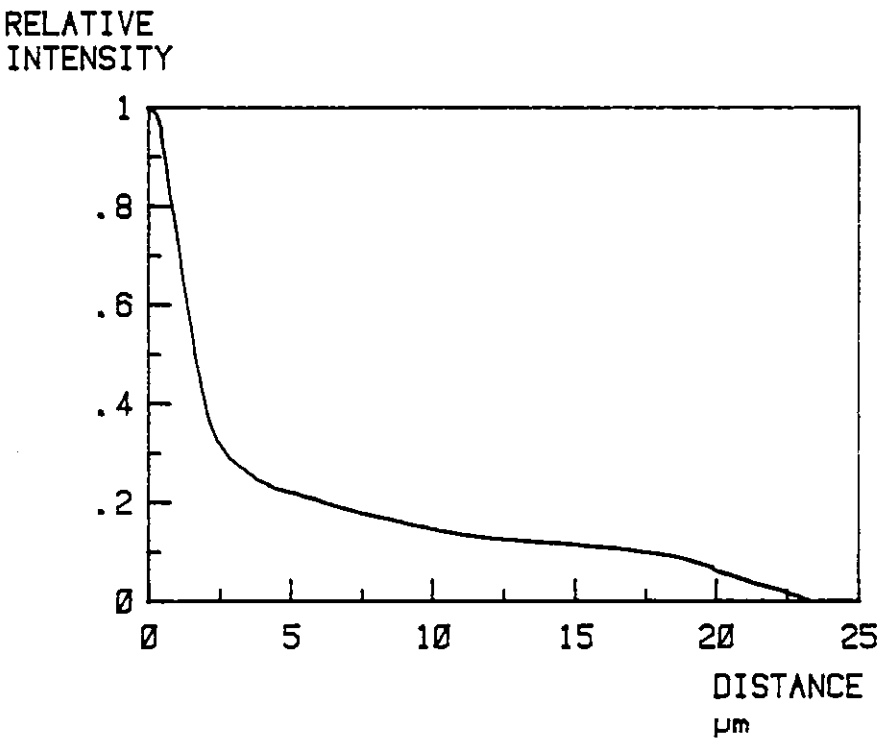

b

Figure 4.4 a) The variation of the transverse ray aberration R, with field angle θ.

b) Discrete differentiation of the curve in 4.4a.

CHAPTER 5

CHAPTER 5 - OVERALL DESIGN

5.1 Layout of System

The system as far as the cameras is all mounted on a 3ft x 4 ft cast iron table which rests on four partially inflated car inner tubes. This provides a rigid base for the optics which is vibrationally isolated from the floor. The degree of isolation necessary is small compared to equipment used for interferometric purposes as the most sensitive variations between components is for the line producing system. A movement of 1 μm of the microscope objective with respect to the line producing cylindrical lens would only cause a 10 μm shift of the line on the object. Experimentally a Twyman Green interferometer was set up on the table with a laser as the source and all components sitting unattached on the table. With people working nearby, movements of less than 0.5 fringes were observed. This stability is obviously desirable when the equipment is installed in an industrial environment.

All components are securely bolted to the table, except for the 3-beam producing prism mount which is held spring loaded on a bolted base and is positioned on the base by a ball, plane and line 3- point mounting system. A minimum of adjustments possible are included in the equipment to allow for alignment. The cameras each have two orthogonal translation and one rotation stages on which they are mounted. One translation stage moves parallel to the faceplate causing an image shift with no defocus whilst the second has both effects. The rotation stages are necessary to ensure the

faceplate lies in the image plane and more importantly, to aid registration of the image in both cameras. Electronic alignment of the two camera image areas is explained in Chapter 7.

Figure 5.1 shows the positions of the components on the table and plate (5.1) is a double exposure of the equipment with a long time exposure of the laser beam to show the ray paths.

5.2 Rotation of the Object

The object is positioned on a ground steel shaft which runs between two bearings. This shaft is driven via a timing belt from a stepping motor. There is provision for a variety of ratios between the stepping motor and shaft to change the object rotation angle, but this is normally carried out by varying the number of steps of rotation between frames when data is being recorded. The step angle desired depends on the object size and the object surface resolution required. With the value of rough diamonds varying exponentially with the radius, smaller stones may only require a larger sampling interval than that given by a single motor step.

The accuracy of the position of the motor after a step is of the order of 0.2^{o}, thus any errors in the rotation system will be caused by the belt drive. This was tested by fixing a mirror to the shaft and reflecting a laser beam off the mirror. On rotation of the shaft by 360 degrees using the stepped drive, the reflected

beam was found to always lie within 0.15 degrees of its original position which, with a 10 mm object, would give a 13 μm error in the rotation coordinate of the data. For a system requiring an higher accuracy, a different form of drive would have to be employed. Replacement of the belt drive with even a perfect zero slip system would leave the stepping motor positioning error of approximately 25% of the step angle.

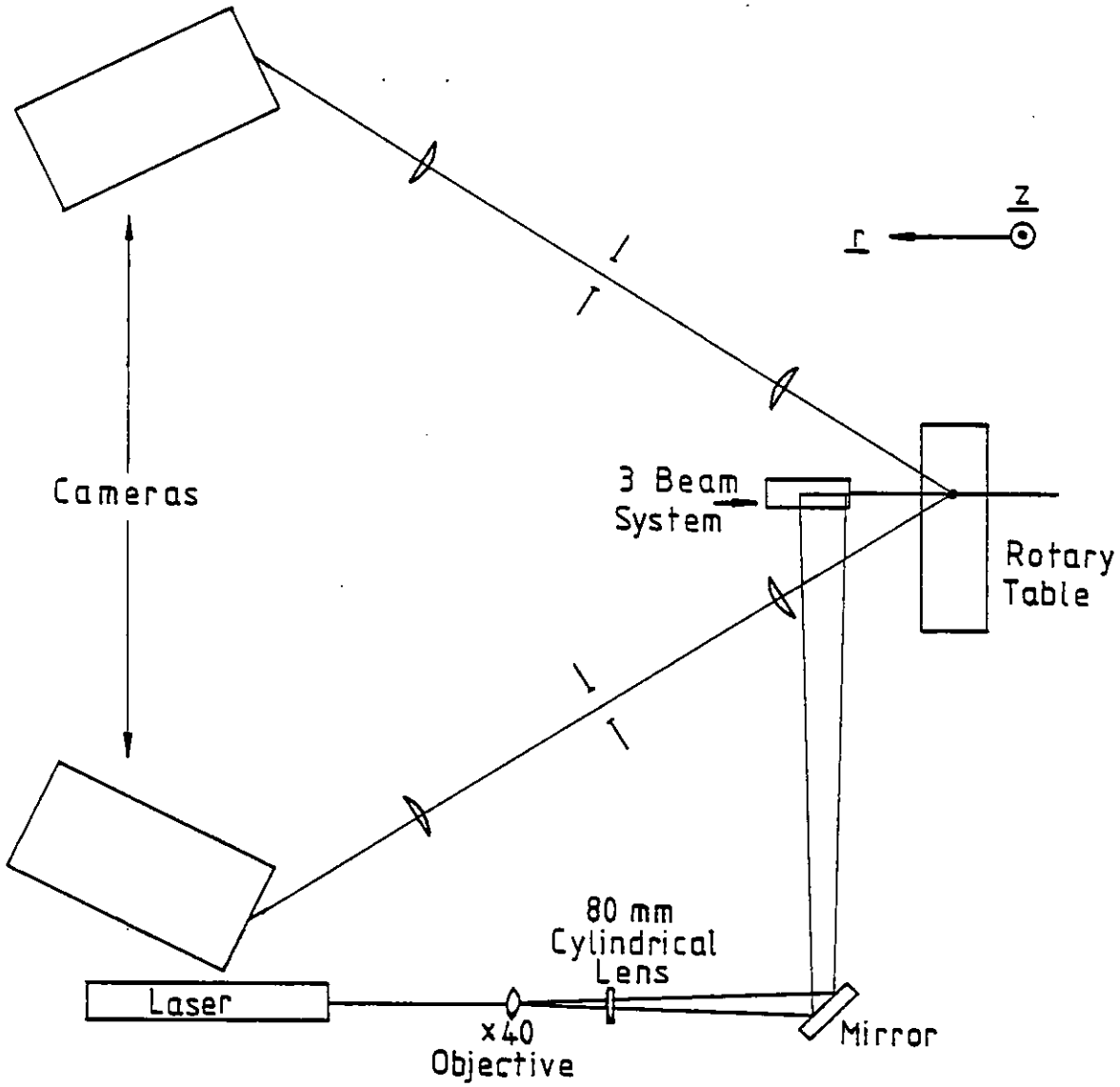

Figure 5.1 General layout of system.

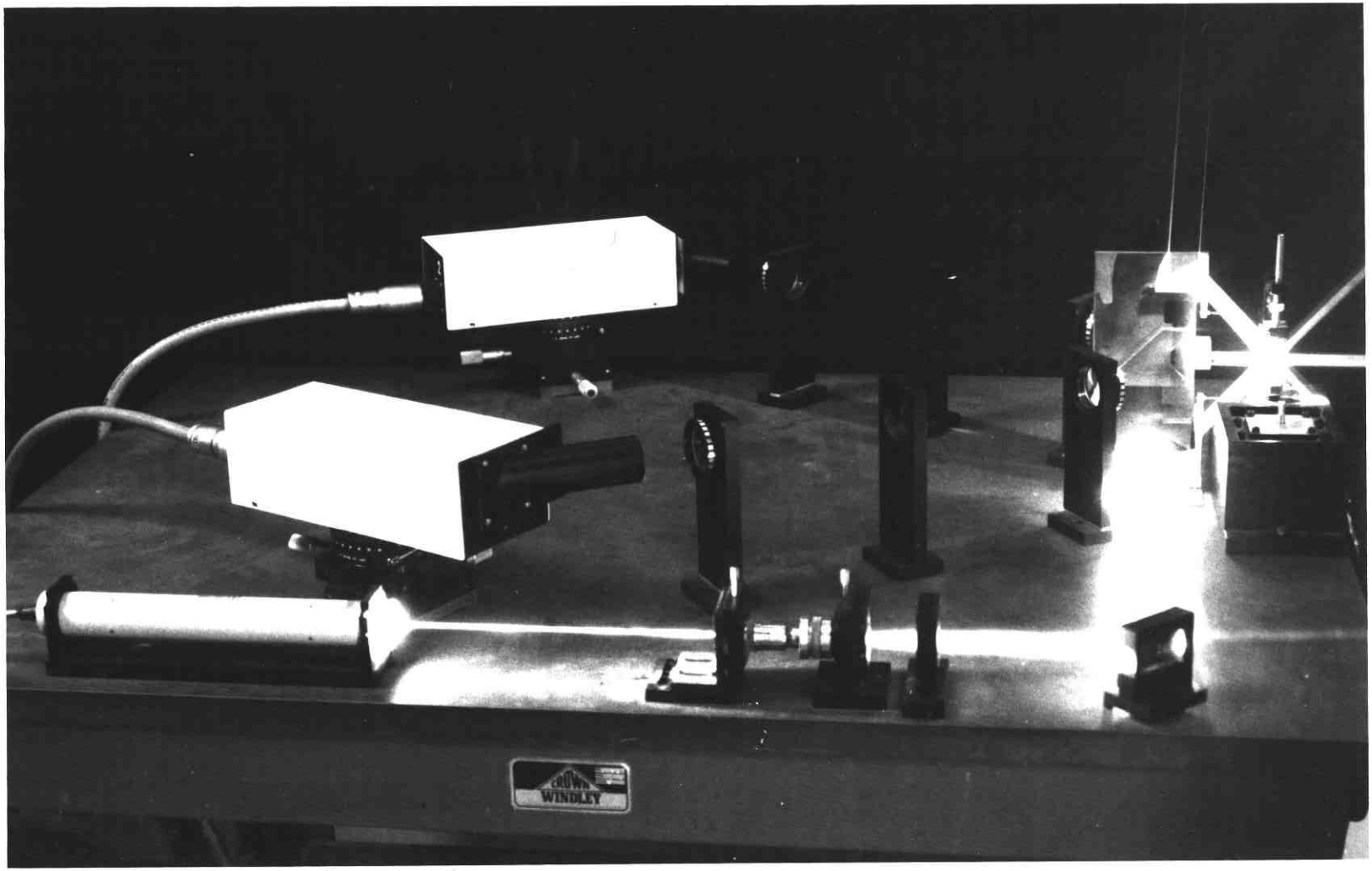
CROWN
WINDLEY

CHAPTER 6

CHAPTER 6 - IMAGE PROPERTIES

6.1 Introduction

In this chapter the various parameters affecting the image are described. In section 6.2 the interaction of the camera electron beam with the image is discussed. Sections 6.4 and 6.5 examine the properties of the "Slick" coating in the production of speckle in the image due to the coherent illumination and estimate the reduction in speckle contrast caused by the beam spot. In section 6.6 experimental variations in image properties due to changes in object orientation are given and theoretical explanations attempted.

6.2 Video Signal Production

When light falls on the photoconductive layer of a TV camera tube, a charge pattern is set up which at any point is proportional to the total flux incident at that point. A focussed electron beam is scanned over the active area of the faceplate and the current in the beam will depend upon the potential at the point where it is incident. This point is then discharged by the beam and the current required to do this measured. This current provides the video signal and it will vary from point to point as the beam scans. Once a point has been discharged, the incident illumination will begin to charge that point up again. The charge at a point is therefore the integral over time of the illumination. The period of integration is the time between discharges by the electron beam which is the frame time of the scanning raster.

Normally the focussed beam has an effective diameter less than the raster line separation and therefore each line scans an image that has not been discharged for a whole frame period; nevertheless, there is a time constant for the discharge of any point and therefore some information from the previous frame will still be stored. This effect is known as lag and is measured by studying the video signal amplitude in successive frames after the illumination is cut off. There are two predominant causes of lag which vary in significance for different types of camera tube. The first cause is the diffusion time for charge carriers crossing from the image side of the photoconductive layer to the beam side. The second reason is the capacitative effect of the photoconductive layer. In "Plumbicon" tubes the first effect is negligible and the majority of the carriers produced during a frame will be detected during the first scan of the beam, and the characteristic lag will depend only on the number of times a point is scanned and not on the time between scans. In vidicon tubes the diffusion process is the predominant cause of lag and the characteristic curve will depend mostly on the time between scans and not on the number.

The tubes used in this system are English Electric Valve Co Ltd P8203 vidicons and their typical lag characteristics, as supplied by the manufacturers are shown in figure 6.1. The lag characteristic curve was measured for a 20 millisecond field rate and from the graph it can be seen that after a 20 millisecond delay the video signal is 60% of the original.

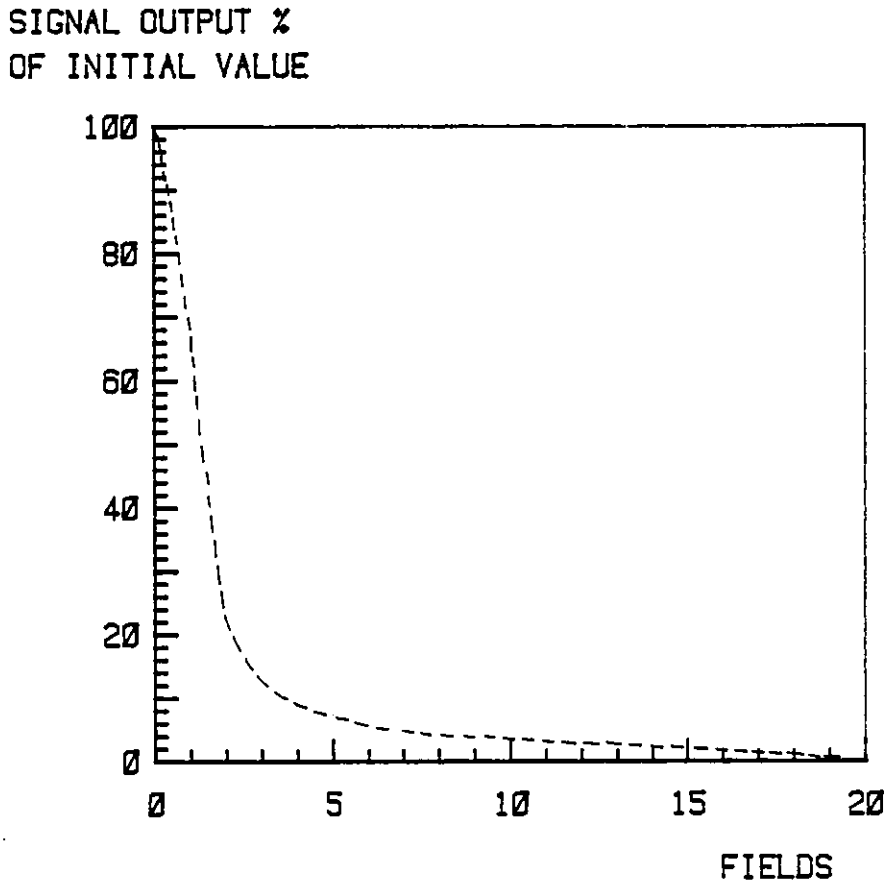

Figure 6.1 The lag characteristics of the camera tubes.

When coherent or partially coherent light is reflected from an optically rough surface the resulting optical wave at any point will consist of many wavelets with randomly distributed phases. The resulting intensity pattern will have a granular appearance known as speckle. The production of the speckle pattern is discussed further in section 6.4.

It will be shown in section 6.5 that to reduce the speckle contrast by a significant amount the beam spot will have to be defocussed to a diameter of approximately 64 μm. This implies that with a 16 μm line separation (i.e. 625 lines in a 10 mm field) the spot will be scanning over a width of 4 lines. If on a single pass of the flying spot all charge were detected on a line, then a defocussed spot would be effectively scanning only one line width (i.e. the previously unscanned line). This situation is shown in figure 6.2. This would imply that a vertical resolution of one line pair per two T.V. scan lines should be able to be achieved with a greatly defocussed spot. This leads to a contradiction that if the beam current depends upon the potential at the photoconductive surface, and a potential exists for only the segment X in figure 6.2 of the beam spot area, the majority of the beam area will not be required, thereby reducing the effective spot size. A precise description does not therefore appear possible without considering the exact interaction between the beam and the target. The evidence for considering the spot as a linear filter is solely from experimental evidence given in section 6.3, where it is shown that the image appears to be a "hard" image which does not interact with the spot whilst it is being scanned. This is clearly important when

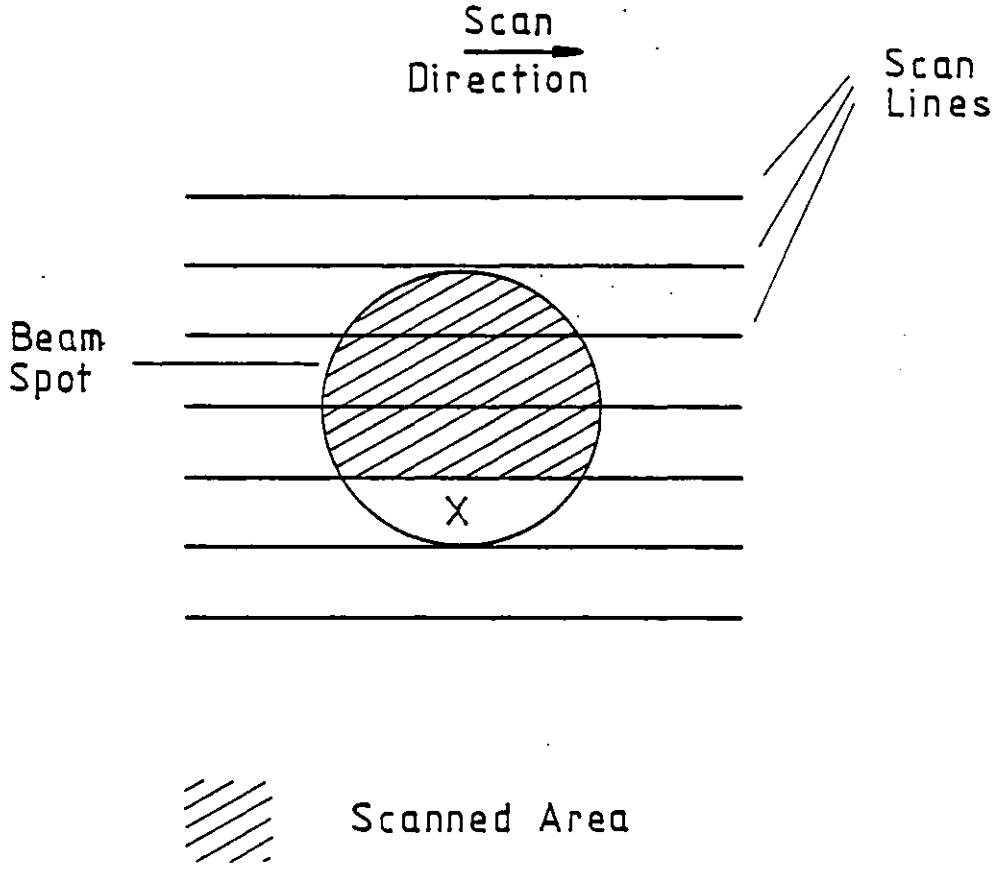

Figure 6.2 The electron beam scanning across 4 raster lines.

considering the reduction in speckle contrast as discussed in section 6.5. A second result of this will be that the video signal from any line will not be independent of other lines and thus a reduction in coordinate measurement accuracy is experienced.

6.3 Camera Resolution

With the flying spot defocussed so as to eliminate any appearance of speckle on the video signal, a 50 mm focal length TV camera lens was fixed to the camera and focussed on a square wave pattern recorded on 35 mm film. The film was positioned approximately one metre from the lens and was illuminated from the rear. The pattern was generated by computer and written directly onto the film. The film consisted of a series of gratings ranging from 0.1 lines/mm to 30 lines/mm. The transmittance of the film was measured on a microdensitometer and found to be constant for all gratings to within $\pm 2\%$. The spatial frequencies and the video signal amplitudes were measured on a 40 MHz bandwidth oscilloscope. For the two lowest line frequencies, significant contributions occur from their harmonics and so their values were adjusted by considering the attenuation values for frequencies above 8 lines/mm to be due to the fundamentals only. This produced the points shown in figure 6.3. The line fitted to these points is given by:

$$\text{Attenuation} = \exp\left[\frac{-u^2}{2\sigma^2}\right]$$

where u = frequency in lines per mm

and σ = 10.0 lines/mm

The fourier transform of this function is ignoring multipli-

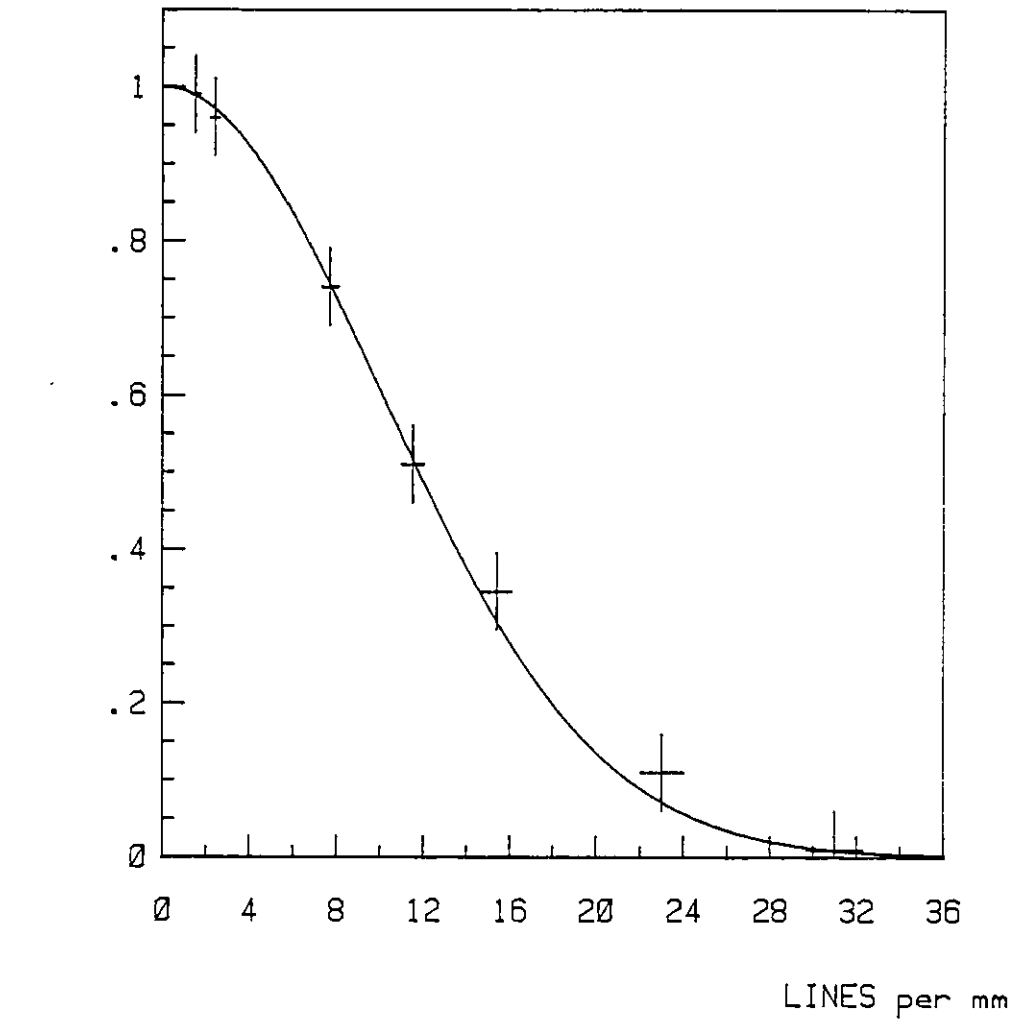

Figure 6.3 The measured transfer function of the camera and lens combination.

cative constants:

$$f(r) = \exp\left[\frac{-r^2}{2a^2}\right]$$

where a = 16 μm

Figure 6.3 includes the effect of the modulation of the image by the camera lens. The system was duplicated with a microscope instead of the camera and the gratings viewed. With an aperture of f/4 the upper limit of the modulation transfer function for a diffraction limited lens would be approximately 500 lines per mm. The image spatial frequency was varied in steps of the order of 30 lines/mm from 1 to 360 when no contrast was detectable. The contrast appeared to fall off smoothly with increasing spatial frequency and the lens was therefore assumed to have a negligible effect on the data in figure 6.3. Measurements of the transfer function were also taken with the gratings parallel to the scan lines and a similar curve to figure 6.3 noted.

6.4 Speckle Formation

In this section the imaging system will be assumed to be aberration free. Goodman [5] has calculated the dependence of the contrast of image plane speckle in telecentric lens systems on the number of independent object scatterers contributing to an image point and the variance in phase of the light scattered from the object. Ouchi [6] continued this work to include speckle in defocussed planes and shows that the contrast is a minimum in the image plane, though for a strong scatterer and a large number of scattering cells, the contrast will be unity in and out of the image plane. The above references both assumed perfectly coherent

illumination. The three beam illuminating system creates a path difference between the 45^{o} beam and the central beam of approximately 80 mm whilst the laser was found to have a coherence length of the order of 200 mm. It will thus be assumed that the illumination is perfectly coherent, but it should be remembered that the addition of two partially coherent speckle patterns will produce a speckle pattern whose contrast will be reduced. The three beams will clearly interfere in the plane of the object, and it is easily shown that the fringe separation in the $\underline{z}$ direction will be $\sqrt{2}\lambda$ and thus well beyond the resolution limit of the optical system.

An experiment was carried out on "Slick" to determine the size of the scatterers and also to show if there was any depth effect which would increase the number of scatterers and also the variance in the reflected wavefront. A glass slide was coated with a 50% "Slick", 50% thinners mixture and then a part of the uncoated slide and a part of the "Slick" had a layer of aluminium vacuum deposited on them. On testing in a Linnik interferometer, the aluminium coating was found to be approximately 25 nm thick and the "Slick" 5 μm on average. The aluminium coating was of the order of 90% reflective and thus any reflections from the coated "Slick" could be considered to be due to surface effects only. This surface was illuminated obliquely via a laser and microscope objective with an area of 1.4 x 2.8 μm and the far field diffraction pattern observed. This pattern showed a strong specular component, but also consisted of several speckles. This implies that within the illuminated area there were at least two independent scatterers.

The maximum value of the correlation length would therefore be 0.7 μm. On illuminating the non-aluminised surface, the far field pattern showed no clear specular component and appeared as a random distribution of speckles. Clearly there is a definite depth effect in the "Slick" coating. On viewing a greatly thinned "Slick" coating under a microscope, micron size particles could be distinguished which explains the depth effect.

With a cell radius of R μm the effective number of scatterers in a cylinder defined by the point spread function and the thickness of the "Slick" coating will be given by

$$N = \frac{r^2 t}{R^3}$$

where r = radius of Airy Disc,

t = thickness of slick coating, assuming no absorption

On substitution with a thickness of 5 μm and for the other variables, a value of 350 for N is obtained. Clearly the phase will have a standard deviation much greater than 2π radians and thus from Ouchi [6], it can be seen that the contrast of the speckle will be unity.

6.5 Reduction of Speckle Contrast

With the object surface normal to the direction of illumination, it has been shown in Chapters 2 and 3 that the image is a gaussian of standard deviation 35 μm. To apply gaussian statistics to the image plane speckle requires at least 8 speckles within the

image. It is well known (e.g. Dainty [7]) that the autocorrelation of the image plane speckle is the point spread function of the imaging system, implying that the average size of the speckles is the same as that of the central maximum of the point spread function. For the optical system described in Chapter 4, the radius of the Airy disc is 5 μm. Except for a small effect due to defocus, the point spread function formed on a plane inclined at an angle to the gaussian image plane will be an ellipse. For the case where the angle is 58°, the speckle size will be approximately 10 x 18 μm. This will give about 8 speckles within the gaussian envelope which for the purposes of the following arguments will be considered large enough to permit the use of gaussian statistics.

The flying spot of the camera tube approximates to having a gaussian cross-section which will be described by

$$f(r) = \exp\left[\frac{-r^2}{2a^2}\right]$$

This acts as a filter with a very fast roll-off which can be used to reduce the speckle contrast without severely broadening the gaussian envelope. The effective area of the filter will be considered to be given by $4a^2\pi$. The contrast, C, of the speckle pattern when averaged over N speckles will be given by

$$C = \frac{1}{2\sqrt{N}} \qquad \text{for } N>8$$

With a speckle area of $45\pi\,\mu m^2$ the contrast will be given by

$$C = \frac{1.6}{a}$$

As in this system high resolution is not required from the cameras, the flying spot can be considerably defocussed without significant loss of ability to measure coordinates. Describing the image envelope by

$$g(r,z) = \frac{1}{\sigma} \exp\left[\frac{-r^2}{2\sigma^2}\right] P(z)$$

(i.e an image line parallel to the z axis) and considering the flying spot as a linear filter, the resultant signal is given by the two-dimensional convolution

$$F(r,z) = \frac{1}{\sigma} \iint_{-\infty}^{\infty} e^{-\frac{(\tau_1^2+z_1^2)}{2a^2}} \; e^{-\frac{(\tau-\tau_1)^2}{2\sigma^2}} P(z-z_1)\, d\tau_1\, dz_1$$

which on integrating gives

$$F(r,0) \propto \frac{\exp\left[\frac{-r^2}{2c^2}\right]}{c}$$

where $c^2 = a^2 + \sigma^2$

Figure 6.4 shows the variation of c and the contrast, C, with changing filter width a, with a value of σ of 35 μm. It would appear that a value for a of 30 μm would be a suitable compromise, but it was found experimentally that a value around 16 μm was sufficient to reduce the speckle contrast in each camera separately such that the electronic signal appeared to be a smooth gaussian. At a period of 20 μm in a 10 mm T.V. field, i.e. 50 lines/mm, the video electronics should not modulate the signal significantly and so the reason for this drop in contrast must be elsewhere. A piece of polaroid was introduced into the randomly polarised laser beam and extinction of the beams in the object space was possible with

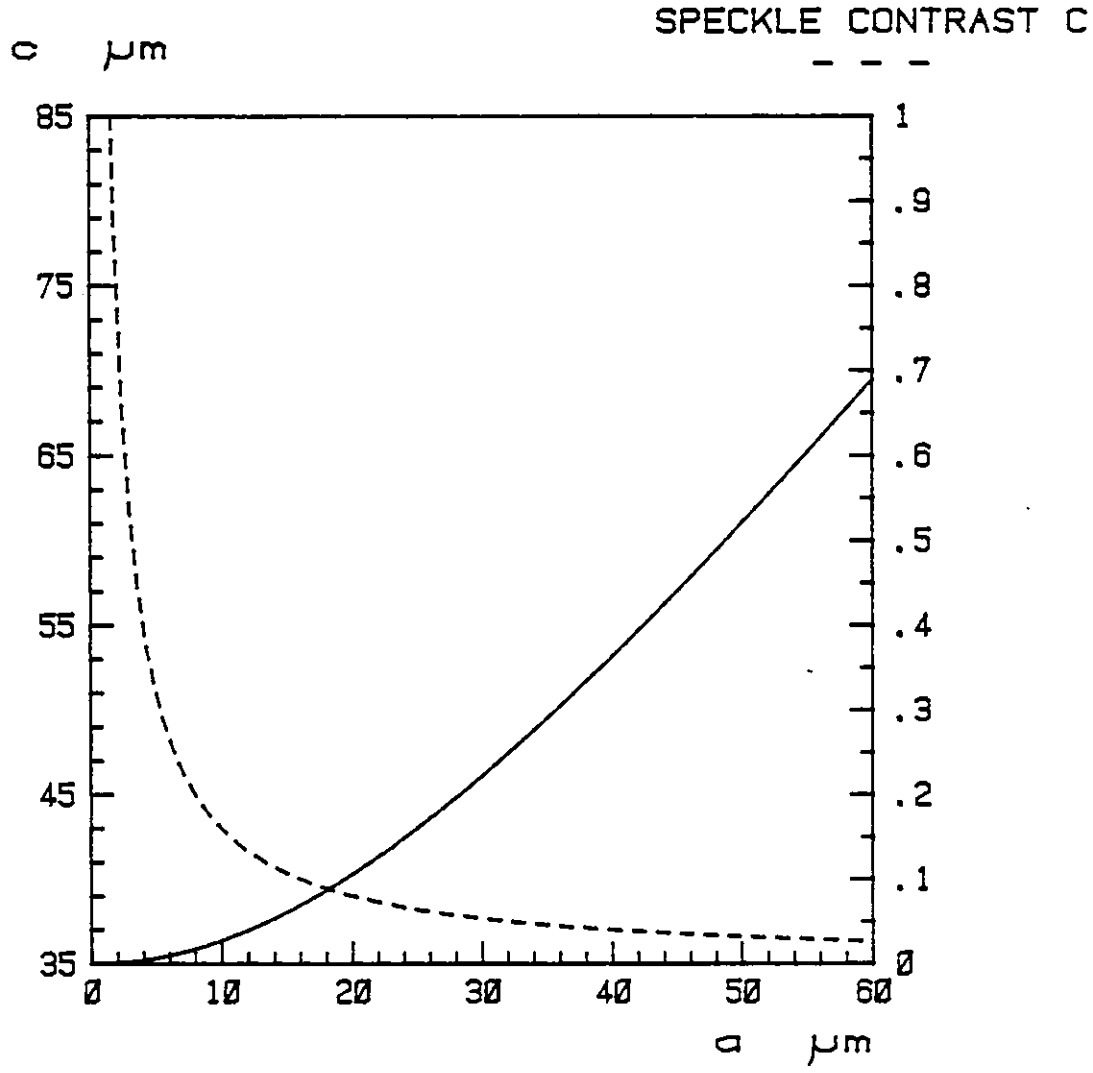

Figure 6.4 The variation of the image width ,c, and speckle contrast ,C, with changing filter width a.

another polarizer. On placing the second polarizer in the plane of the aperture of the imaging system, no distinguishable variation of video signal occurred for a rotation of the polaroid. Thus the "Slick" coating depolarized the laser illumination by random multiple reflections and the image plane will therefore consist of two mutually incoherent speckle patterns with orthogonal axes of polarisation. Each will have unit contrast with the addition of the two having a contrast of $1/\sqrt{2}$.

In section 6.2 it was stated that the electron beam scans over a point on the tube on four successive lines. This may cause some local charge dispersion and thus further reduce the speckle contrast.

6.6 Effects of Object Orientation on the Image

In Chapter 2 the image size was calculated for the case when the plane of the object was normal to the direction of illumination. For objects such as rough diamonds, the surface will more probably be illuminated obliquely and the ability of the system to measure coordinates of such surface points is clearly an important consideration when trying to estimate the accuracy of these measurements.

Figure 6.5 shows a segment of the surface rotated about the z axis by an angle α from the position of normal illumination and viewed at an angle θ by the camera.

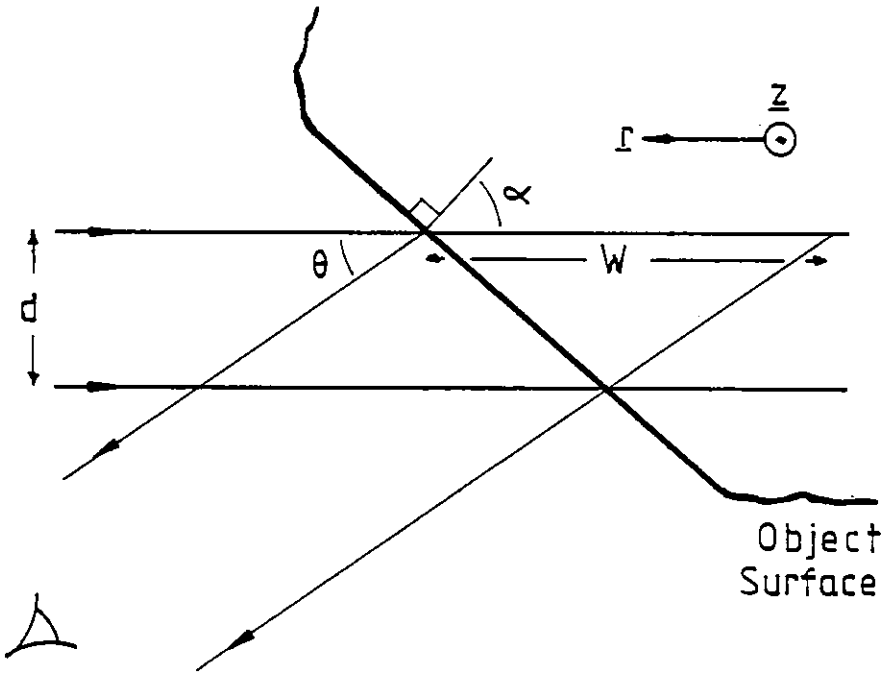

Figure 6.5 The object surface rotated by an angle α from the direction of normal illumination and viewed at an angle θ.

The width of the illuminated surface in the object plane, W, is given by:

$$W = d\ (\tan\alpha + \cot\theta) \tag{6.2}$$

where d is the $\frac{1}{e^2}$ width of the illuminating line.

Let the convolution of the point spread function with a gaussian of variance $\left[\frac{W}{4}\right]^2$ produce a gaussian of variance σ_1^2

$$\text{where}\quad \sigma_1^2 = \left[\frac{W}{4}\right]^2 + \left[\frac{R}{2}\right]^2 \tag{6.3}$$

where R is the radius of the Airy disc. This image is then convolved with the electron beam gaussian of variance a^2 giving a video signal of the form,

$$f(r) = \frac{S}{c} \exp\left[\frac{-r^2}{2c^2}\right] \tag{6.4}$$

where S is a reflection coefficient describing the intensity of light reflected from the surface in the direction θ and c is given by

$$c^2 = a^2 + \sigma_1^2 \tag{6.5}$$

Substituting the values:

$\theta = 32^\circ$

$d = 90\ \mu m$

$R = 9\ \mu m$

$a = 16\ \mu m$

and equation (6.2) into (6.5) the variance c^2 of the gaussian is described by

$$c^2 = 2.76 + 506(\tan\alpha + \tan 58)^2 \qquad (6.6)$$

Experimentally, a piece of plate glass was coated with "Slick" and positioned on the rotary table perpendicular to the central beam. It was then rotated using the stepper motor by a well defined angle and the width of the video signal measured on a 40 MHz bandwidth oscilloscope. These measurements are shown in figure 6.6 together with the line described by equation (6.6). The experimental results show fairly good agreement with the predicted values and it would appear valid to use this equation to describe the effects of rotation of the object surface on the image width. At high positive angles the theory predicts slightly larger widths than were measured and this may be due to the difficulty in establishing a zero level for the video signal, due to the low signal levels involved.

In Chapter 7 the method of extracting the coordinates of a surface point from the video signal will be described, but for the purposes of this section, it is sufficient to say that the centre of the Gaussian is measured by differentiating the video signal and finding the point when the differentiated signal is zero. The uncertainty in defining this point will depend on the rate of change of the differentiated signal and thus on the second derivative of the gaussian input. Describing the input signal as

$$f(t) = \frac{S}{c} \exp\left[\frac{-t^2}{2c^2}\right] \qquad (6.7)$$

were S and c depend on the object orientation angle α , we can

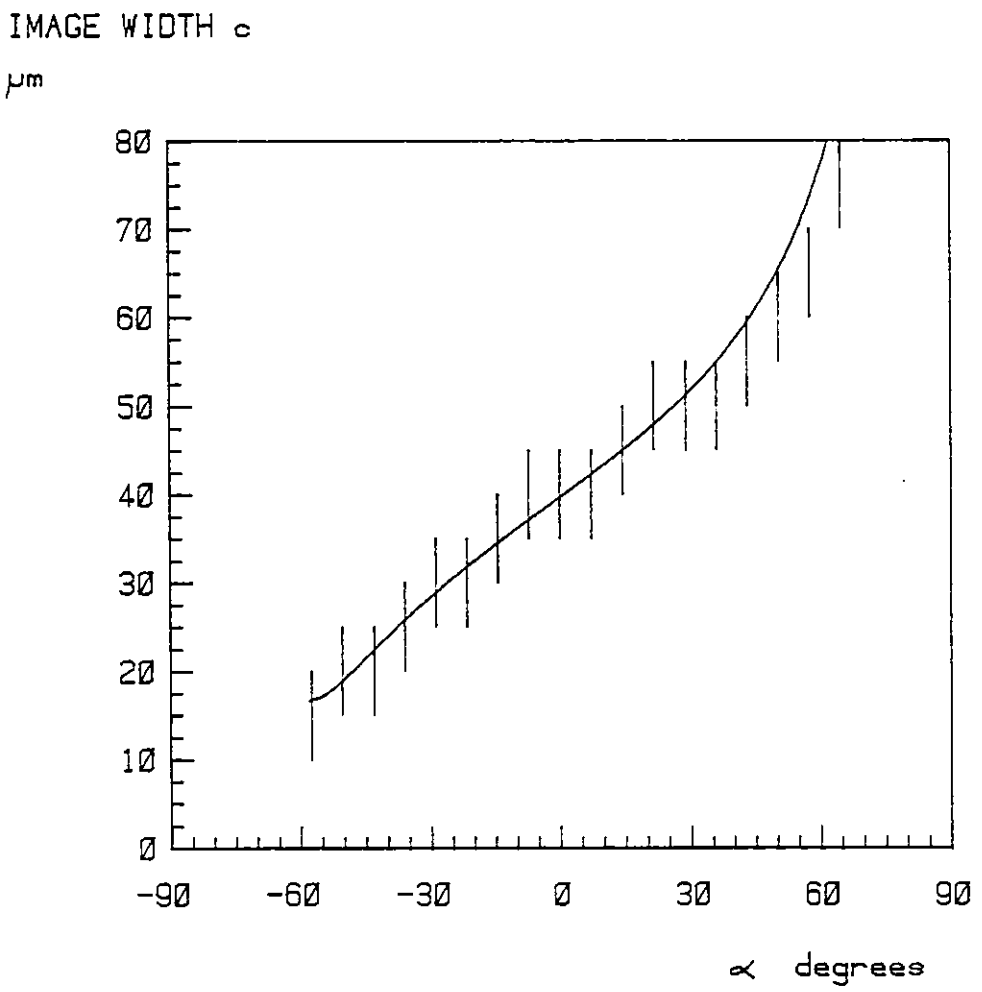

Figure 6.6 The theoretical curve and measured data for the variation of image width with object orientation angle ∝.

easily obtain the equation

$$f''(0) = \frac{-S}{c^3} \tag{6.8}$$

For the addition of two cameras with the surface orientated at angles of α and $-\alpha$ we have

$$f''(0) = -\left[\frac{S(\alpha)}{c^3(\alpha)} + \frac{S(-\alpha)}{c^3(-\alpha)}\right] \tag{6.9}$$

If $S(\alpha)$ is normalised so that $S(0) = 1$, and similarly for $c(\alpha)$ such that $c(\alpha) = \frac{c(\alpha)}{40}$ where c is defined as in figure 6.6, then we can redefine a normalised equation (6.9)

$$f''(0) = 0.5\left[\frac{S(\alpha)}{c^3(\alpha)} + \frac{S(-\alpha)}{c^3(-\alpha)}\right] \tag{6.10}$$

Experimentally the signal amplitude corresponding to $\frac{S(\alpha)}{c(\alpha)}$ was measured using the oscilloscope and is shown in figure (6.7). For a substance like "Slick", it was thought that it may behave as a Lambertian reflector, such that all light incident was scattered and reemitted uniformly over a solid angle of 2π steradians. This would give a simple form of $S(\alpha)$ of

$$S(\alpha) = \frac{\cos(\alpha-32)}{\cos 32} \tag{6.11}$$

The theoretical value of $\frac{S(\alpha)}{c(\alpha)}$ given by equations (6.11) and the normalised form of (6.6) is also shown in figure 6.7. The experimental results are for the central beam only, but it was found that the 45° beams gave similar values .

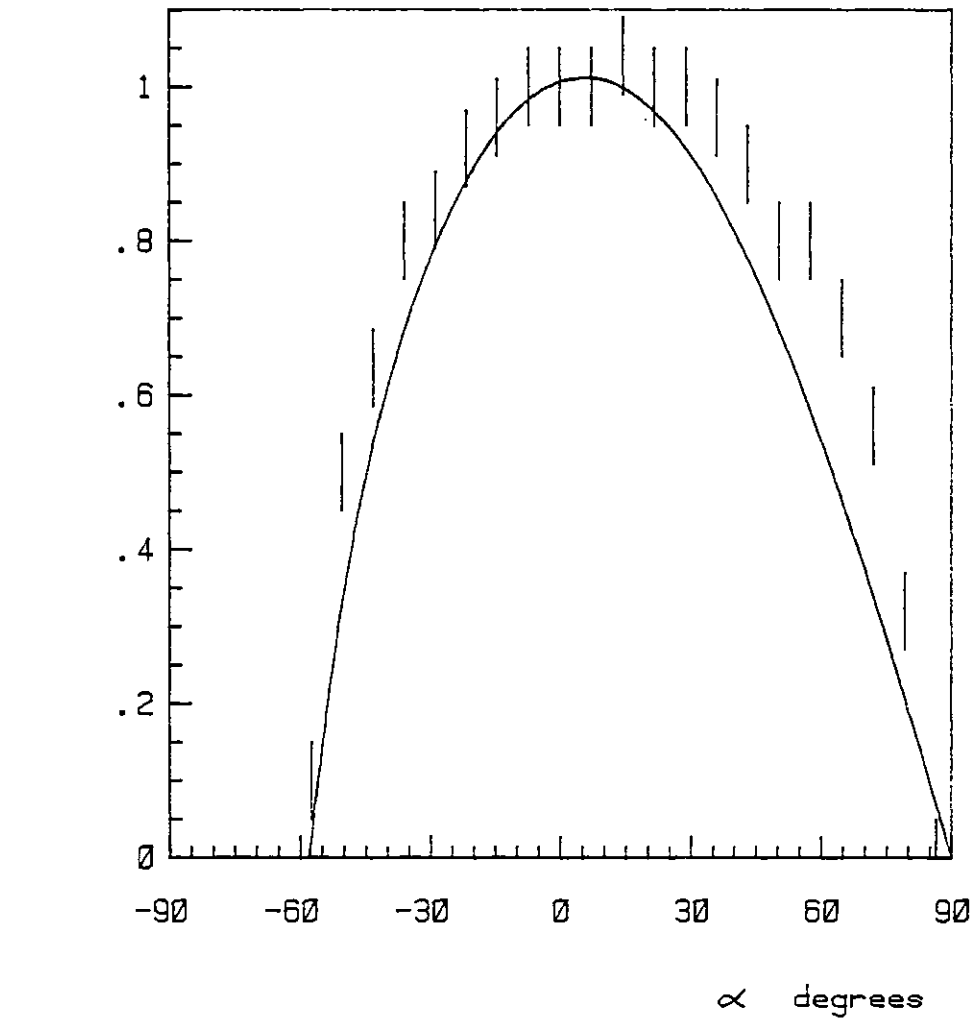

Figure 6.7 The variation of the signal amplitude with object orientation angle α . The graph shows both experimental and theoretical results based on a Lambertian reflector.

The experimental results show a much broader curve which indicates that at angles greater than 30° light has a tendency to be retroreflected. This could be due to particles in the coating shadowing neighbouring particles in such a way so as to increase the probability of an incident ray being retroreflected. Such a case is shown in figure 6.8. This effect has been described and measured in many works on illumination and photometry, e.g. Keitz [8] . Clearly from figure 6.6, the absolute maximum permissible angle of rotation of the object plane will be 58° when the surface becomes hidden from one camera and the image in the other camera is a very broad gaussian. Using the experimental results from figures 6.6 and 6.7, the ability of the electronics to define the centre of the gaussian images as given in equation (6.10) is shown in figure 6.9. The errors in the curve calculated from experimental data are of the order of ± 0.3 for the ordinate. Also shown are experimental results from oscilloscope measurements of the gradient of the video signal after the differentiator. All the experimental points lie within the error limits of the curve. As will be shown in Chapter 7, a value of 0.1 for the normalised second derivative of the gaussian signal permits a high degree of certainty in the electronic processing of the signal. Thus the governing factor in the determination of the maximum angle with which there is a reasonable certainty in the data is the angle at which the object becomes invisible to one of the cameras. Therefore, for the system described in this thesis, it can be said that for object surface rotations of up to 55° about the $\underline{z}$ axis

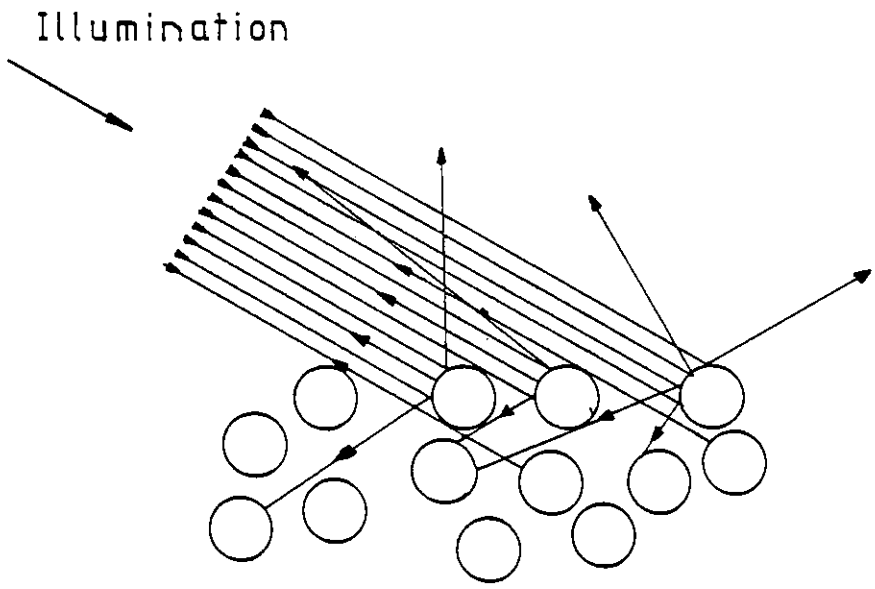

Figure 6.8 An example of retroreflection from a surface consisting of particles suspended in a lightly adsorbing liquid.

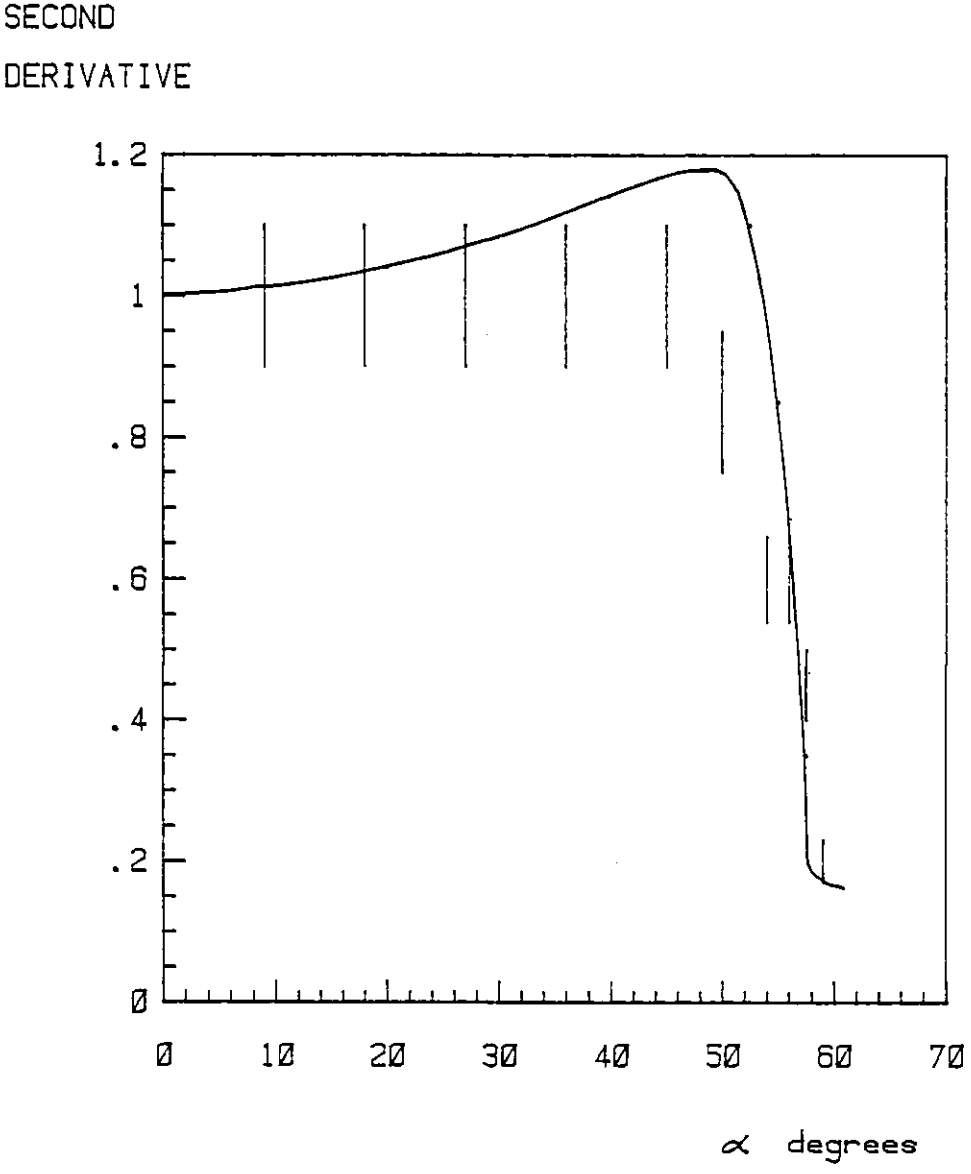

Figure 6.9 The variation of the second derivative of the image signal with orientation angle α .

from the direction of normal illumination, the properties of the image are such that there is no appreciable loss in ability to measure the gaussian centre.

Also to be considered are object surfaces perpendicular to the $\underline{r}$, $\underline{z}$ plane but rotated in this plane. Assuming a point on a surface rotated an angle β from the position where it is illuminated normally by the central beam, the illumination on the surface will be given by

$$I = \frac{1}{1+\sqrt{2}} (\cos\beta + \cos(45-\beta) + \cos(45+\beta)) \qquad \beta < 45^{\circ} \qquad (6.12a)$$

$$= \cos\beta$$

$$I = \frac{1}{1+\sqrt{2}} (\cos\beta + \cos(45-\beta)) \qquad \beta > 45^{\circ} \qquad (6.12b)$$

assuming the 3 beams are of equal intensity. Equation (6.12b) shows a small increase in illuminance above that of a single beam.

In Chapter 7 it will be shown that for the system to work within the limits imposed by the data storage methods used, only one coordinate point per T.V. line can be obtained. As the direction of the line scan is along the direction of illumination of the central beam, then any surface point that provides data will have been illuminated by the central beam. This, therefore, brings into question the necessity for the three beam system. As will be shown in this section, the three beam system does increase the light reflected from a surface in the viewing direction for angles of β greater than 45° and a decision on the use of one or all

three beams will depend on the properties of a particular object. It was shown in Chapter 2 that after an object has been rotated 360° and the data stored, to obtain data on the poles the object must be rotated by 90° about some axis orthogonal to the $\underline{z}$ axis. This rotation will cause a change in orientation of a point to the direction of illumination. If before the 90° rotation a point was not detected due to its orientation to the direction of illumination, there is a possibility that after the rotation the new orientation will still be such that no data can be acquired for that point. It is therefore desirable that the range of measurable β is as great as possible, and it might be necessary to use all three beams for highly pitted objects so as to reduce the number of surface points not included in the data. Considering an illuminated surface whose normal lies in the $\underline{z},\underline{r}$ plane and at an angle β to the $\underline{r}$ axis, the projection of this line onto the geometrical object plane gives a line whose variance $(\sigma')^2$ is given by

$$\sigma' = \frac{\sigma_o \cos\theta}{(1 + \sin^2\theta \tan^2\beta)^{0.5}} \qquad (6.13)$$

where σ_o^2 is the variance of the illuminating beam, and θ is the angle between the $\underline{r}$ axis and the viewing optical axis. For values of σ_o and θ of 22.5 μm and 32° respectively, the effect of the Airy disc of radius 2.5 μm will be negligible for angles of β of less than 80°. The imaged line will therefore be considered as a line described by

$$I(r,z) = \exp\left[\frac{-(r + z\tan\beta)^2}{2\sigma^2}\right] \qquad (6.14)$$

where $\sigma = \sigma_o \tan 58$

The video signal will be given by the two dimensional convolution of equation (6.14) with the electron beam of the vidicon tube. The electron beam will be described by

$$f(r,z) = \exp\left[\frac{-(r^2+z^2)}{2a^2}\right] \qquad (6.15)$$

The output will therefore be

$$G(r,0) = \iint_{-\infty}^{\infty} e^{-\frac{(\tau'+z'\tan\beta)^2}{2\sigma^2}} \; e^{-\frac{(\tau-r')^2}{2a^2}} \; e^{-\frac{z'^2}{2a^2}} \; dz'dr' \qquad (6.16)$$

The straightforward solution of this integral produces a gaussian of variance $(\sigma')^2$ given by

$$\sigma' = \left[\frac{a^2}{\cos^2\beta} + \sigma^2\right]^{0.5}$$

The normalised form will be

$$\sigma' = \left[1 + \frac{a^2\tan^2\beta}{a^2+\sigma^2}\right]^{0.5}$$

substituting the values

$a = 16\ \mu m$

$\sigma = 22.5 \tan 58$

we obtain

$$\sigma' = (1 + (0.4 \tan\beta)^2)^{0.5} \qquad (6.17)$$

This curve is plotted in figure 6.10 with experimental results obtained from a glass slide coated in "Slick". The experimental results show greater broadening in the range measured

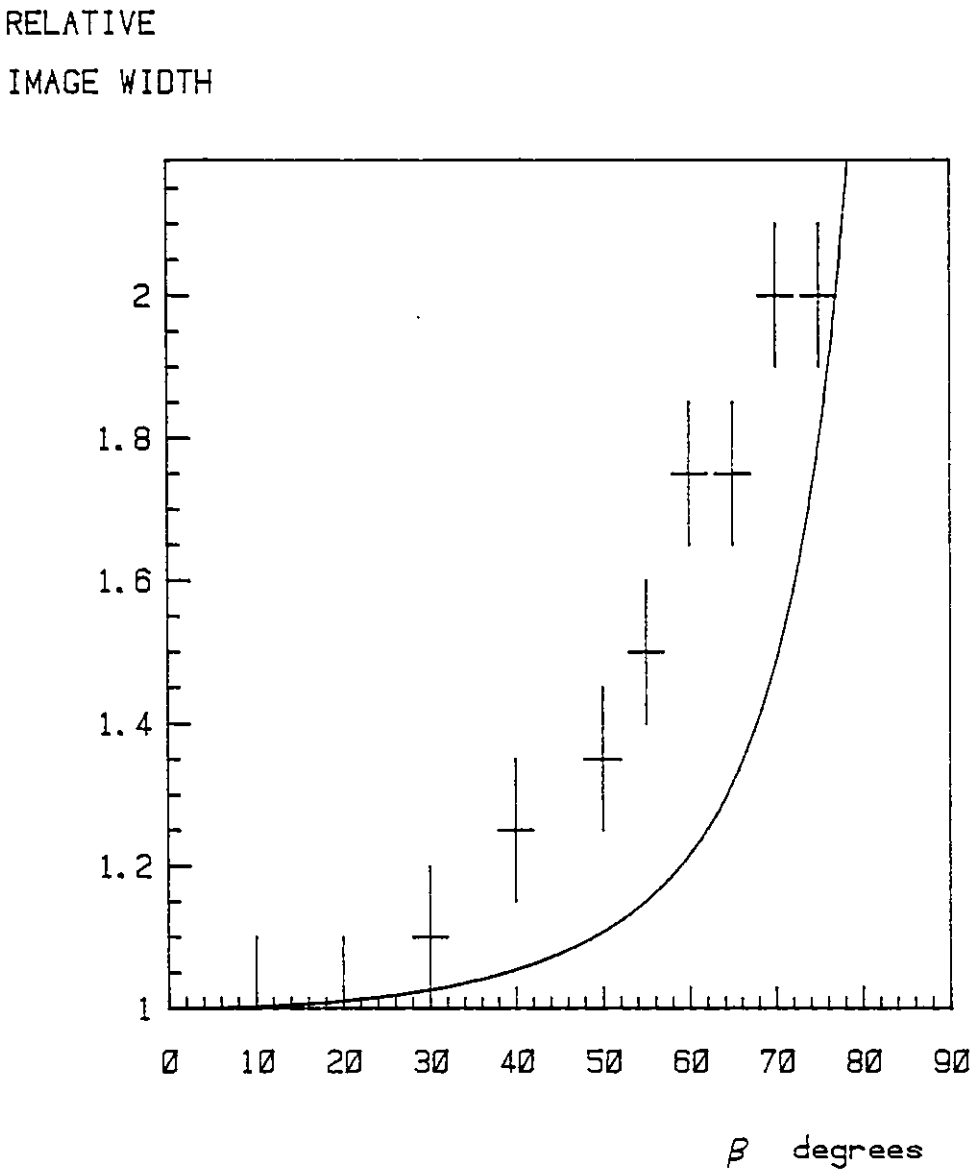

Figure 6.10 Experimental and theoretical results for the variation of video signal width with orientation angle β.

than can be explained by experimental error. The values of the width agree for single and 3 beam illumination and so the discrepancy must be assumed to be due to a broadening effect on the vidicon faceplate. With a defocussed electron beam and an image line not orthogonal to the direction of scan the multiple scanning of a line may cause the extra broadening. When both cameras have the same image the ability of the electronics to determine the centre of the gaussian profile will be given by equation (6.8).

$$f''(0) = \frac{S(\beta)}{c^3(\beta)} \qquad (6.18)$$

Figure 6.10 shows that to achieve a value of f"(0) greater than 0.1 for angles of β less than 70°, the function $S(\beta)$ must be reasonably flat in this region. The amplitude of the video signal which corresponds to the function $\frac{S(\beta)}{c(\beta)}$ was measured and with the experimental values of $c(\beta)$ from figure 6.10, $S(\beta)$ was calculated and is shown in figure 6.11 for both one and three beam illumination. Also shown for comparison, is the curve expected from a Lambertian reflector which is $\cos^2\beta$ for the single beam illumination. Clearly there is a high degree of retroreflection occurring and it can be seen that f"(0) = 0.1 for $\beta = 60^\circ$ and 67° for single and three beams respectively. It is whether this gain in measurable angles compensates for the complexity of the three beam system that the user will have to decide.

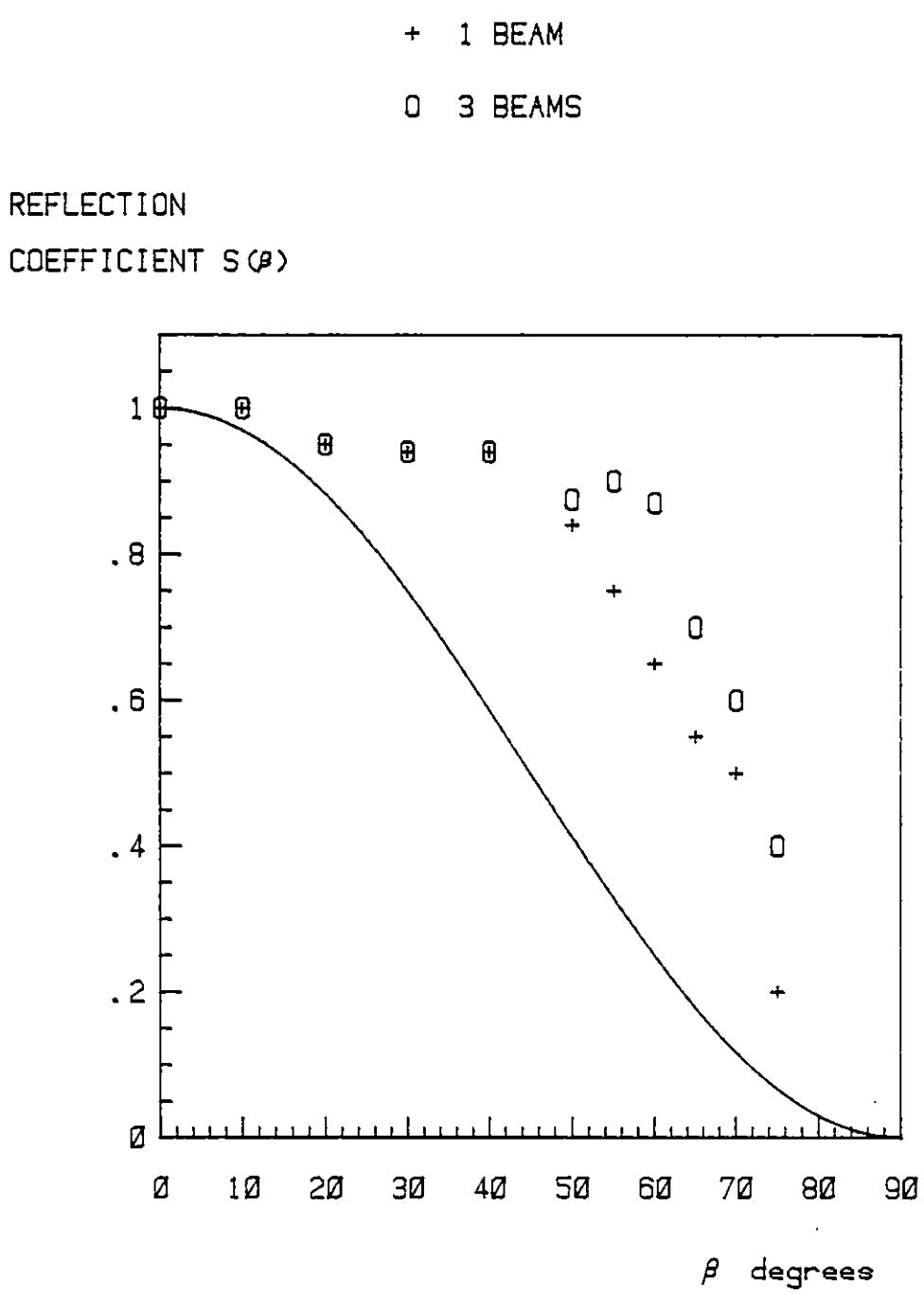

Figure 6.11 The variation of the experimental reflection coefficient ,S(β), and that for a Lambertian reflector.

6.7 Conclusions

It has been shown that to decrease the speckle contrast in the image, the flying spot has to be defocussed to such an extent that though the gaussian profile is not broadened considerably for object points whose normal is orthogonal to the z axis, the line width is affected for rotations of the normal in the z, r plane. This is due to the flying spot width being greater than the line separation. The limit of reliable measurement of the centroid of the profile for rotations about the z axis is governed by the angle between the r axis and the viewing optical axis, whilst the limit for rotations of the normal in the z, r plane is affected by the flying spot size. For most points on a surface with large incident angles, the rotation of the object by 90° in a plane through the poles will reduce the incident angle of illumination. The number of immeasurable points on an object will depend on its "roughness" and this will decide whether the three beam illumination is necessary. It has also been shown that the reflection properties of "Slick" are ideal for the system in having retroreflective components at high angles of incidence. Clearly a reduction in the flying spot size is desirable and for a fixed contrast reduction, the ratio of spot diameter to optical system f/number is fixed. For the resolution of the system to be decreased to 16 μm in the z direction, such that the video signal from a line is independent of the image on other lines, the spot diameter would have to be decreased to 16 μm, implying an imaging system aperture of f/1.6 requiring lenses of 120 mm diameter if the focal length of 180 mm is to be kept.

CHAPTER 7

CHAPTER 7 - SIGNAL PROCESSING AND DATA STORAGE

7.1 Introduction

In this Chapter the system from the cameras to the final storage on disc is described. The complete circuit diagrams are confined to Appendix B and the operating programmes to Appendix A, whilst in this Chapter block diagrams explaining the processes are used. In section 7.4, the methods of aligning the two camera scans, electronically and mechanically, are given. For the purposes of studying the response of the electronics to the incoming video signal, this signal is assumed to be gaussian in form with the highest frequencies involved taken from the gaussian of least variance as measured in Chapter 6.

7.2 Electronic Processing

The two cameras have opposite scan directions enabling the addition of the two video signals assuming correct alignment of their scanned areas. The cameras scan 625 line non-interlaced frames at a rate of 25 frames/second. This rate causes "flicker" when the image is viewed on a monitor as it is just within the ability of the eye and brain to distinguish separate pictures. As a monitor is only an aid in viewing the object and plays no part in the data storing process the decrease in bandwidth of the electronics, from that of a 50 frame/second rate, was felt to be a valuable gain. The advantage of non- interlaced frames is that it enables sequential T.V. lines to have their data extracted and stored. The basic method of storing coordinates thus only needs

one number to be acquired as the z coordinate is given by the integer number of the line multiplied by some conversion factor and the angle of rotation by the integer number of the frame multiplied by the stepping angle of the object between frames. The method of measuring the centre of the gaussian profile is to count pulses from a master clock from the beginning of a T.V. line to the point where the differentiated signal goes to zero. This count will then be stored as a binary word. The clock rate will decide the minimum r resolution of the system and the line separation the z resolution. For a 625 line system and a 10 mm field, each line corresponds to a distance of approximately 16 μm. When designing such a system, the amount of storage space on the floppy disc or other storage medium specifies the resolution that can be measured by the system. A floppy disc storage area is normally divided into blocks, where each block is capable of storing a number of 8 bit bytes. In the case of the disc used in this system, there are 960 blocks available, each capable of storing 512 bytes. For a resolution in r of better than 40 μm in a 10 mm field, each stored count will be a 2 byte word and therefore if each block is to represent a frame of data, only 256 T.V. lines can have their data extracted. As shown in Appendix A, the program DRVEG1 which operates the system for normal data storage requests the input step number to be used. If a step angle of 0.9^{o} i.e. 2 steps/frame, or more is used, then there will be a maximum of 400 frames and 512 words can be stored/frame, using two blocks for each frame. As the original specifications for the system were for a 25 μm accuracy, data is taken from every alternate T.V. line, i.e.

approximately every 32 μm allowing storage of 256 words out of 312 possible with a 0.45^{o} stepping angle or of all 312 words with a larger stepping angle. There is therefore an ability to decrease the resolution of the system if a larger storage area is available.

Figure 7.1 shows a block diagram of the analogue electronics. The two camera video signals can be either added or monitored separately via the large bandwidth mixer, and this signal is then low pass filtered to remove any noise. This filter is a passive second order filter with a -3db response at about 5 MHz where there is a negligible component from the gaussian signal. The signal is then differentiated and passed to a zero level comparator. This comparator is only enabled when the differentiator input signal is above a reference level, thus ensuring that spurious signals are not detected. If this signal is above a clipping reference level, then an error LED is switched on informing the operator that the cameras gains are too high. The final output to the timing electronics is a 0.5 μsec pulse.

The line time is approximately 50 μsecs for the 10 mm field giving a conversion factor from μms to μsecs of 0.005. The total delay times involved after the differentiator and through the digital electronics may be of the order of a few μsecs but will be constant to within a few nanoseconds. Possible errors in coordinate measurement are therefore likely to be due to the differentiator. The frequency response of a perfect differentiator is proportional to the frequency, so any high frequency noise will

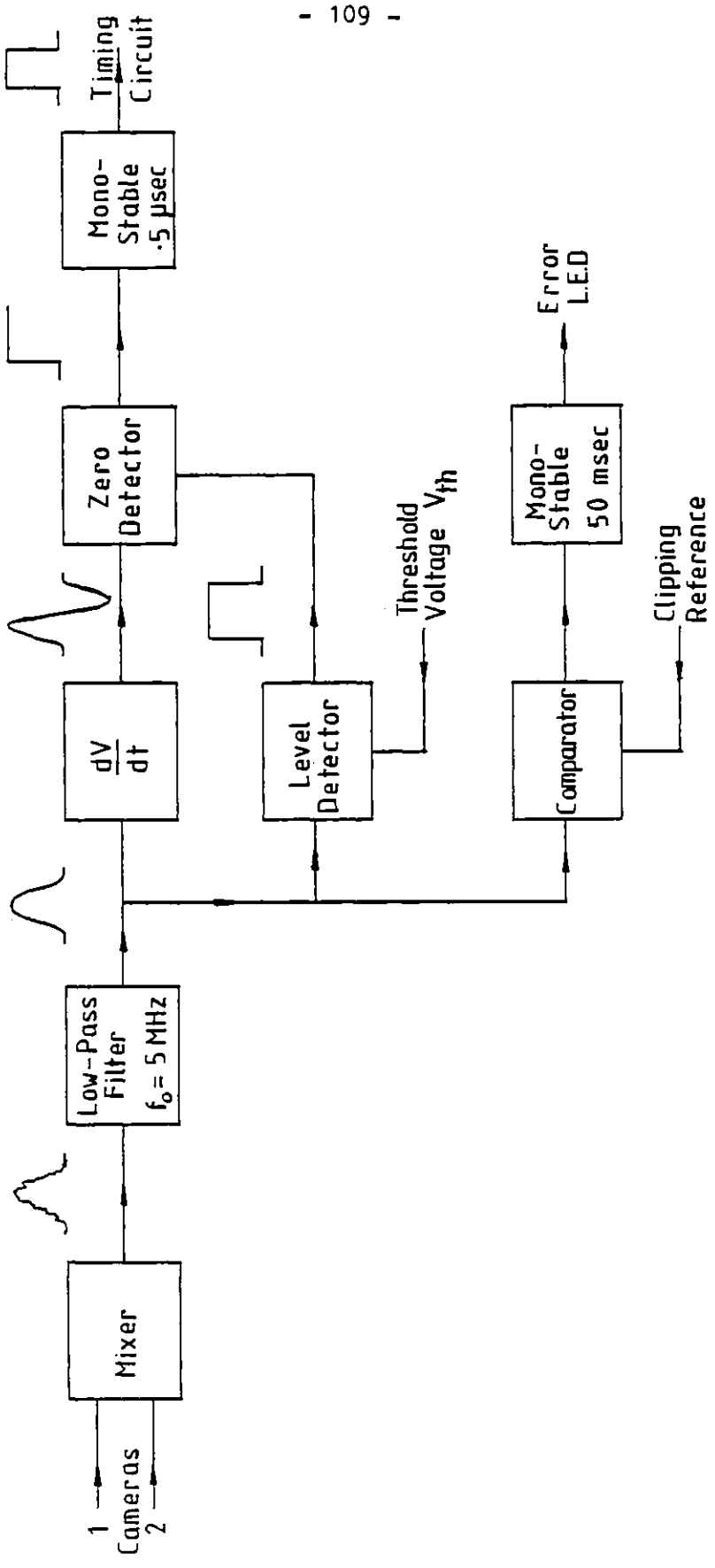

Figure 7.1 A block diagram of the analogue electronics.

produce large outputs and render the circuit unstable. To prevent this happening, the circuit is designed so that at high frequencies its response is that of an integrator. This causes phase shifts that may vary the delay in the output signal and thus be a source of error in coordinate measurement for different variance input gaussians.

The circuit used is shown in Figure 7.2. The operational amplifier is assumed to have an infinite input impedance such that all input currents through R_1C_1 flow through R_2C_2. Also assumed is an infinite gain such that both inputs must be at the same voltage for linear operation. The transfer function is therefore given by:

$$A = \frac{-(R_2/iwC_2)}{(R_1+1/iwC_1)(R_2+1/iwC_2)} \qquad (7.1)$$

on rearranging, this leads to

$$A = \frac{-iR_2wC_1}{(1+iwC_1R_1)(1+iwC_2R_2)} \qquad (7.2)$$

At low frequencies the response will approximate to

$$A = -iwR_2C_1$$

and at high frequencies to,

$$A = \frac{i}{wC_2R_1}$$

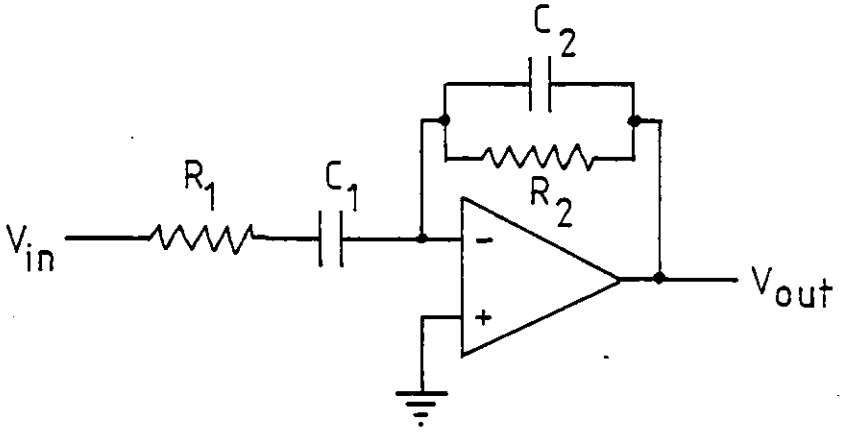

$$\text{Gain} = A = \frac{V_{out}}{V_{in}}$$

Figure 7.2 The differentiator.

To simplify equation (7.2), the relationship

$$R_1C_1 = R_2C_2$$

is used. This gives a response of

$$A = -\frac{R_2}{R_1} \frac{iwC_1R_1}{(1+iwC_1R_1)^2}$$

defining $w_oC_1R_1 = 1$ and $x=w/w_o$, we obtain

$$A = -\frac{R_2}{R_1} \frac{ix}{(1+ix)^2}$$

$$= -\frac{R_2}{R_1} \frac{ix(1-x^2) + 2x^2}{(1+x^2)^2} \qquad (7.3)$$

The phase ϕ will be given by

$$\tan\phi = \frac{1 - x^2}{2x}$$

and the modulus of the transfer function ignoring multiplicative constants by;

$$A = \frac{x}{(1+x^2)}$$

Figure 7.3 shows the functions $A(x)$ and $\phi(x)$. It is desirable to have as low a value for the cross over point w_o in the response which does not cause any error in the centroid measurement of gaussian inputs. To evaluate this, we consider the filter as the sum of its real and imaginary parts given by

$$G_R(x) = \frac{2x^2}{(1+x^2)^2} \qquad (7.4)$$

$$G_I(x) = \frac{x(1-x^2)}{(1+x^2)^2}$$

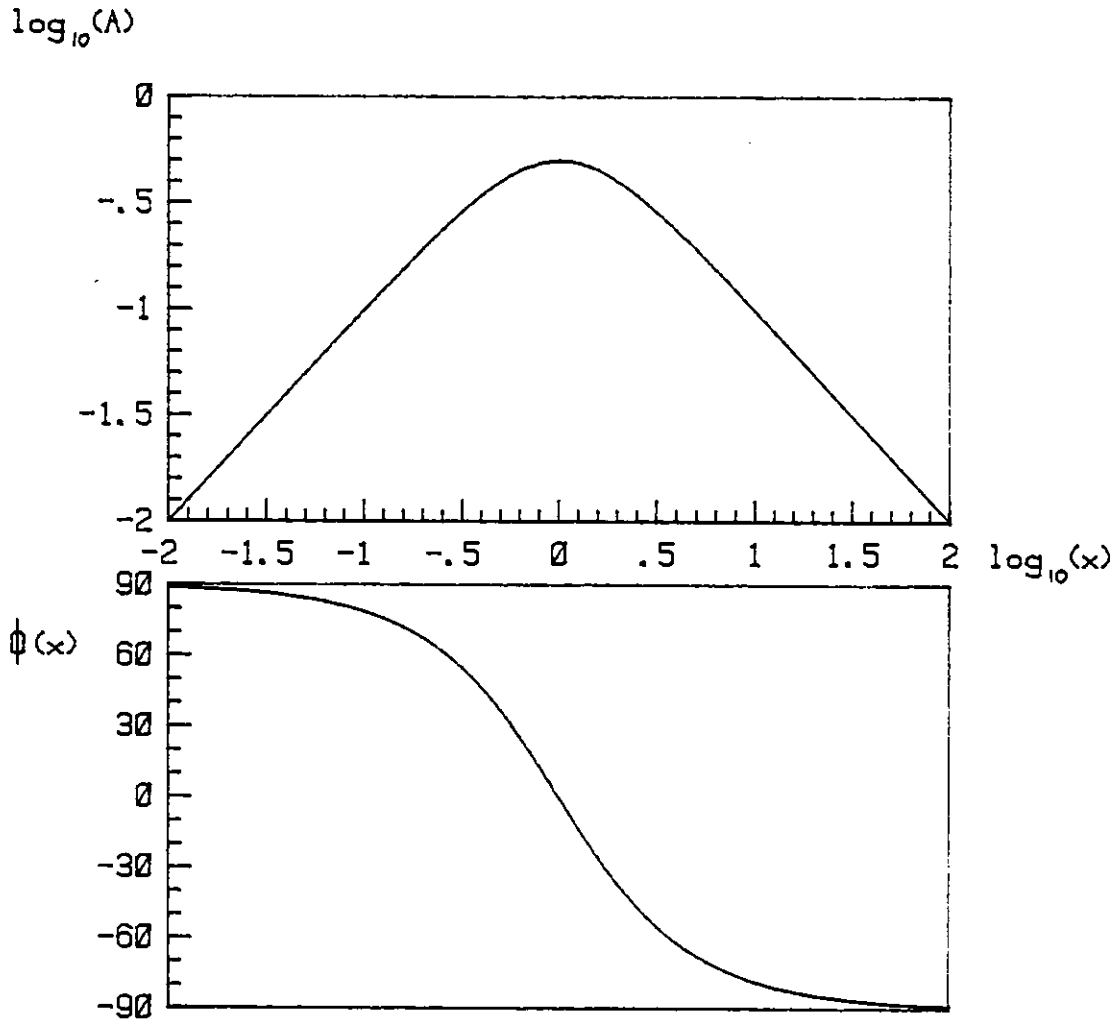

Figure 7.3 The phase and amplitude transfer functions for the differentiator.

The output from this filter with a gaussian input variance σ^{-2} will be given by

$$f(t) = \int_{-\infty}^{\infty} \left(G_R\left(\frac{w}{w_o}\right) + iG_I\left(\frac{w}{w_o}\right)\right) e^{-(iwt)} e^{-\left[\frac{w^2}{2\sigma^2}\right]} dw$$

Making the substitution $x = w/w_o$ we obtain,

$$f(w_o t) = w_o \int_{-\infty}^{\infty} (G_R(x)+iG_I(x)) e^{-(iw_o xt)} e^{-\left[\frac{(xw_o)}{2\sigma^2}\right]^2} dx \tag{7.5}$$

$G_R(x)$ is an even function and $G_I(x)$ is odd, reducing equation (7.5) to

$$f(w_o t)=w_o \int_{-\infty}^{\infty} \frac{\left[2x^2\cos(w_o xt)-x(1-x^2)\sin(w_o xt)\right]}{(1+x^2)^2} e^{-\left[\frac{(xw_o)}{2\sigma^2}\right]^2} dx \tag{7.6}$$

If $w_o >> \sigma^-$ then the integral reduces to

$$f(w_o t) = w_o \int_{-\infty}^{\infty} \left[2x^2\cos(w_o xt)-x\sin(w_o xt)\right] e^{-\left[\frac{(xw_o)}{2\sigma^2}\right]^2} dx$$

for $xw_o t<<1$ we have

$$f(w_o t) = w_o \int_{-\infty}^{\infty} \left[2x^2-x^2 w_o t\right] e^{-\left[\frac{(xw_o)}{2\sigma^2}\right]^2} dx$$

If $f(w_o t) = 0$ we obtain the time when the output signal goes to zero as,

$$t=2/w_o$$

This would be the ideal situation when the time delay is constant for all gaussian inputs but requires a higher w_o than may be necessary. Equation (7.6) was solved numerically for various values of σ/w_o and the values $(w_o t)$ when the function goes to zero recorded. Figure 7.4 shows the relationship between $w_o t$ and σ/w_o. As shown in Chapter 6, the standard deviation of the imaged gaussian is between 20 μm and 80 μm, which converted to the frequency domain gives values of σ between 2.5 and 10 megaradians/sec. A value of w_o of 20 megaradians/sec will thus give delay times between 0.1 μsecs and 0.086 μsecs, corresponding to an error in timing of $\pm$0.007 μsecs. This is an error in the r coordinate of 1.5 μm. The differentiator was found to work very well with this value of w_o and the delay time was measured to be of the order of .1 μsecs.

The other parameter to be decided upon is the gain of the differentiator R_2C_1. Typical values for the gains of high speed comparators are of the order of 2000 and thus for a normal 5 volts output swing the input switching level is 2.5 millivolts. If the differentiator output near the time when it is zero is changing at V' volts/μsec, the time for the comparator to switch is 1/400V' μsecs corresponding to 1/2V' μm.

The operational amplifier in the differentiator has a maximum slew rate of 50 volts/μsec which far exceeds the desired rate. The gain was chosen to give a 10 volts/μsec slew for an object illuminated normally by the central beam, thus ensuring that the

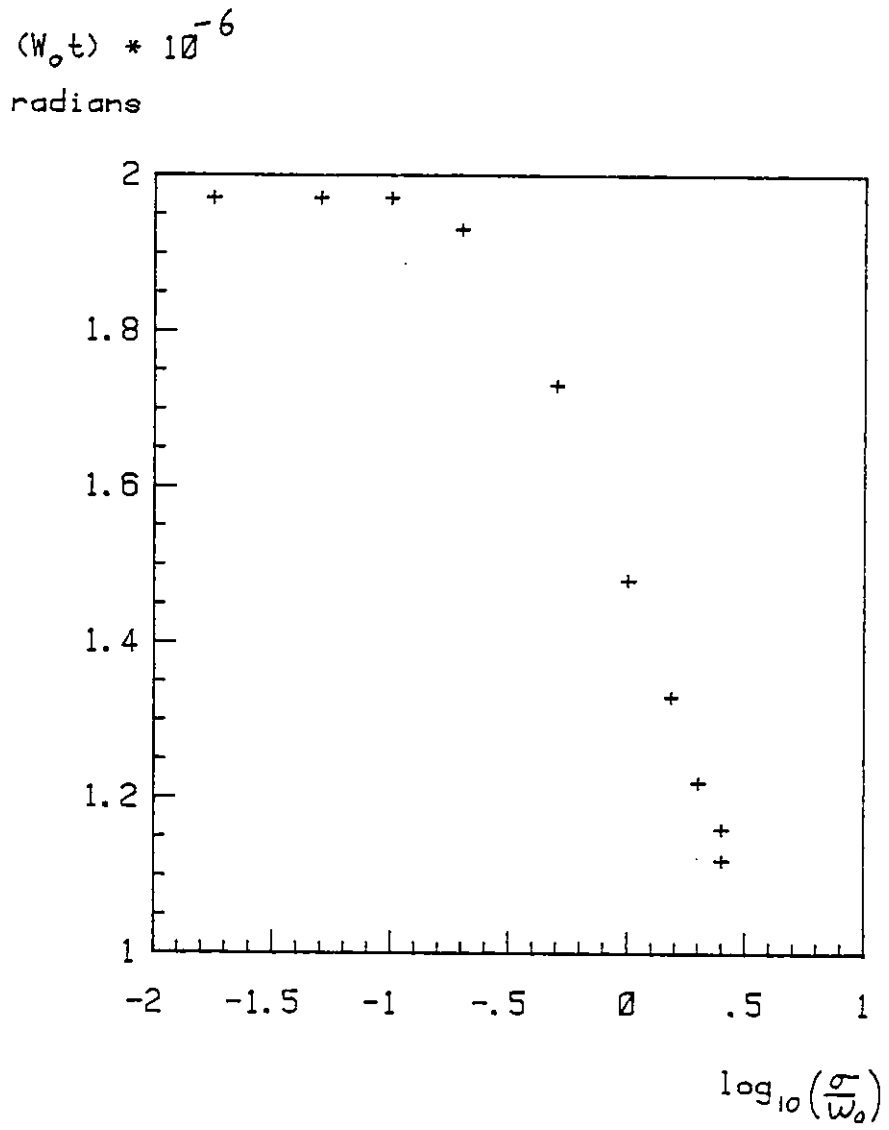

Figure 7.4 The variation of the response time of the differentiator with the standard deviation of the input gaussian.

response of the differentiator is such that any errors in timing an incoming signal amount to only a few micrometers at the worst.

In Chapter 6, consideration of the various image properties required a minimum value of dV/dt below which the data would be considered unreliable. Clearly from the above calculations if we define the variance σ_R^2 of the input gaussian with respect to the "normal" gaussian of variance 1600 μm^2 and of relative amplitude A we obtain,

$$\frac{dV}{dt} = \frac{10\ A}{\sigma_R^2} \qquad \text{Volts/}\mu\text{Sec.}$$

giving an error in the coordinate r of

$$\Delta r = \frac{\sigma_R^2}{20\ A} \quad \mu m$$

If the worst error allowed is 10 μm, the input gaussian must be defined by

$$\frac{\sigma_R^2}{A} < 200$$

The maximum value of A will be $1/\sigma_R$, implying that the system can measure gaussians with a value of σ_R=6. This would assume that the profile was so noise free that over the relatively long time during the signal, no point on the signal had a zero gradient. From observation of the video signal, the reference level for the level comparator in figure 7.1 was chosen to be approximately 0.4 of the clipping level giving a maximum value for σ_R of 2.5 and a minimum value of (A/σ_R^2) of 0.064. The value used in Chapter 6 is 0.1.

The digital electronics shown in figure 7.5, with timing diagram in figure 7.6, receive the line sync pulse, 6 MHz clock and the 0.5 μsec analogue timing pulse. The negative edge of the line sync pulse clears the counters and 0.5 μsec later a 0.5 μsec pulse is inputed to the data decision box. If in the previous line there had been no input from the analogue board, the decision box sends a 0.5 μsec pulse to Latch 1 and as the counter has been cleared, 10 zeros are latched. At the end of the 0.5 μsec pulse from the monostable the data on the outputs of Latch 1 is entered into Latch 2. The positive going edge of the line sync pulse restarts the counter and requests the computer to accept data from Latch 2. When a pulse from the analogue board is received, if it is not the first pulse on a TV line, it is ignored, otherwise it causes the counter to stop, and .15 usec later instructs Latch 1 to store the count reached. On receipt of the delayed line sync pulse, the decision box will now not send a latching pulse and the count in Latch 1 will be passed to Latch 2. All signals between the counters and Latch 1 are clocked by the master clock to ensure synchronisation such that output data is settled before being latched as input data.

7.3 Computer Control

The computer is a DIGITAL VT103 with a twin drive floppy disc system. The interface between the computer and the rest of the system is via a Direct Memory Access (DMA) Board. This board is capable of taking control of the computer busses and storing input

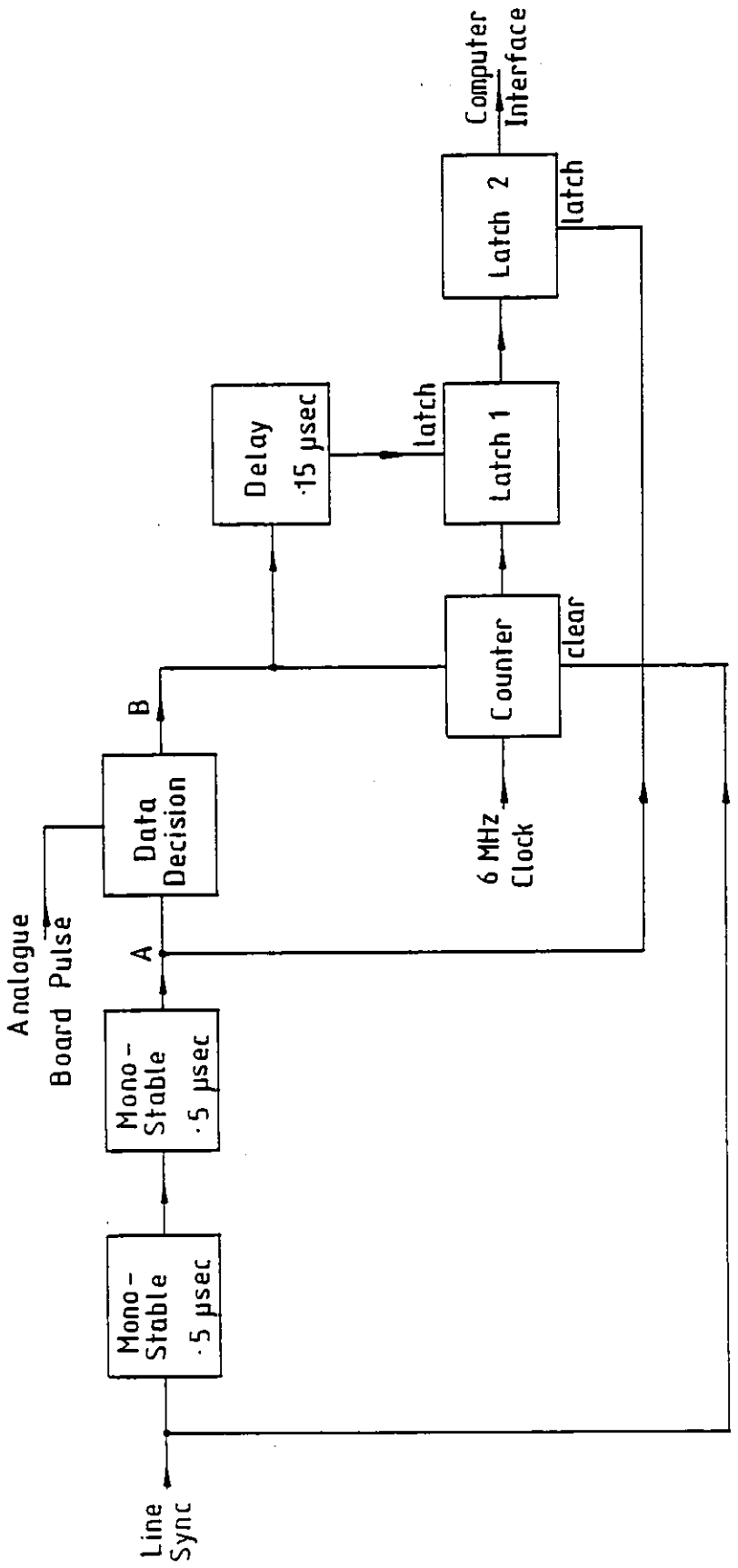

Figure 7.5 The digital electronics.

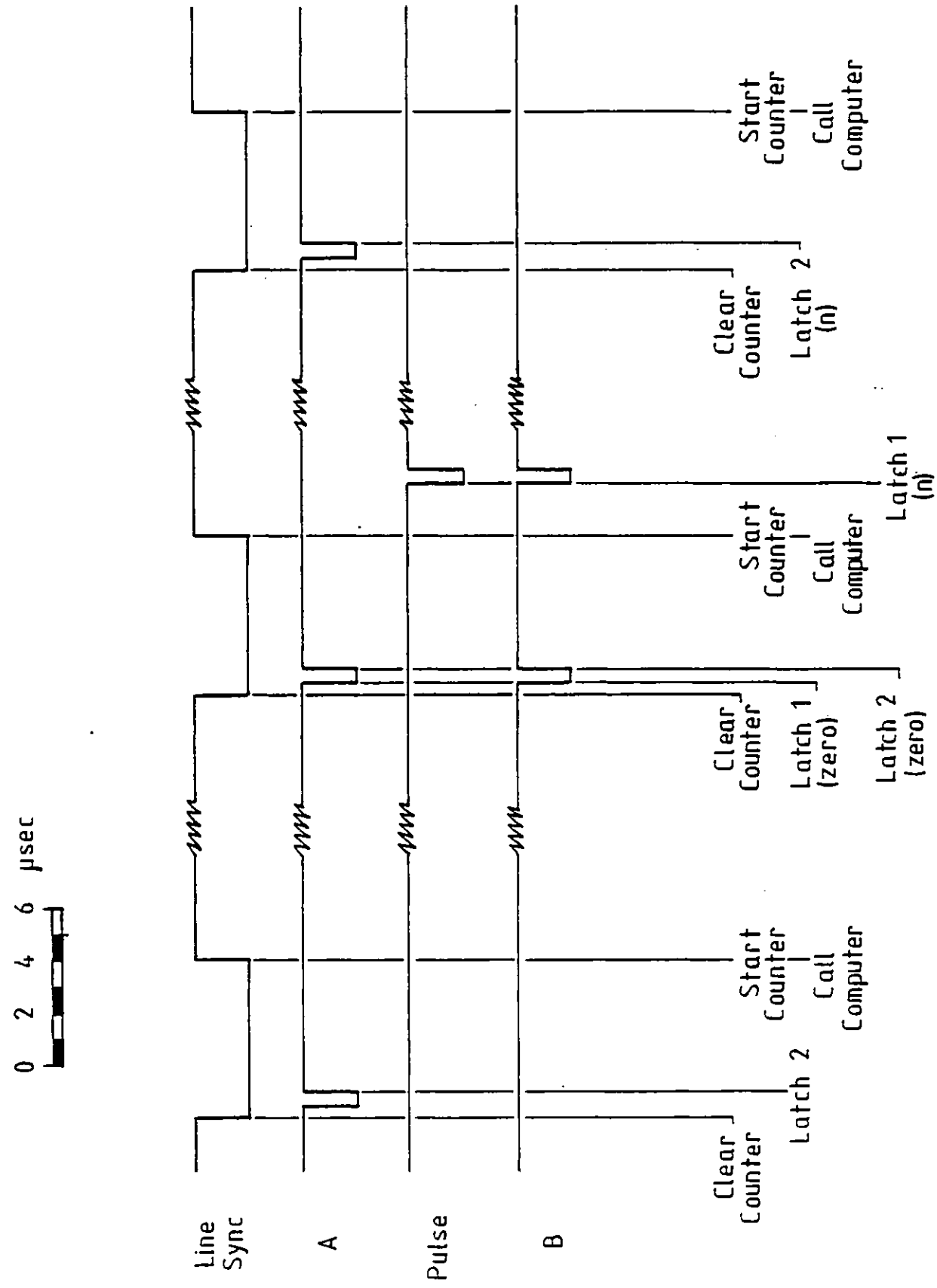

Figure 7.6 The timing diagram for the digital electronics.

data directly to a specified memory location and is necessary when a high data transfer rate is required. For the system described so far, a 2 byte word is transferred every two T.V. lines, i.e. every 128 μsecs, and for such a rate, normal input/output ports could be used. The provision of the DMA board allows the system to be changed such that the frame rate could be increased to 50 frames/sec and data from every line stored. This would require a 32 μsec cycling time and the DMA board would be necessary. The operation of the data storage program DRVEG1 is shown in figure 7.7. If the step number was not 1 and more than 256 words were to be stored, then the value "NFRAME" would be incremented by two for each frame. The starting memory address P for each new frame is assigned by the computer. The time to store one frame is the frame time plus the time taken for the transfer of one frame of data from core memory to disc which is about 140 milliseconds. This allows storage of 800 frames each with 256 words to be stored in 2 1/2 minutes. The complete FORTRAN program is given in Appendix A.

7.4 Camera Alignment Procedure

The cameras have to be individually adjusted so that the image plane is in the plane of the photoconductive surface of the tubes. This is achieved by adjustment of two translation and one rotation stages to which the cameras are fixed, whilst viewing the video signal. The tubes are then adjusted so that the raster scans in a direction orthogonal to the $\underline{z}$ axis of the object. A tri-square is placed on the table in the centre of the object field and a section

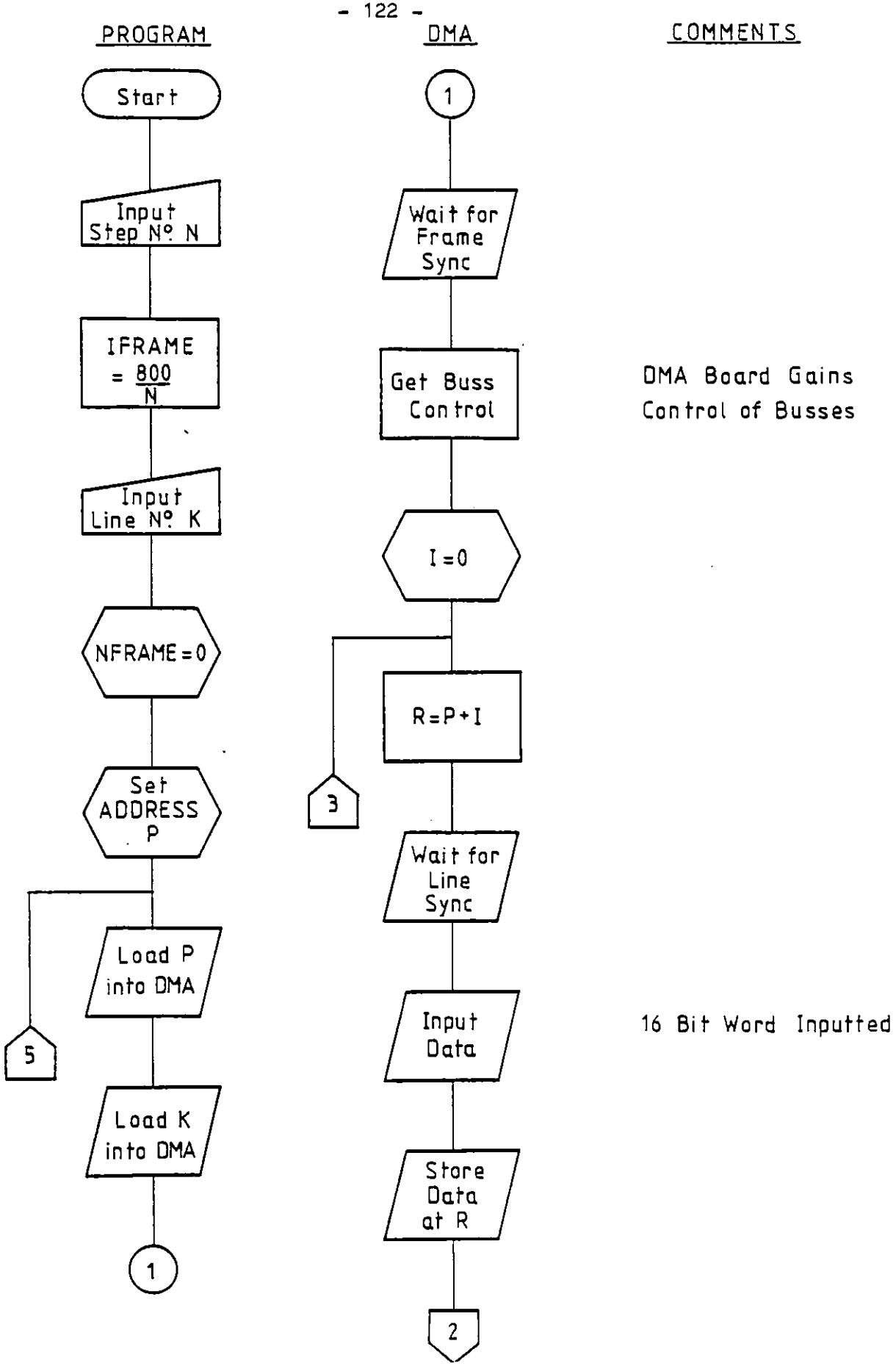

Figure 7.7 Operation of the main data aquisition program DRVEG1.

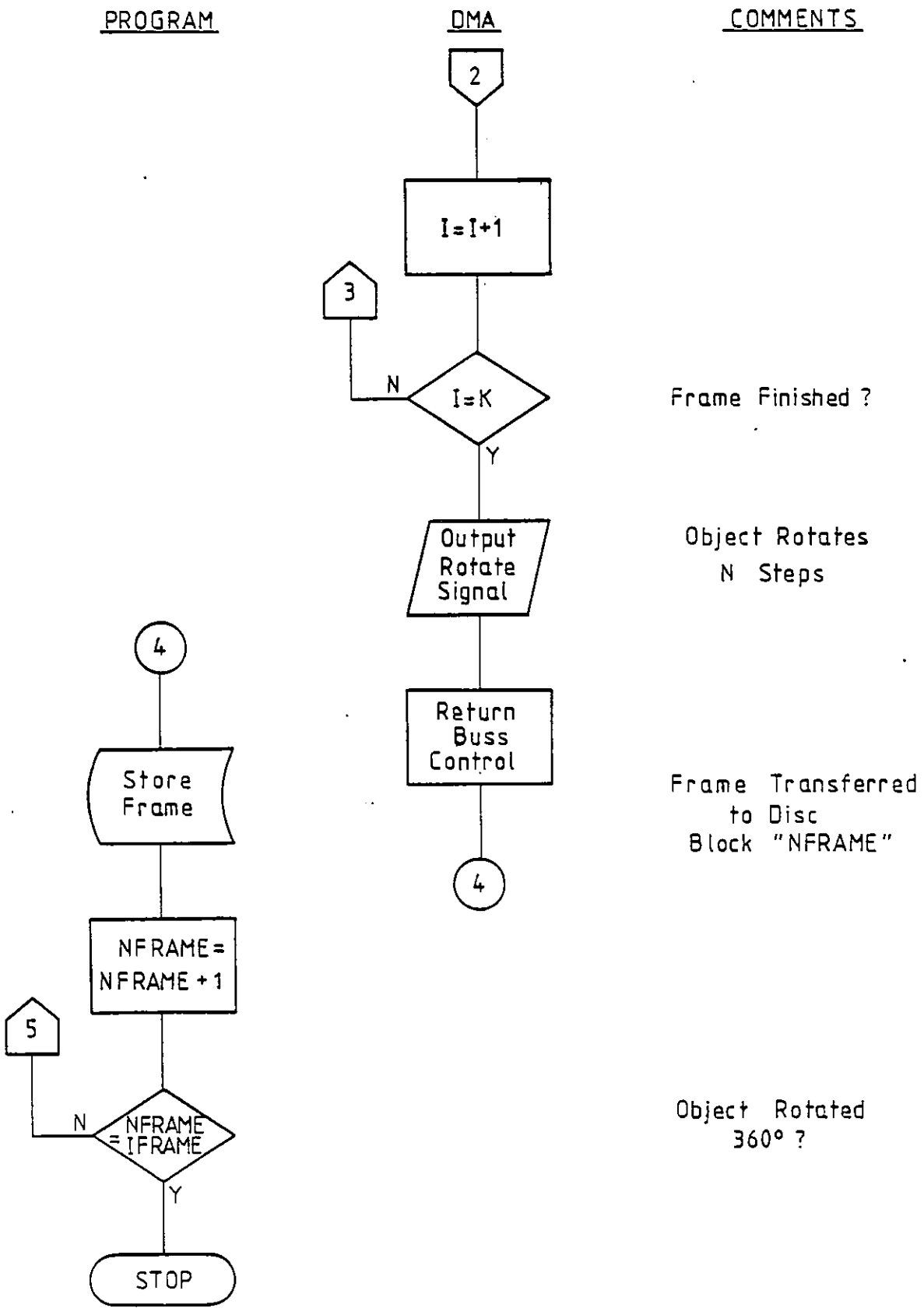
PROGRAM
DMA
COMMENTS
2
I=I+1
3
N
I=K
Y
Frame Finished ?
Output Rotate Signal
Object Rotates N Steps
Return Buss Control
4
4
Store Frame
Frame Transferred to Disc Block "NFRAME"
NFRAME = NFRAME + 1
5
N
NFRAME = IFRAME
Y
Object Rotated 360° ?
STOP

coated with "Slick". Program TUBROT, listed in Appendix A, takes data from the top and bottom of the frame and instructs, via the Visual Display Unit (VDU), the operator to rotate the camera tubes until the line count is identical for both extremities of the frame. The height and vertical scale of the scanned areas are registered using Program DRVEG3 which with a knife edge object prints on the VDU the line number of the first non-zero count. The height and scale are adjusted using potentiometers in the camera scan drive boards.

The $\underline{r}$ axis scale is also adjusted in the drive boards, whilst running Program DRVEG4 and using the tri-square on a micrometer driven slide. The program extracts one frame of data and the number of lines with the same, one more or one less counts as the central line are displayed. Fine adjustment is carried out by using program ROTATE which on input of line counts from both cameras, obtained from Program DRVEG4, calculates the angle a camera must be rotated, to equalise the $\underline{r}$ axis scales.

Using these programs, the time to align the rasters of the two cameras is approximately one hour. The degree to which they can be aligned depends upon the different distortions in each camera, whilst common nonlinearities due to errors in the drive electronics will not affect the registration. Chapter 8 describes experimental results on camera registration and linearity.

7.5 Conclusions

It has been shown that the electronic processing of the video signals does not introduce any appreciable error in the coordinate measurement. Nethertheless the restrictions on the measureable orientations described in Chapter 6 are due to low signal to noise ratios. The inclusion of a variable gain amplifier, whose gain is a function of the video signal on any TV line, would enable signals of low amplitude to be measured providing the noise levels in the cameras could be reduced.

The data storage method has the capability for improved performance in both speed and capacity.

CHAPTER 8

CHAPTER 8: RESULTS

8.1 Introduction

In this chapter various results obtained from the system are presented. In section 8.2, possible errors in the data are calculated. Sections 8.3 and 8.4 describe results on the linearity of the system and least square error curves are fitted to the data. In section 8.5, data obtained from a steel ball is presented.

8.2 Error Analysis

In this section the camera scans are assumed to be geometrically linear. Only objects illuminated normally by the central beam are considered, as the linearity of the total system will be measured using such object orientations. Possible errors arise from the misalignment of the three-beam system, the viewing optical system and noise in the video signal.

It was stated in Chapter 3 that the three illuminating beams were coplanar to within ± 5 μm. If we assume equal intensities for the three beams, the resultant intensity distribution will be of the form:

$$I(x,z) = e^{\frac{-x^2}{2a^2}} + e^{\frac{-(x+bz)^2}{2a^2}} + e^{\frac{-(x+cz)^2}{2a^2}} \qquad (8.1)$$

where a^2 is the variance of the illuminating beams and interference terms are ignored. Equation (8.1) assumes that the three beams intersect at $z = 0$, where the object field is described by $|z| < 5$ mm. This particular case allows the maximum possible values of b and c

which describe the orientations of two of the beams with respect to the first. It is easily shown that for the case where b = c, the function I(x,z) is a maximum when x is given by:

$$x = \frac{2bz}{3} + g(z)$$

With a maximum value of b of 0.001, the departure of x from a linear relationship with z can be shown to be less than 0.1 μms. The object line can therefore be considered to be solely dependant on the object.

In Chapter 4 it was shown that the maximum antisymmetric aberration in the image will cause a shift of less than 1 μm of the centre of the gaussian from the geometrical image point. Variations in the response of the analogue electronics, as described in Chapter 7, with an evenly illuminated object will depend on noise in the system. For a normally illuminated object, the variation in response time of the differentiator will be small due to the large input signal. A precise figure for the variation is not known, but is certainly less than 2 μm in the object space. Variations above this would have been detected using the 40 MHz bandwidth oscilloscope. The errors in the signal can therefore be summarized as

$\leq \pm$ 2 μm random

$\leq \pm$ 1 μm systematic

The systematic error produced in the viewing system will appear as a pin cushion form of distortion in the data. The random error implies that for an object point positioned within 2 μm of a

digitising coordinate, it has a probability of being described by either of two consecutive counts.

8.3 r Linearity of the System

To measure the linearity of the system in the r direction, the edge of a tri-square was coated with thinned "Slick" and mounted on a micrometer driven slide. As the tri-square is moved in the r direction in the plane of illumination, a digitised coordinate will be given by the curve in Figure 8.1. The shaded areas are places where due to the random error E, as described in section 8.2, the count will be indefinite. Experimentally 2E was found to be less than 5 μm over the whole object field for a large majority of measurements. It was noted that it was possible for a count to change momentarily whilst the object point was away from the undefined area. This is believed to be due to the high sensitivity of the large bandwidth electronics to radio waves which can cause unusually high noise levels.

The maximum number of data words from any frame was given in Chapter 7 as 312. This is further modified as the first seven and the last two words occur during blanked T.V. lines. The useful number of words is therefore 303. Describing the count of the 156th line as c, and the number of lines in a frame with this count as N(c), program DRVEG4 (described in Appendix A) outputs to the VDU.

N(c), N(c+1) and N(c-1)

Defining the maximum value of this set of N as N_{max} and the other two values as N_1 and N_2, figure 8.2 shows the variation of the three values as the object moves. The plateau level of N_{max} varied

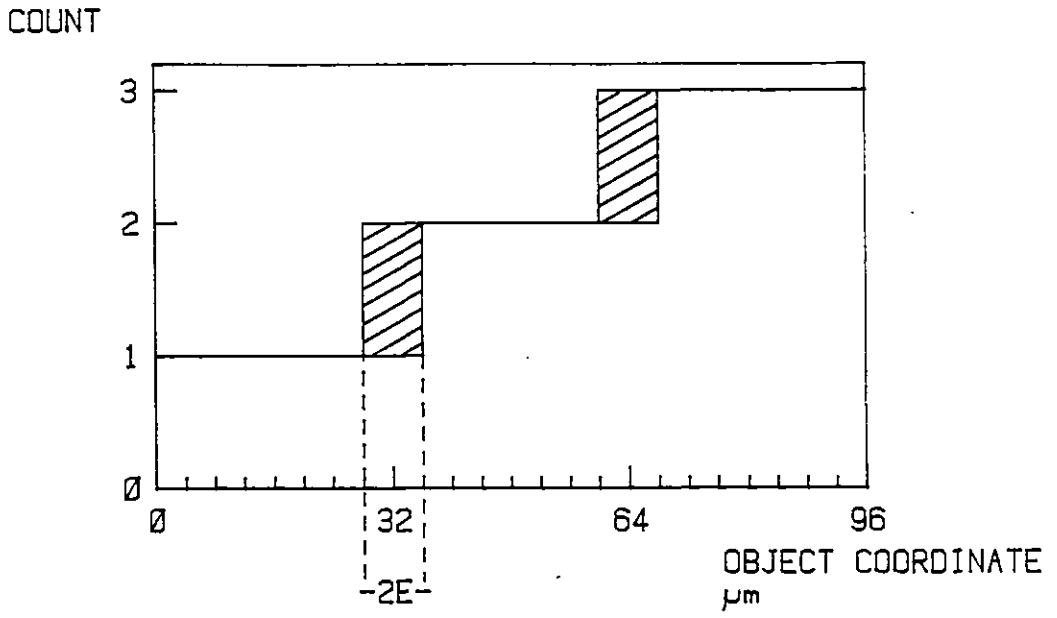

Figure 8.1 The positions which have an undefined coordinate due to random errors.

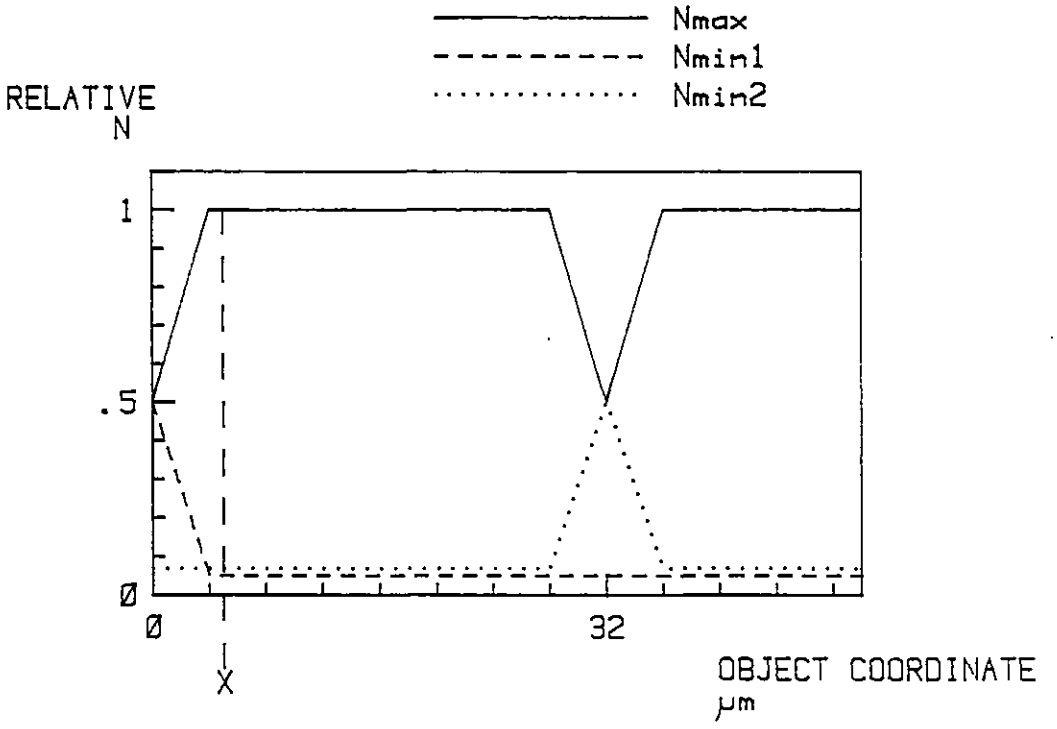

Figure 8.2 The variation of the number of lines with a certain count for three different counts.

across the object field between 295 and 303. This variation is attributed to two factors. The coating of the tri-square produced an object that varied by up to 5 μm from a straight line and also an error will be introduced by the raster scan lines not being precisely registered in time along the r direction. In the majority of cases, the non-consistent counts occurred at the top and bottom of the frame, but no systematic curvature of the scan lines could be detected. Readings were taken from the micrometer as the position X in figure 8.2 were reached. The data was taken for the two cameras separately and combined and identical results to within the 5 μm resolution of the micrometer were obtained. The readings were taken at intervals of the count of 30 from 55 to 355. Cubic, quadratic and linear curves were fitted to the data using a least squares method (Program SQFIT). Figure 8.3 shows the departure from the quadratic and linear curves of the data. The standard deviations of the errors are 17 and 25 μms respectively. The cubic showed a negligible improvement and is therefore not included. The data were repeatable to within ±5 μms and to check that the errors in figure 8.3 were systematic, readings were taken for every count and for a unit change in count the movement was always between 30 and 35 μm. This implies that a continous curve fitted to the data would be smooth between the data points. The constant of proportionality between r and the count was 31.43 μm/count.

A rotation of the cameras of 2' arc will produce a change in scale of 0.1%. If the linearity of the system is known, a quick method of restoring the scale to a known value is desirable. This

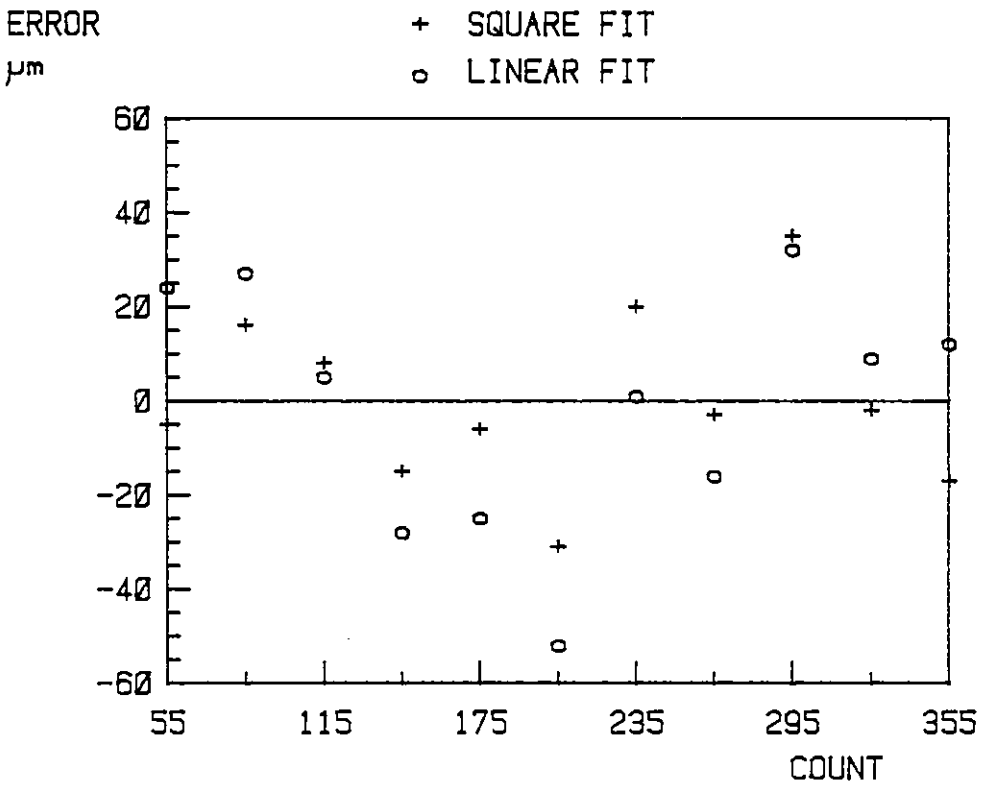

Figure 8.3 The departures from quadratic and linear curves for the r coordinate.

could be accomplished with a standard object using either computer control of stepping motor driven camera rotation and translation stages, or by manual adjustment. A possible object is shown in Figure 8.4. Rotation of the object will provide object points defined by

$$r = -R_1 \text{ or } R_2$$

The cameras could then be adjusted to provide correct counts for the object.

8.4 z linearity

A knife edge was coated with "Slick" and moved vertically through the object field. The line spread function of the viewing system and the defocussed electron beam of the camera will cause the video signal to increase to a plateau level over a number of lines, as shown in figure 8.5. Experimentally, the number of lines was found to be approximately 6. The first line to provide data will have a video signal of amplitude greater than the threshold voltage V_{th}, as described in Chapter 7. If the image profile is identical over the total object field then this line provides a valid description of the position of the knife edge.

Using program DRVEG3, data was taken on the vertical linearity of the system. The data was identical to within 5 μm throughout the object field. Using program SQFIT 3, least square error curves were fitted and the remaining errors are shown in figure 8.6 for a linear fit. The errors suggest that the relationship between the z coordinate and the line number has a discontinuity at a line number of approximately 150, where the constant of proportionality appears to

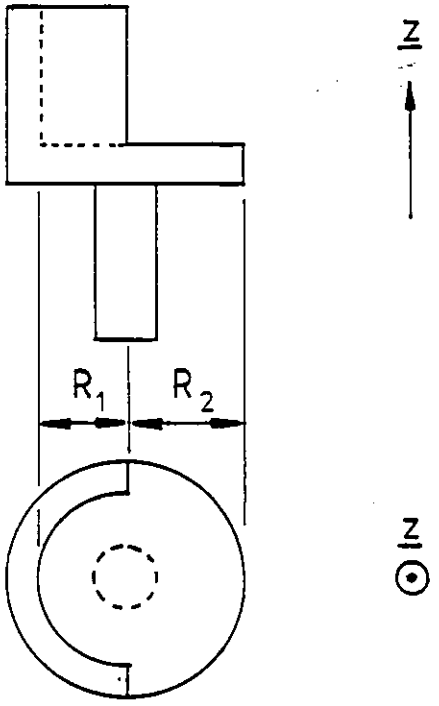

Figure 8.4 A possble object to enable automatic alignment of the two cameras.

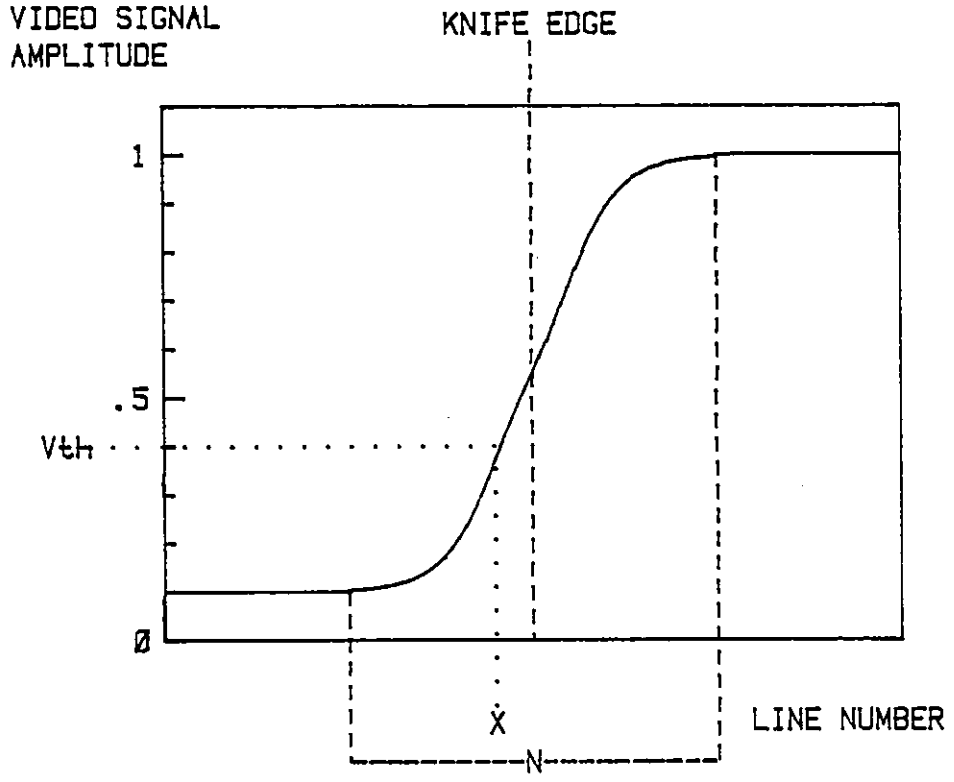

Figure 8.5 The variation of the amplitude of the video signal across a number of lines for a knife edge as the object.

change. The first six points lie on a straight line to better than 1 μm and the last four lie on a line of different gradient to within 5 μm. The standard deviation of the errors is 25 μm and for a quadratic fit is 17 μm. Both the r linearity as in figure 8.3 and the z linearity can best be fitted to two lines which intersect in the centre of the object field. This can be explained by considering the method by which the camera scans are generated. With no deflection voltages applied to the camera tube, the beam would rest at the centre of the image field. The line and frame scan drive voltages are produced by "push-pull" amplifiers. With this method, one transistor supplies the positive voltages and another transistor the negative voltages, thereby causing the beam to scan across the image area. If the transistors are not perfectly matched, a different scan rate will occur for the two halves of the scan. There is also an uncertainty in the scan signal at the cross-over point when one transistor is switching off and the other on. This is shown clearly in the seventh point in figure 8.6. If digitised data are to be reconverted to a linear coordinate system and the r and z linear curves are considered to be too inaccurate, then a two line conversion method would be a considerable improvement.

8.5 Measurements on a Steel Ball

In order to obtain estimates of the ability of the system to measure shapes of objects, precisely known objects must be used. A steel ball of radius 3.175 mm had data taken from it. The ball was spherical to better than ± 2 μm. The coating with "Slick" of the ball

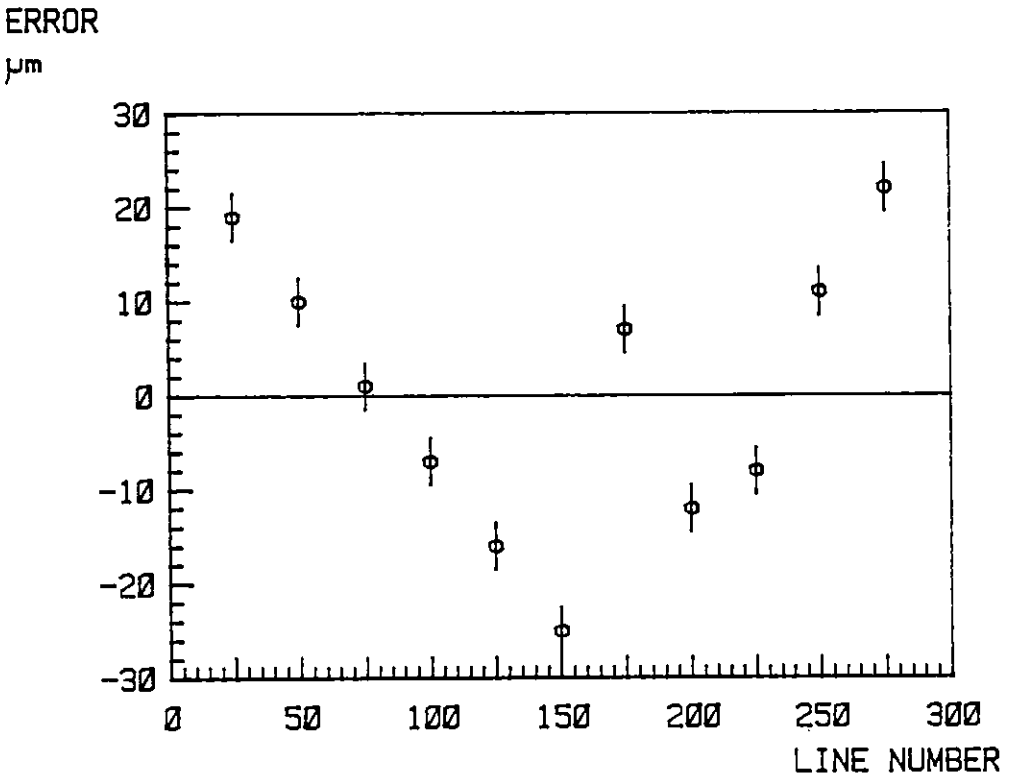

Figure 8.6 The departures of the z coordinate from a linear relationship with the TV line number.

produced a spherical surface to within 5 μm. Twenty two frames of data were taken and for each frame a least squares error circle was fitted. For a sphere held off axis by the rotary table, the intersection of the illumination will be described by:

$$r = r_o + (R^2 - (z - z_o)^2)^{0.5}$$

where r_o and z_o are the coordinates describing the centre of the circle and R is the radius. R and r_o are functions of the rotation of the ball and their dependence can be determined after the first frame of data is taken. However, any error in the calculation of their dependence would be carried over to the following frames of data. For this reason, R and r_o were treated as constants, found for each frame of data by ascertaining the minimum standard deviation in the errors. Each frame is therefore fitted to a circle independent of other frames, rather than fitting all the frames to a sphere.

If we consider the case in figure 8.7 where a circle is digitised in the $\underline{r}$ direction with a digitising step of e starting at a position given by $r = a_o$, it is clear that the error will not be evenly distributed in the interval $-\underline{e} \rightarrow \underline{e}$. The error E, for a point on the circle described by z is given by:

$$E = (R^2 - z^2)^{0.5} - a_o - Me \qquad (8.2)$$

where M is an integer chosen such that;

$$|E| < 0.5e$$

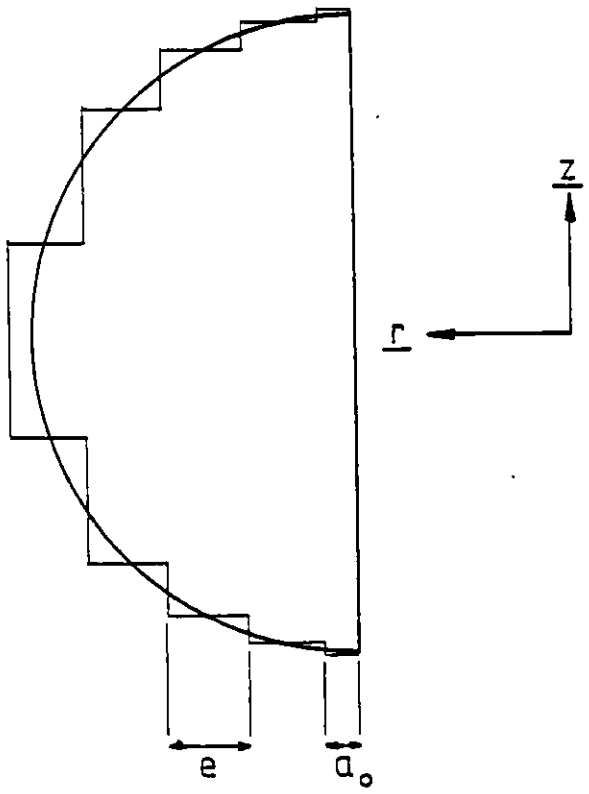

Figure 8.7 The effect of digitising a circle.

If $z = n\Delta z$ where n is an integer and Δz the T.V. line separation, the standard deviation S of the errors is given by

$$S^2(a_o) = \frac{1}{N} \sum_{n=1,N} E_n^2$$

$S(a_o)$ was calculated for values of:

$N = 90$

$\Delta z = 32$ μm

$e = 32$ μm

$R = 3200$ μm

This value of N implies that data exists on the circle for surface tangents inclined by up to 64^o to the $\underline{r}$ axis. It was found that although the standard deviation only varied from 9.7 μm to 10.0 μm for a_o lying between $\pm$16 μm, the error distribution is far from flat. The distribution is shown approximately in figure 8.8 for a_o equal to zero. If the ball is mounted off centre such that for twenty two frames of data a_o varies throughout its range, the curve in figure 8.8 would be smoothed. Figure 8.9 shows the experimental data obtained on 4000 points with a bin size of 4 μm. Clearly insufficient variation in a_o occurred for a statistical averaging of the errors between $\pm$16 μm. A gaussian of the same area and variance is drawn. The standard deviation is 14.9 μm implying that over 95% of the data is accurate to within 30 μm. It is reasonable to assume that the coating of the ball and the nonlinearity of the raster scans of the cameras increased the standard deviation of the errors. Elimination of these contributions would be expected to reduce the error distribution to closely resemble a top hat function between $\pm$16 μm

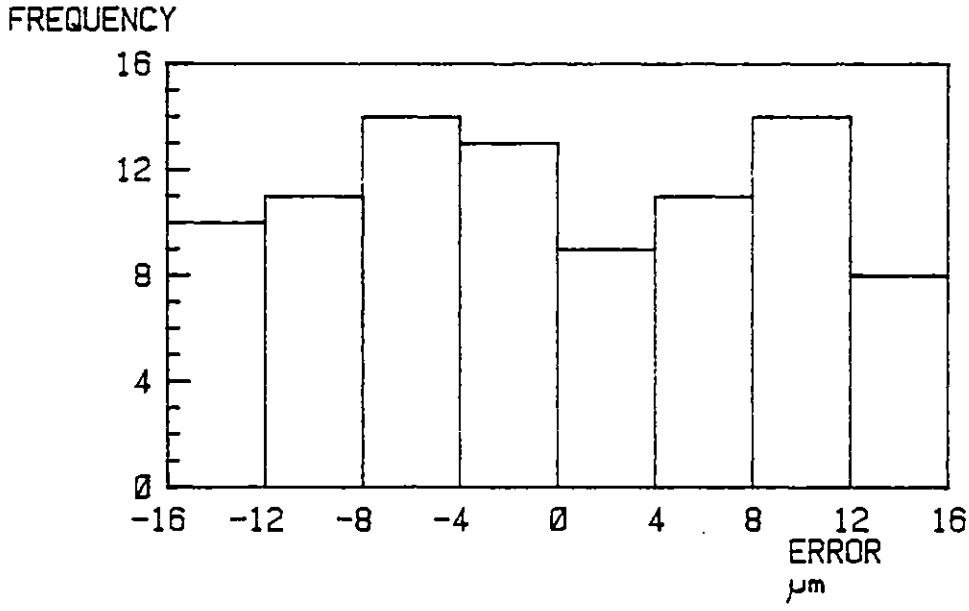

Figure 8.8 The error distribution for a digitised circle.

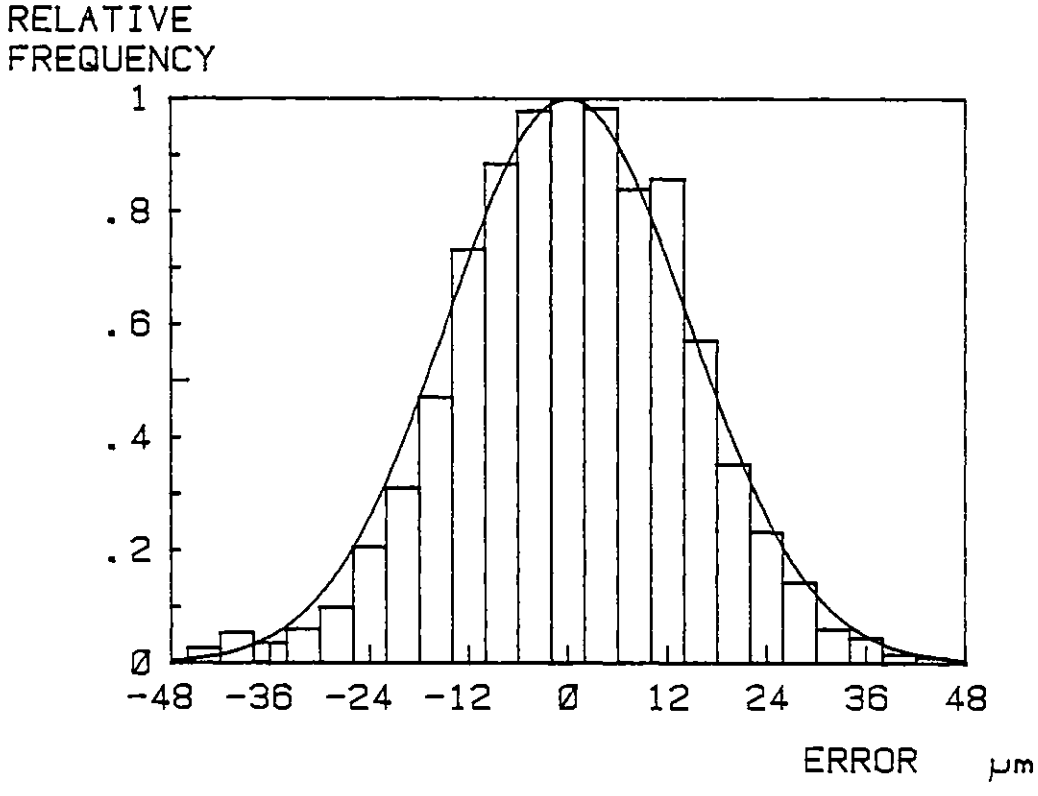

Figure 8.9 The error histogram obtained from 4000 points on a steel ball.

for a smooth object such as a ball.

8.6 Conclusions

It has been shown that the application of a linear relationship between the digitized data and the r and z coordinates can lead to errors as high as 50 μm. If speed is important in the handling of large amounts of data, then a two line relationship reduces the errors significantly.

To assess the measuring ability of the system further, known objects of greater complexity must be used. These objects should have surface points which have normals to the surface out of the z, r plane and may even be invisible to one of the cameras. For comparison of the measured and true shapes, complex data handling programs would be a necessity.

CHAPTER 9

CHAPTER 9: CONCLUSIONS

9.1 Introduction

This thesis has described a new system for measuring the coordinates describing the surface of an object. The system has been shown to be close to achieving the performance as described in Chapter 1. The basic method as given in Chapter 2 is simple and refinements on the system would be expected to greatly enhance its measuring ability. In this chapter, the theoretical and experimental results obtained in this thesis are presented, and possible areas of improvement in the design given.

9.2 A Resumé

In Chapter 2, the method of obtaining information on an object was described. The viewing angle was shown to affect the imaged line width and the number of object points not measured by the system. The results presented in Chapter 6 show that if the ability to measure various object surface orientations is to be improved by using a smaller viewing angle then the illumination beam width will also have to be reduced. This assumes that the electronic signal processing is unchanged. Chapter 3 showed that the optimum illuminating beam width, w_o, is a function of the required depth of field z, and of the wavelength λ of the illumination, described by

$$w_o^2 = \frac{\lambda z}{\pi}$$

Clearly, little variation in the beam diameter is possible with visible illumination. A wavelength of 488 nm would allow a viewing

angle of 29^{o} for the image line width to remain constant. The depth of field is decided by the size of the object that is to be measured and is therefore not a variable in this discussion. The affect on the system of different object sizes is discussed in section 9.3. A small improvement in the line width is possible by increasing the aperture of the illuminating system and the alignment of the three beam producing prisms. Chapter 6 showed the necessity of a defocussed camera electron beam. This beam is used as an high order filter to reduce the speckle contrast. It also causes video signals of large variance with obliquely illuminated object surfaces. A large increase in the aperture of the viewing optics and a resultant reduction in speckle size would enable the use of a focussed electron beam. With a unit magnification telecentric viewing system the aberrations due to the large aperture should be small if well corrected lenses are used.

Chapter 7 described the signal processing and showed that given a noise free signal, the errors in measurement due to the electronics was only a few μms. Problems in measurement of obliquely illuminated object points occurred due to the broad profile and hence low amplitude of the signal. Noise in the cameras causes a great reduction in the certainty with which the centre of the gaussian profile can be determined with low signal levels. The noise experienced is believed to be greater than that due to statistical effects. Introduction of cameras with lower noise levels would enable the use of variable gain amplifiers in the processing electronics. These amplifiers would help to achieve a constant signal amplitude to the differentiator thereby reducing variations in its response.

In Chapter 6 results obtained on the ability of the system to measure object points with varying orientations were given. It was shown that the "Slick" coating exhibited retroreflective properties which greatly increased signal amplitudes above those expected for a Lambertian reflector. For surfaces whose normal was orthogonal to the $\underline{z}$ axis and at an angle α to the $\underline{r}$ axis, the critical value of α above which no data could be collected was shown to depend on the viewing angle. A reduction in the camera electron beam diameter and an increase in the viewing optics aperture would allow signals with greater bandwidths to be passed to the differentiator, than at present. This, coupled with a decrease in the viewing angle would enable measurements of surfaces with a larger range of α to be made with a greater certainty. In section 6.6, it was noted that object surfaces with normals in the r, z plane and at an angle β to the $\underline{r}$ axis, had profiles broader than theoretical explanations could justify. This was assumed to be an effect of the defocussed electron beam and it is therefore assumed that it could be reduced. It seems possible that if all the above improvements were implemented with a 20° viewing angle, a ± 16 μm accuracy could be obtained on object points defined by

$$\alpha < 70^{\circ}$$

$$\beta < 70^{\circ}$$

The data storage system as described in Chapter 7 is capable of increased storage volume and speed. Transfer of data from the core

memory to disc accounts for nearly half the total data acquisition time and is easily reduced by increasing the number of frames transferred at any one time. The remainder of the acquisition time depends upon the T.V. frame rate which could be increased by a factor of two providing the signal processing electronics have the necessary bandwidth. The z resolution of the system is the T.V. line separation which can be increased with the present camera tubes to 1500 lines. The r resolution is decided by the clock frequency in the counters and could be increased greatly if sufficient data storage exists.

9.3 Object Field Size

This thesis has been concerned with the measurement of objects of up to 10 mm in size. With the detectors used, this has enabled a unit magnification in the viewing system. The effect of a larger or smaller object field is discussed here and the effects on the design of the system considered. The optimum illuminating beam waist has been shown to be proportional to the square root of the depth of field required. If the accuracy of a measurement is assumed to be a linear function of the beam width, then the useful number of measurable cells or pixels across an object is proportional to the square root of the depth of field. If a unit magnification was possible with a 100 mm object, it would be expected that the system could achieve a 50 μm accuracy i.e. 2000 pixels. If, however, a 25 mm camera tube was the detector, the imaging system must produce a X10 demagnification. This has the advantage that the image plane is closer to being normal to the optical axis, whilst it also requires a ratio of the focal lengths of the two lenses of 4:1 for a 20^{o} viewing angle. Clearly such an

asymmetrical system with large off-axis object points could introduce large aberrations, even with well corrected lenses. An object field of only 1 mm would only provide 200 pixels of information and would require a ratio of the focal lengths of the lenses of 0.3. This also requires an image plane at 6^{o} to the optical axis for a 20^{o} viewing angle. From the above discussion it can be seen that for a fixed detector size, the possible range of object field sizes is controlled at the upper limit by the aberrations of the viewing system and at the lower limit by the image plane-optical axis angle.

9.4 Conclusions

This thesis has given the underlying principles and design criteria for an automatic shape measuring system. The basic method of obliquely viewing a projected plane of illumination has been shown to fill a gap in methods for three dimensional measurement.

APPENDIX A. LISTING OF THE FORTRAN ROUTINES

DRVEG1	This requires the step number,line number and filenames for data storage.
DRVEG2	This inputs 312 line counts ,and on the input of camera number and X distance outputs the frame to logical unit 7.
DRVEG3	This continuously inputs 312 line count frames and displays on the terminal the line number with the first non-zero count.
DRVEG4	This continuously inputs 312 line count frames and displays on the terminal the number of lines with the same count as the 156 th line and of the number of lines with a count of 1 more or less than the 156 th line.
TUBROT	This continuously inputs 312 line frames, averages the 11-20 line counts and the 291-300 lines and indicates on the terminal the direction of movement of the tube necessary to correct the rotation.
STEP	This rotates the rotary table a given number of step,delays for a certain time and repeats for a given number of times.
ROTATE	On alligning the two cameras at one point and then moving the object to a new position, inputing the counts of cameras 1 and 2 the program calculates the angle of rotation necessary to give identical linear scales for both cameras.
SQFIT	On inputing the object distance data for 11 points (every 30 counts) this fits a cubic,quadratic and linear curve and outputs the results to logical unit 7.
SQFIT2	This the same as SQFIT but for 21 points (every 15 counts).

SQFIT3	This is the same as SQFIT but for the vertical adjustment of the cameras taking 11 readings of Z from line 25 to line 175.
DGET	This prints to logical unit 7 the first block of DY0:DAAAAA.DAT and then any other block requested showing the differences between it and block 0.
BALL	This fits a least square error circle to data from a ball-bearing and outputs either the data or a histogram of the errors to logical unit 7.

```
      PROGRAM DRVEG1
      DIMENSION IARR(312)
      REAL*4 FILNA(3),FILNB(3),FILNC(3)
      DATA FILNB(1)/4HDY1D/
      WRITE(6,*)'Input parameter filename    (10 letters or less)'
      READ(6,10)FILNA
10    FORMAT(3A4)
      WRITE(6,*)' Input data filename in format *****DAT'
      READ(6,15)FILNB(2),FILNB(3)
15    FORMAT(2A4)
      N=IRAD50(12,FILNB,FILNC)
      WRITE(6,*)'Type 1 for rotation,    0  for single frame.'
20    ACCEPT*,IROT
      IF(IROT.EQ.1)GOTO 30
      IF(IROT.NE.0)GOTO 25
      ISTEP=800
      GOTO 50
25    WRITE(6,*)'Invalid input.Try again.'
      GOTO 20
30    WRITE(6,*)'Step number?'
40    ACCEPT*,ISTEP
      IF(ISTEP.NE.3.AND.ISTEP.NE.6.AND.ISTEP.NE.7.AND.
     C  ISTEP.LE.8)GOTO 45
      WRITE(6,*)'Invalid step number.Try again.'
      GOTO 40
45    NBI=2
      NLINE=312
      IF(ISTEP.NE.1) GOTO 50
      NBI=1
      NLINE=256
50    WRITE(6,*)'Line number not greater than ',NLINE
60    ACCEPT*,NWCR
      IF(NWCR.LE.NLINE) GOTO 70
      WRITE(6,*)'Invalid line number.Try again.'
      GOTO 60
70    NFRAM=800/ISTEP
      NBLK=NBI*NFRAM
C
C     Number of blocks needed.
C
      OPEN(UNIT=4,NAME=FILNA,TYPE='NEW',INITIALSIZE=1)
      WRITE(4,100)ISTEP,NWCR,NFRAM,ISTEP,NWCR,NFRAM
100   FORMAT(3I3,/,10X,15HSTEP NUMBER IS ,I3,10X,15HLINE NUMBER IS ,
     C  I3,/,5X,16HFRAME NUMBER IS ,I3)
      CLOSE(UNIT=4)
      ICHAN=IGETC()
      IF(ICHAN.LT.0)STOP              'No channel available'
      I=IENTER(ICHAN,FILNC,NBLK)
      IF(I.LT.0) STOP                 'IENTER error'
C
C
C     Channel successfully opened.
```

```
C
C
      IWCR="172410
      IBAR="172412
      ISCR="172414
      NSCR="000001
      IAD=IADDR(IARR(1))              !Gets memory location of IARR!
C
C     DMA registers loaded.
C
      DO150 KOUNT=1,NFRAM
      IBLK=NBI*(KOUNT-1)
      CALL IPOKE(IWCR,-NWCR)
      CALL IPOKE(IBAR,IAD)
      CALL IPOKE(ISCR,NSCR)
130   I=IPEEK(ISCR)
      J=I.AND.128
      IF(J.EQ.0)GOTO 130
      WRITE(6,*)KOUNT
      I=IWRITW(NWCR,IARR,IBLK,ICHAN)
      IF(I.GT.0)GOTO 150
      WRITE(6,*)'IENTER error number.....',I
      STOP
150   CONTINUE
      CALL CLOSEC(ICHAN)
      CALL IFREEC(ICHAN)
      STOP
      END
```

```
      PROGRAM DRVEG2
      DIMENSION IARR(312)
      IWCR="172410
      IBAR="172412
      ISCR="172414
      NSCR="000001
      IAD=IADDR(IARR(1))              !Gets memory location of IARR!
C
C     DMA registers loaded.
C
10    IBLK=0
      CALL IPOKE(IWCR,-312)
      CALL IPOKE(IBAR,IAD)
      CALL IPOKE(ISCR,NSCR)
130   I=IPEEK(ISCR)
      J=I.AND.128
      IF(J.EQ.0)GOTO 130
      WRITE(6,*)'X Distance in MM ?'
      ACCEPT*,XMM
      WRITE(6,*)'CAMERA ?'
      ACCEPT*,ICAM
      WRITE(7,150)ICAM,XMM,IARR
150   FORMAT(10X,11HCAMERA.....,I1,/,10X,
     C  17HX  DISTANCE MM...,F6.3,///,20(5X,16(3X,I3),/))
      WRITE(6,*)'TYPE 1 FOR REPEAT.'
      ACCEPT*,NGAIN
      IF(NGAIN.NE.1) GOTO 180
      WRITE(7,160)
160   FORMAT(5(/))
      GOTO 10
180   WRITE(7,200)
200   FORMAT(10(/,))
      STOP
      END
```

```
      PROGRAM DRVEG3
      DIMENSION IARR(312)
      IWCR="172410
      IBAR="172412
      ISCR="172414
      NSCR="000001
      IAD=IADDR(IARR(1))              !Gets memory location of IARR!
C
C     DMA registers loaded.
C
      WRITE(6,5)
5     FORMAT(1H1,30(/))
10    CALL IPOKE(IWCR,-312)
      CALL IPOKE(IBAR,IAD)
      CALL IPOKE(ISCR,NSCR)
30    I=IPEEK(ISCR)
      J=I.AND.128
      IF(J.EQ.0)GOTO 30
      DO 50 K=1,312
      IF(IARR(K).EQ.0) GOTO 50
      WRITE(6,40)K,IARR(K)
40    FORMAT(1H+,5X,18HLINE NUMBER ......,I3,5X,I3)
      GOTO 10
50    CONTINUE
      GOTO 10
      STOP
      END
```

```
      PROGRAM DRVEG4
      DIMENSION IARR(312),MVAL(3),IA(3),MVFIN(3),IAFIN(3)
      IWCR="172410
      IBAR="172412
      ISCR="172414
      NSCR="000001
      IAD=IADDR(IARR(1))              !Gets memory location of IARR!
C
C     DMA registers loaded.
C
      WRITE(6,5)
5     FORMAT(30(/))
10    CALL IPOKE(IWCR,-312)
      CALL IPOKE(IBAR,IAD)
      CALL IPOKE(ISCR,NSCR)
30    I=IPEEK(ISCR)
      J=I.AND.128
      IF(J.EQ.0)GOTO 30
      DO 100 J=1,3
      IA(J)=IARR(128)+J-2
      MVAL(J)=0
      DO 50 K=1,312
      IF(IARR(K).EQ.IA(J)) MVAL(J)=MVAL(J)+1
50    CONTINUE
100   CONTINUE
C
C
C     Test for largest value.
C
C
      IF(MVAL(1).GT.MVAL(2)) GOTO 160          !1st value greatest!
      IF(MVAL(3).GT.MVAL(2)) GOTO 130          !3rd value greatest!
      DO 120 LI=1,3                            !2nd value greatest!
      L=3-LI
      IF(L.EQ.0)L=3
      MVFIN(L)=MVAL(LI)
      IAFIN(L)=IA(LI)
120   CONTINUE
      GOTO 180
130   DO 150 LI=1,3
      L=4-LI
      MVFIN(LI)=MVAL(L)
      IAFIN(LI)=IA(L)
150   CONTINUE
      GOTO 180
160   DO 170 LI=1,3
      MVFIN(LI)=MVAL(LI)
      IAFIN(LI)=IA(LI)
170   CONTINUE
180   MTOT=MVFIN(1)+MVFIN(2)+MVFIN(3)
190   WRITE(6,200) ((IAFIN(I),MVFIN(I)),I=1,3),MTOT
200   FORMAT(1H+,5X,10HVALUES    ,3(I3,4H....,I3,5X),5X,
     C  8HTOTAL...,I3,10X)
      GOTO 10
      STOP
      END
```

```
      PROGRAM TUBROT
      DIMENSION IARR(312),MVAL(2),VAL(2)
      IWCR="172410
      IBAR="172412
      ISCR="172414
      NSCR="000001
      IAD=IADDR(IARR(1))              !Gets memory location of IARR!
C
      WRITE(6,*)'INPUT CAMERA TO BE ADJUSTED.'
      ACCEPT*,ICAM
C
C     DMA registers loaded.
C
      WRITE(6,5)
5     FORMAT(30(/))
10    CALL IPOKE(IWCR,-312)
      CALL IPOKE(IBAR,IAD)
      CALL IPOKE(ISCR,NSCR)
30    I=IPEEK(ISCR)
      J=I.AND.128
      IF(J.EQ.0)GOTO 30
      DO 50 K=1,2
      MVAL(K)=0
      INIT=280*(K-1)+10
      DO 100 L=1,10
      MVAL(K)=MVAL(K)+IARR(INIT+L)
100   CONTINUE
      VAL(K)=FLOAT(MVAL(K))/10.0
50    CONTINUE
      IF(ICAM.EQ.1) GOTO 80
      IF(VAL(1).GT.VAL(2)) GOTO 130
      IF(VAL(1).LT.VAL(2)) GOTO 150
      GOTO 90
80    IF(VAL(1).GT.VAL(2)) GOTO 150
      IF(VAL(1).LT.VAL(2)) GOTO 130
90    WRITE(6,*)'CAMERA CORRECT.'
      GOTO 10
130   WRITE(6,*)'RAISE TUBE ADJUSTMENT.'
      GOTO 10
150   WRITE(6,*)'LOWER TUBE ADJUSTMENT'
      GOTO 10
      STOP
      END
```

```
      PROGRAM STEP
      DIMENSION IARR(312)
      IWCR="172410
      IBAR="172412
      ISCR="172414
      NSCR="000001
      NWCR=200
      IAD=IADDR(IARR(1))              !Gets memory location of IARR!
C
C     DMA registers loaded.
C
      WRITE(6,5)
5     FORMAT(1H1,30(/))
10    WRITE(6,*)'Input step number.'
      ACCEPT*,ISTEP
      WRITE(6,*)'Input delay in Milli-seconds.'
      ACCEPT*,IDELAY
      NFRAM=800/ISTEP
20    DO 50 K=1,NFRAM
C
C
C     PRODUCE DELAY.
C
C
      DO 25 L=1,IDELAY
      A=FLOAT(L)**2.0
25    CONTINUE
      CALL IPOKE(IWCR,-NWCR)
      CALL IPOKE(IBAR,IAD)
      CALL IPOKE(ISCR,NSCR)
30    I=IPEEK(ISCR)
      J=I.AND.128
      IF(J.EQ.0)GOTO 30
50    CONTINUE
      WRITE(6,*)'Type 1 for repeat,2 for new data.'
      ACCEPT*,IFLAG
      IF(IFLAG.EQ.1) GOTO 20
      IF(IFLAG.EQ.2) GOTO 10
      STOP
      END
```

```
      PROGRAM ROTATE
C
C
C     This program calculates the required change of angle
C     of camera 2 to adjust the two cameras linear scales.
C
C
      DIMENSION ANAME(3)
      DATA ANAME/4HINCR,4HDECR,4HEASE/
      PI=3.14159
      TH=32.0*PI/180.0
      THTAN=SIN(TH)/COS(TH)
10    IVAL=1
      WRITE(6,*)'INPUT CAMERAS 1 AND 2 COUNT.'
      ACCEPT*,COUNT1
      WRITE(6,*)'MOVE SET-SQUARE TO NEW POSITION.'
      WRITE(6,*)'INPUT CAMERA 1 COUNT.'
      ACCEPT*,COUNT2
      WRITE(6,*)'INPUT CAMERA 2 COUNT.'
      ACCEPT*,COUNT3
      SCALE1=ABS(COUNT2-COUNT1)
      SCALE2=ABS(COUNT3-COUNT1)
      THETA=ABS((1.0-SCALE1/SCALE2)*THTAN)
      DELTAC=THETA*130.0*31.6
      THEMIN=THETA*57.0*60.0
      IF(SCALE1.GT.SCALE2) IVAL=2
      WRITE(6,50) ANAME(IVAL),ANAME(3),THEMIN,
     C ANAME(IVAL),ANAME(3),DELTAC
50    FORMAT(30(/),5X,2(A4),23H CAMERA 2 ANGLE BY.....,F3.0,
     C 9H  MINUTES,//,2X,3HOR ,2(A4),23H CAMERA 2 COUNT BY.....,F5.1)
      WRITE(6,*)'TYPE 1 FOR REPEAT'
      ACCEPT*,IREP
      IF(IREP.EQ.1) GOTO 10
      STOP
      END
```

```
      PROGRAM SQFIT
      DIMENSION XVAL(11),AVAL(4),COUNT(11),COUNTS(11),COUNTC(11)
      DIMENSION COUTOT(11),ICOUNT(11),DIFF(11)
      WRITE(6,*)'ENTER 205 COUNT X VALUE'
      ACCEPT*,XVA
      DO 10 I=1,11
      IA=25+30*I
      WRITE(6,*)'ENTER ',IA,' COUNT   X VALUE'
      ACCEPT*,XV
      XVAL(I)=XVA-XV
10    CONTINUE
      DO 30 K=1,4
      IPO=K-1
      AVAL(K)=0.0
      DO20 I=1,11
      IA=I-6
      IF(I.EQ.6)GOTO15
      AVAL(K)=AVAL(K)+XVAL(I)*FLOAT(IA**IPO)
      GOTO 20
15    IF(K.EQ.1)AVAL(K)=AVAL(K)+XVAL(I)
20    CONTINUE
30    CONTINUE
C
C
C     SIGMA(X*COUNT**N)       N=0,1,2,3       CALCULATED
C
C
      C=1.0
      D=1.0
      DO 150 L=1,3
      IF(L.EQ.1) GOTO 40                                  !CUBIC!
      D=0.0
      C=1.0
      IF(L.EQ.2) GOTO 40                                  !QUADRATIC!
      C=0.0                                               !LINEAR!
40    C=(AVAL(3)-10.0*AVAL(1))/858.0/900.0*C
      A=AVAL(1)/11.0-9000.0*C
      D=(AVAL(4)-17.8*AVAL(2))/6177.6/27000.0*D
      B=(AVAL(2)/110.0-17.8*D*27000.0)/30.0
C
C
C     COEFFICIENTS    CALCULATED
C
C
      DIFTO=0.0
      DIFTOT=0.0
      DO50 I=1,11
      ICOUNT(I)=(I-6)*30
      ACOUNT=FLOAT(ICOUNT(I))
      COUNT(I)=B*ACOUNT
      COUNTS(I)=C*ACOUNT**2
      COUNTC(I)=D*ACOUNT**3
      COUTOT(I)=A+COUNT(I)+COUNTS(I)+COUNTC(I)
      DIFF(I)=XVAL(I)-COUTOT(I)
      DIFTO=DIFF(I)**2+DIFTO
50    CONTINUE
```

```
      DIFTOT=SQRT(DIFTO/11.0)
      WRITE(7,70)A,B,C,D
70    FORMAT(5X,2HX=,F6.3,3H + ,F8.5,10H(C-205) + ,1PE9.2,
     C  13H(C-205)**2 + ,1PE9.2,10H(C-205)**3,/,/,/)
      WRITE(7,100)ICOUNT,COUNT,COUNTS,COUNTC,COUTOT,XVAL,DIFF,DIFTOT
100   FORMAT(5X,26HX   COUNT-205.............,11(I4,5X)/,5X,
     C  26HA* (COUNT-205).............,11(F6.3,3X),/,5X,
     C  26HB* (COUNT-205)  SQUARED...,11(F6.3,3X),/,5X,
     C  26HC* (COUNT-205)  CUBED.....,11(F6.3,3X),/,/,5X,
     C  26HTOTAL.....................,11(F6.3,3X),/,/,5X,
     C  26HDATA......................,11(F6.3,3X),/,/,5X,
     C  26HDIFFERENCE................,11(F6.3,3X),/,/,5X,
     C  26HROOT MEAN SQUARED DIFF....,1PE9.2,5(/,))
150   CONTINUE
      STOP
      END
```

```
      PROGRAM SQFIT2
      DIMENSION XVAL(22),AVAL(4),COUNT(22),COUNTS(22),COUNTC(22)
      DIMENSION COUTOT(22),ICOUNT(22),DIFF(22)
      WRITE(6,*)'ENTER 205 COUNT X VALUE'
      ACCEPT*,XVA
      DO 10 I=1,21
      IA=40+15*I
      WRITE(6,*)'ENTER ',IA,' COUNT   X VALUE'
      ACCEPT*,XV
      XVAL(I)=XVA-XV
10    CONTINUE
      XVAL(22)=0.0
      DO 30 K=1,4
      IPO=K-1
      AVAL(K)=0.0
      DO20 I=1,21
      IA=I-11
      IF(I.EQ.11)GOTO15
      AVAL(K)=AVAL(K)+XVAL(I)*FLOAT(IA**IPO)
      GOTO 20
15    IF(K.EQ.1)AVAL(K)=AVAL(K)+XVAL(I)
20    CONTINUE
30    CONTINUE
C
C
C     SIGMA(X*COUNT**N)       N=0,1,2,3       CALCULATED
C
C
      SIGC2=770.0
      SIGC4=50666.0
      SIGC6=3956810.0
      C=1.0
      D=1.0
      DO 150 L=1,3
      IF(L.EQ.1) GOTO 40                                  !CUBIC!
      D=0.0
      C=1.0
      IF(L.EQ.2) GOTO 40                                  !QUADRATIC!
      C=0.0                                               !LINEAR!
40    C=(AVAL(1)*SIGC2-AVAL(3)*21.0)/(SIGC2**2-21.0*SIGC4)*C/225.0
      A=(AVAL(1)-C*SIGC2*225.0)/21.0
      D=(AVAL(2)*SIGC4-AVAL(4)*SIGC2)/(SIGC4**2-SIGC6*SIGC2)
     C                *D/3375.0
      B=(AVAL(2)-D*SIGC4*3375.0)/SIGC2/15.0

C
C     COEFFICIENTS    CALCULATED
```

```
C
C
      IAO=1
      DIFTOT=0.0
      DIFTO=0.0
      DO50 I=1,22
      IF(I.EQ.22) IAO=0
      ICOUNT(I)=(I-11)*15*IAO
      ACOUNT=FLOAT(ICOUNT(I))
      COUNT(I)=B*ACOUNT
      COUNTS(I)=C*ACOUNT**2
      COUNTC(I)=D*ACOUNT**3
      COUTOT(I)=A*FLOAT(IAO)+COUNT(I)+COUNTS(I)+COUNTC(I)
      DIFF(I)=XVAL(I)-COUTOT(I)
      DIFTO=DIFF(I)**2+DIFTO
50    CONTINUE
      DIFTOT=SQRT(DIFTO/21.0)
      WRITE(7,70)A,B,C,D
70    FORMAT(5X,2HX=,F6.3,3H + ,F8.5,10H(C-205) + ,1PE9.2,
     C 13H(C-205)**2 + ,1PE9.2,10H(C-205)**3,/,/,/)
      DO 200 LNU=1,2
      N=(LNU-1)*11+1
      M=N+10
80    WRITE(7,100)(ICOUNT(I),I=N,M),(COUNT(I),I=N,M),
     C (COUNTS(I),I=N,M),(COUNTC(I),I=N,M),(COUTOT(I),I=N,M),
     C (XVAL(I),I=N,M),(DIFF(I),I=N,M)
100   FORMAT(5X,26HX   COUNT-205.............,11(I4,5X)/,5X,
     C 26HA* (COUNT-205).............,11(F6.3,3X),/,5X,
     C 26HB* (COUNT-205)  SQUARED...,11(F6.3,3X),/,5X,
     C 26HC* (COUNT-205)  CUBED.....,11(F6.3,3X),/,/,5X,
     C 26HTOTAL.....................,11(F6.3,3X),/,/,5X,
     C 26HDATA......................,11(F6.3,3X),/,/,5X,
     C 26HDIFFERENCE................,11(F6.3,3X),/,/,/)
200   CONTINUE
      WRITE(7,170) DIFTOT
170   FORMAT(5X,25HROOT MEAN SQUARED DIFF...,1PE9.2,5(/,))
150   CONTINUE
      STOP
      END
```

```
      PROGRAM SQFIT3
      DIMENSION XVAL(11),AVAL(4),COUNT(11),COUNTS(11),COUNTC(11)
      DIMENSION COUTOT(11),ICOUNT(11),DIFF(11)
      WRITE(6,*)'ENTER X COUNT VALUE'
      ACCEPT*,IVA
      DO 10 I=1,11
      IA=25*I
      WRITE(6,*)'ENTER ',IA,' LINE   Z VALUE'
      ACCEPT*,XVAL(I)
10    CONTINUE
      DO 30 K=1,4
      IPO=K-1
      AVAL(K)=0.0
      DO20 I=1,11
      IA=I-6
      IF(I.EQ.6)GOTO15
      AVAL(K)=AVAL(K)+XVAL(I)*FLOAT(IA**IPO)
      GOTO 20
15    IF(K.EQ.1)AVAL(K)=AVAL(K)+XVAL(I)
20    CONTINUE
30    CONTINUE
C
C
C     SIGMA(X*COUNT**N)       N=0,1,2,3       CALCULATED
C
C
      WRITE(7,35)IVA
35    FORMAT(5X,8HX COUNT=,I3,///)
      C=1.0
      D=1.0
      DO 150 L=1,3
      IF(L.EQ.1) GOTO 40                                  !CUBIC!
      D=0.0
      C=1.0
      IF(L.EQ.2) GOTO 40                                  !QUADRATIC!
      C=0.0                                               !LINEAR!
40    C=(AVAL(3)-10.0*AVAL(1))/858.0/625.0*C
      A=AVAL(1)/11.0-6250.0*C
      D=(AVAL(4)-17.8*AVAL(2))/6177.6/15625.0*D
      B=(AVAL(2)/110.0-17.8*D*15625.0)/25.0
C
C
C     COEFFICIENTS    CALCULATED
```

```
C
C
      DIFTO=0.0
      DIFTOT=0.0
      DO50 I=1,11
      ICOUNT(I)=(I-6)*25
      ACOUNT=FLOAT(ICOUNT(I))
      COUNT(I)=B*ACOUNT
      COUNTS(I)=C*ACOUNT**2
      COUNTC(I)=D*ACOUNT**3
      COUTOT(I)=A+COUNT(I)+COUNTS(I)+COUNTC(I)
      DIFF(I)=XVAL(I)-COUTOT(I)
      DIFTO=DIFF(I)**2+DIFTO
50    CONTINUE
      DIFTOT=SQRT(DIFTO/11.0)
      WRITE(7,70)A,B,C,D
70    FORMAT(5X,2HZ=,F6.3,3H + ,F8.5,13H(LINE-150) + ,
     C  1PE9.2,16H(LINE-150)**2 + ,1PE9.2,13H(LINE-150)**3,/,/,/)
      WRITE(7,100)ICOUNT,COUNT,COUNTS,COUNTC,COUTOT,XVAL,DIFF,DIFTOT
100   FORMAT(5X,26H   LINE-150.............,11(I4,5X)/,5X,
     C  25HA* (LINE-150).............,11(F6.3,3X),/,5X,
     C  25HB* (LINE-150)  SQUARED...,11(F6.3,3X),/,5X,
     C  25HC* (LINE-150)  CUBED.....,11(F6.3,3X),/,/,5X,
     C  25HTOTAL.....................,11(F6.3,3X),/,/,5X,
     C  25HDATA.....................,11(F6.3,3X),/,/,5X,
     C  25HDIFFERENCE................,11(F6.3,3X),/,/,5X,
     C  26HROOT MEAN SQUARED DIFF....,1PE9.2,5(/,))
150   CONTINUE
      STOP
      END
```

```
      PROGRAM DGET
      DIMENSION IARR(256),LARR(256),NARR(256)
      REAL*4 DNAM(2)
      DATA DNAM/6RDY1DAA,6RAAADAT/
      ICHAN=IGETC()
      IF(ICHAN.LT.0)STOP              'No channel available'
      I=LOOKUP(ICHAN,DNAM)
      IF(I.GE.0)GOTO 10
      WRITE(6,*)'LOOKUP error number....',I
      STOP
10    IBLK=0
      I=IREADW(256,LARR,IBLK,ICHAN)
      WRITE(7,20)IBLK,LARR
20    FORMAT(10X,17HBLOCK NUMBER.....,I3,/,/,16(5X,16(3X,I3),/))
30    WRITE(6,*)' Block number.?'
      ACCEPT*,IBLK
      IF(IBLK.NE.0)GOTO35
      WRITE(6,*)'Block 0 has been recieved.'
      GOTO 30
35    I=IREADW(256,IARR,IBLK,ICHAN)
      IF(I.GT.0)GOTO 40
      WRITE(6,*)'IREADW error number',I
      STOP
40    DO 50 K=1,256
      NARR(K)=LARR(K)-IARR(K)
50    CONTINUE
      WRITE(7,100)IBLK,((IARR(I),NARR(I)),I=1,256)
100   FORMAT(10X,17HBLOCK NUMBER.....,I3,
     C       /,/,22(5X,12(3X,I3,2X,I2),/))
      GOTO 30
      CALL CLOSEC(ICHAN)
      CALL IFREEC(ICHAN)
      STOP
      END
```

```
      PROGRAM BALL
      DIMENSION IARR(312),Z(201),XREAL(201),XCAM(201)
     C  ,XDIFF(312),DIFZ(21),DIFX(11)
      IWCR="172410
      IBAR="172412
      ISCR="172414
      NSCR="000001
      IAD=IADDR(IARR(1))              !Gets memory location of IARR!
C
C     DMA registers loaded.
C
10    IBLK=0
      CALL IPOKE(IWCR,-312)
      CALL IPOKE(IBAR,IAD)
      CALL IPOKE(ISCR,NSCR)
20    I=IPEEK(ISCR)
      J=I.AND.128
      IF(J.EQ.0) GOTO 20
      NLINE=0
      IFLAG=1
      IARMAX=0
30    DO 50 K=1,312
      IF(IARR(K).LE.IARMAX) GOTO 50
      IARMAX=IARR(K)
50    CONTINUE
      DO 100 K=1,312
      IF(IARR(K).LT.IARMAX) GOTO 100
      NLINE=NLINE+1
      IF(IFLAG.EQ.0) GOTO 100
      MAXLIN=K
      IFLAG=0
100   CONTINUE
      ILIMAX=MAXLIN+NLINE/2

C
C
C     MAXIMUM X DISPLACEMENT FOUND
C
C
120   WRITE(6,*)'INPUT BALL RADIUS.'
      ACCEPT*,RBALL
      NIX=1
      LIX=21
      XOFF=0.0
      MFLAG=0
110   DIFMIN=1.0
      DO 200 LM=1,LIX
      IF(LIX.EQ.1) GOTO 140
      ZOFF=FLOAT(LM-11)/100.0
140   DO 210 IX=1,NIX
      IF(NIX.EQ.1) GOTO 170
      XOFF=FLOAT(IX-6)/200.0
170   DIFTOT=0.0
      NDIFF=0
```

```
      DO 190 L=1,201
      ILINE=L-101+ILIMAX
      Z(L)=.03165*FLOAT(L-101)+ZOFF
      A=RBALL**2.0-Z(L)**2.0
      IF(A.LE.0.0) A=0.0
      XREAL(L)=SQRT(A)+XOFF
      XCAM(L)=RBALL-FLOAT(IARMAX-IARR(ILINE))*.03143
      XDIFF(L)=XREAL(L)-XCAM(L)
      IF(IARR(ILINE).NE.0) GOTO 180
      XCAM(L)=100.0
      XDIFF(L)=100.0
180   IF(ABS(XDIFF(L)).GT.0.2) GOTO 190
      NDIFF=NDIFF+1
      DIFTOT=DIFTOT+XDIFF(L)**2
190   CONTINUE
      DIFTO=SQRT(DIFTOT/FLOAT(NDIFF))
      IF(LIX.EQ.1) GOTO 205
      IF(DIFTO.GT.DIFMIN) GOTO 192
      DIFMIN=DIFTO
      LMIN=LM
192   WRITE(6,195)DIFTO,ZOFF,XOFF
195   FORMAT(5X,12HRMS DIFF....,F5.3,5X,10HOFFSET....,F6.3,5X,F6.3)
      GOTO 210
205   WRITE(6,195) DIFTO,ZOFF,XOFF
      IF(DIFTO.GT.DIFMIN) GOTO 210
      DIFMIN=DIFTO
      IXMIN=IX
210   CONTINUE
200   CONTINUE
      IF(MFLAG.EQ.1) GOTO 230
      IF(LIX.EQ.1) GOTO 215
C
C     ZOFF CALCULATED
C
      ZOFF=FLOAT(LMIN-11)/100.0
      NIX=11
      LIX=1
      GOTO 110
C
C     XOFF CALCULATED
C
215   XOFF=FLOAT(IXMIN-6)/200.0
      NIX=1
      LIX=1
      MFLAG=1
      GOTO 110
230   WRITE(6,240)
240   FORMAT(/////,5X,5HTYPE:,//,5X,14H1...NEW RADIUS,/5X,
     C  14H2........PRINT,/,5X,14H3.....NEW DATA)
      ACCEPT*,IRAD
      IF(IRAD.EQ.1) GOTO 120
      IF(IRAD.EQ.2) GOTO 350
      IF(IRAD.EQ.3) GOTO 10
      GOTO 250
```

```
350      WRITE(7,220) RBALL,DIFTO
220      FORMAT(////////,5X,20HBALL RADIUS.........,F5.3,//,5X,
     C   47HROOT MEAN SQUARED DIFFERENCE   (DIFF < 0.2)....,F5.3,////)
         WRITE(6,*)'TYPE 1 FOR LISTING OF DATA.'
         ACCEPT*,ILIST
         IF(ILIST.NE.1) GOTO320
         WRITE(7,295)
295      FORMAT(3(8X,1HZ,7X,6HREAL X,4X,8HCAMERA X,5X,4HDIFF,2X))
         DO 310 N=1,67
         WRITE(7,300)(Z(I),XREAL(I),XCAM(I),XDIFF(I),I=N,N+134,67)
300      FORMAT(5X,3(3(F5.2,6X),F6.3,6X))
310      CONTINUE
320      WRITE(6,*)'TYPE 1 FOR HISTOGRAM DATA.'
         ACCEPT*,IHIST
         IF(IHIST.NE.1) GOTO 330
         CALL HISTO(XDIFF)
330      WRITE(6,*)'TYPE 1 FOR NEW RADIUS  2 FOR NEW TV DATA'
         ACCEPT*,IREP
         IF(IREP.EQ.2) GOTO 10
         IF(IREP.EQ.1) GOTO 120
250      STOP
         END
```

```
         SUBROUTINE HISTO(XDIFF)
         DIMENSION N(160),MAX(160),MINX(160),XDIFF(201)
20       WRITE(6,*)'INPUT BIN WIDTH  (1,2,4,8,16).'
         ACCEPT*,IBIN
         NUMB=0
         M=160/IBIN
         DO 50 I=1,M
         MAX(I)=I*IBIN-80
         MINX(I)=MAX(I)-IBIN
         N(I)=0
50       CONTINUE
         DO 200 L=1,201
         IF(ABS(XDIFF(L)).GT.0.08) GOTO 200
100      NERR=IFIX((XDIFF(L)*1000.0+80.0)/FLOAT(IBIN))+1
         N(NERR)=N(NERR)+1
         NUMB=NUMB+1
200      CONTINUE
         WRITE(7,350) NUMB
350      FORMAT(/////,10X,15HTOTAL NUMBER...,I3,
     C   ///,12X,6(5HERROR,4X,6HNUMBER,5X))
         WRITE(7,400) (MINX(I),MAX(I),N(I),I=1,M)
400      FORMAT(10X,27(6(I3,3H - ,I3,3H...,I3,5X),/,10X))
         WRITE(6,*)'INPUT 1 FOR NEW BIN SIZE.'
         ACCEPT*,NBIN
         IF(NBIN.EQ.1) GOTO 20
         RETURN
         END
```

VIDEO MIXER

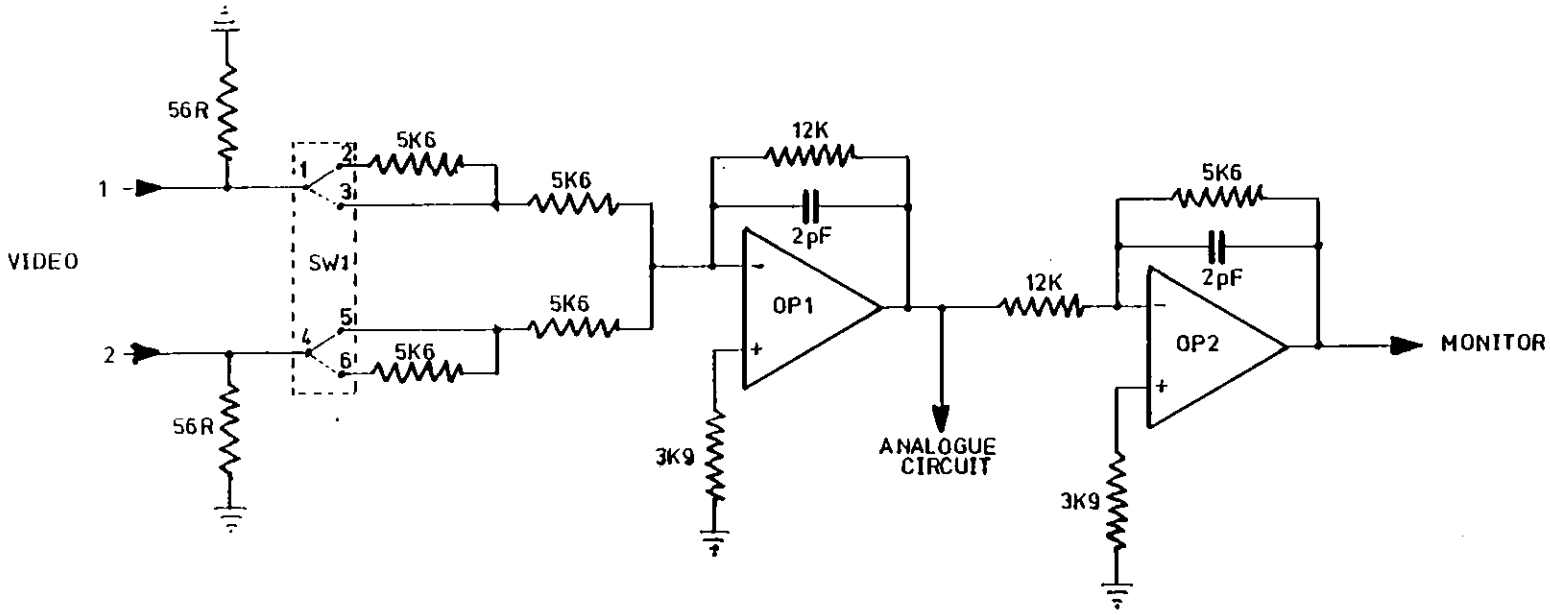

SWITCH SETTINGS

Output Channel	
1	1 - 3
2	4 - 5
1+2	1 - 2 & 4 - 6

ANALOGUE CIRCUIT

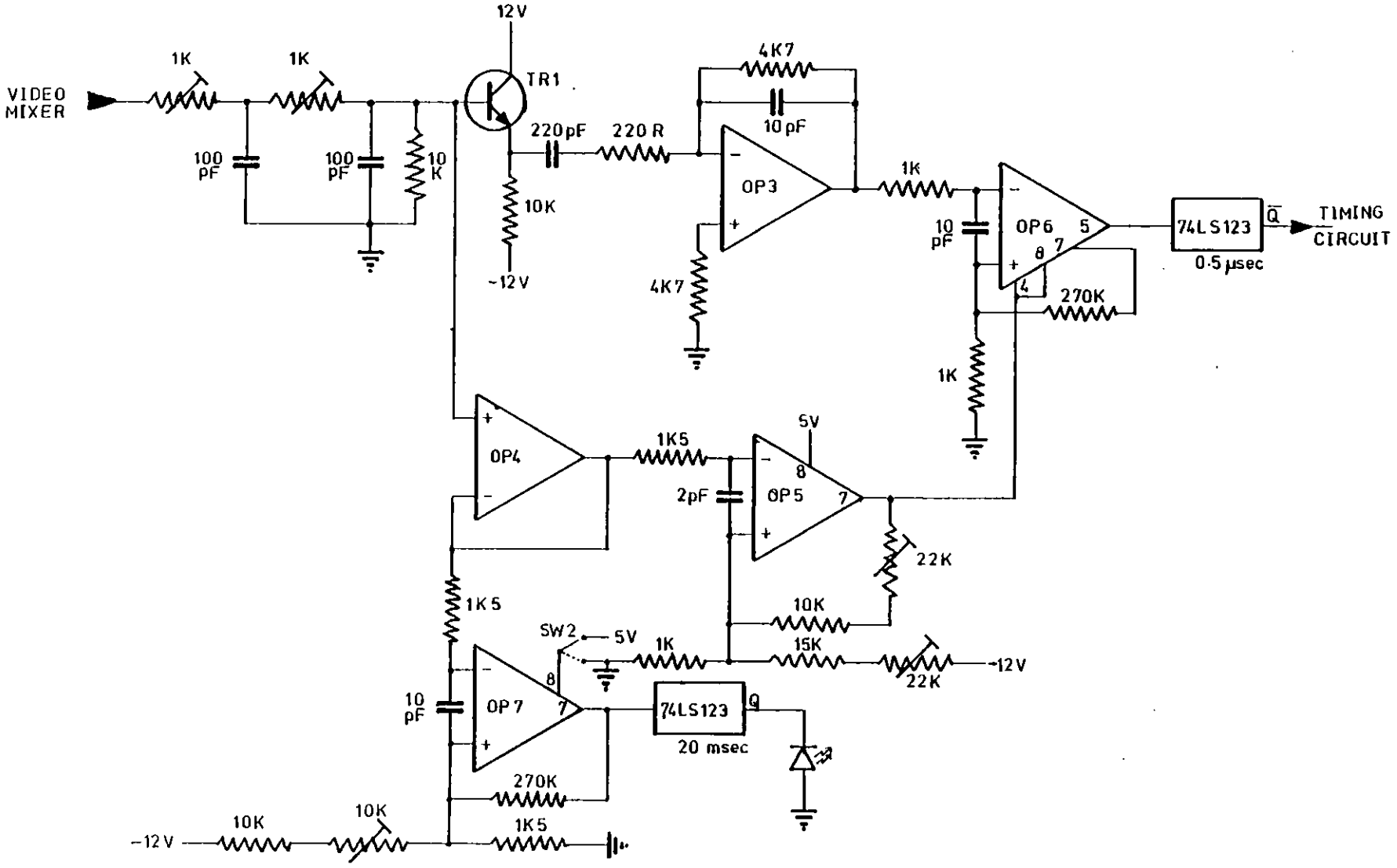

TIMING CIRCUIT

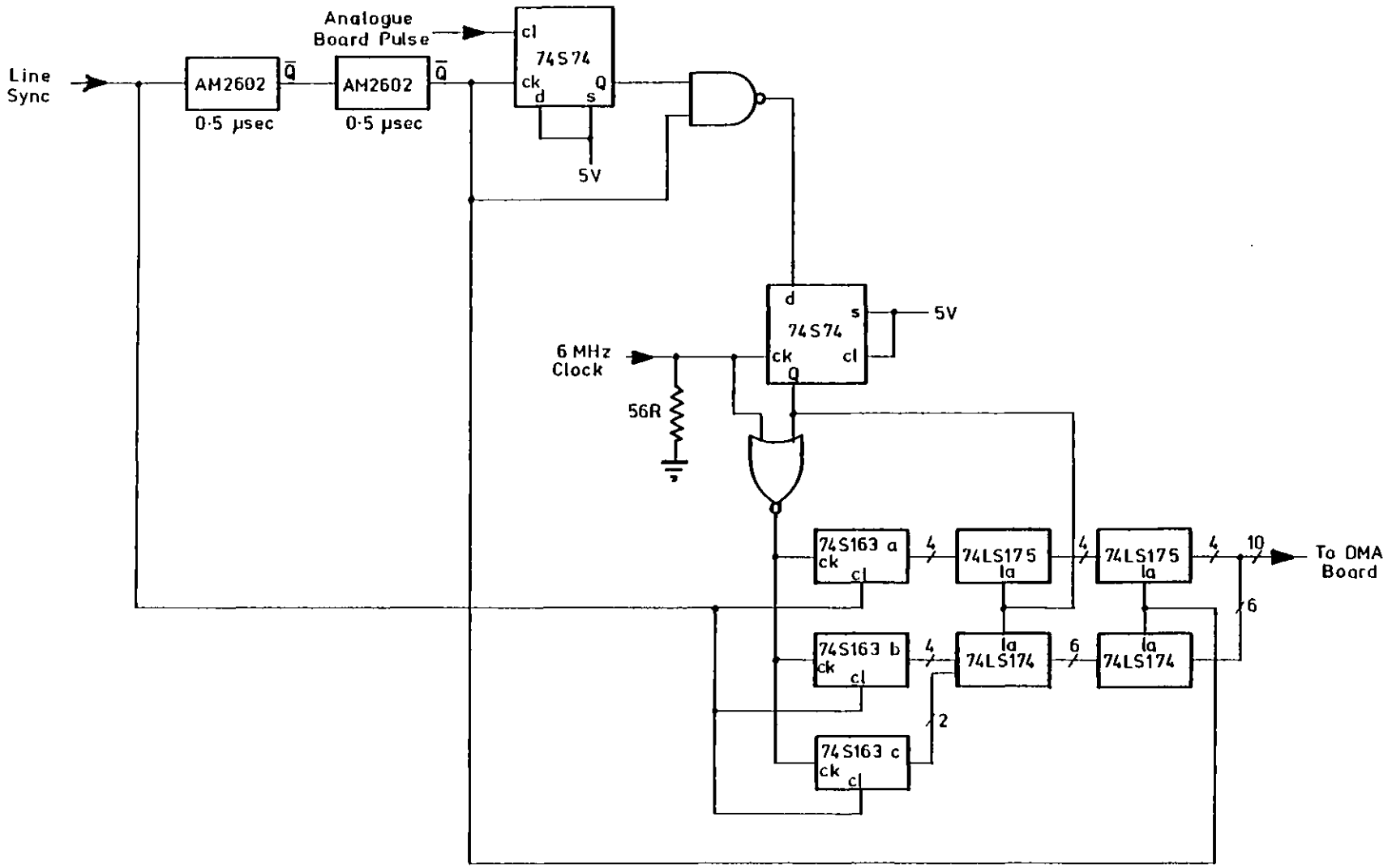

KEY to ANALOGUE CIRCUITS.

TR1	BC184
OP 1,2,3,4	LM318H
OP 5,6,7	NE527K
SW1	Analogue Switch HEF4066
SW2	SPST

Compensation for LM318H

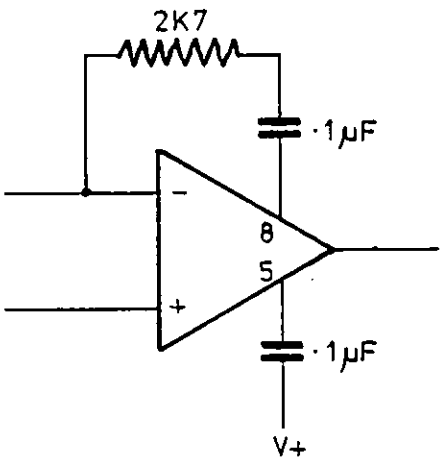

KEY to DIGITAL CIRCUIT

ck	clock
cl	clear
d	data
s	set
la	latch

The carry from counter a enables counter b. The carries from counters a and b are added to enable counter c.

REFERENCES

1). DODSON.J.S. Diamond Trading Co. Private communication.

2). FROBIN.W. HIERHOLZER.E. Journel of the American Society of Photogrammetry vol XLV111. No 2. p215-220. Feb 1980.

3). SCHLESSINGER.G. Surface Finish. Report of the Research Dept of the Institute of Production Engineers 1942.

4). KOGELNICK, LI Applied Optics vol 5. p1550-1559. Oct 1966.

5). GOODMAN.J.W. Optics Commumications vol 14. p324-327. July 1975.

6). OUCHI.K. Optical and Quantum Electronics vol 12. p237-243 1980.

7). DAINTY.J.C. Optica Acta vol 17. p761-772. 1970.

8). KEITZ.H.A.E. Light Calculations and Measurements. Phillips Technical Library. p143-149. 1955.

This paper will be published in March 1983 by S.P.I.E. as part of the proceedings of the MAX BORN CENTENARY CONFERENCE held in Edinburgh in September 1982. The conference was a joint meeting of the European Conference on Optical Systems, ECOSA 82, and the Institute of Physics Optics Group, OPTICS 82.

Surface coordinate measurement using high resolution T.V. cameras

Laurence J. Robinson

Blackett Laboratory, Imperial College, London SW7 2BZ, UK

Abstract

This paper describes a system capable of measuring and storing the cylindrical coordinates describing the surface of a small object (< 10 mm). Two T.V. cameras are used to view an illuminated section of the surface and the z and r coordinates are extracted from the video signals and stored on floppy disc. The resolution of these coordinates is ≈ 32 μm. The θ coordinate is supplied by rotating the object so that a new section of the surface is analysed. The process is repeated until the whole surface has been covered.

Introduction

Several approaches have been utilized for locating objects in a three-dimensional space. Typical methods use stereo photogrammetry or a probe on a three degress of freedom instrumented arm. The first method requires computation on the data from the two images in order to ascertain the object's coordinates. The second method necessitates the probe being moved mechanically over the object surface and is therefore a slow process. If the surface coordinates of an object are required to even one hundredth of its overall dimensions the large amount of data to be recorded requires a different method than those above if the storage time is to be reasonable.

A system was constructed which is capable of storing the coordinates describing the surface of an object using a non-contact method without the need for any computation.

General principle

In Figure 1 A is the axis about which the object can be rotated. The object is illuminated by a plane of light which passes through the axis A and intersects the object surface at a point B. Viewing the object at an angle θ from the plane of illumination, the point B will appear to be a distance r' from A given by

$$r' = r \sin(\theta)$$

The viewed surface will therefore be a segment of the whole surface from which its r and z coordinates can be extracted. Rotation of the object will enable data from the whole surface within certain limitations to be measured.

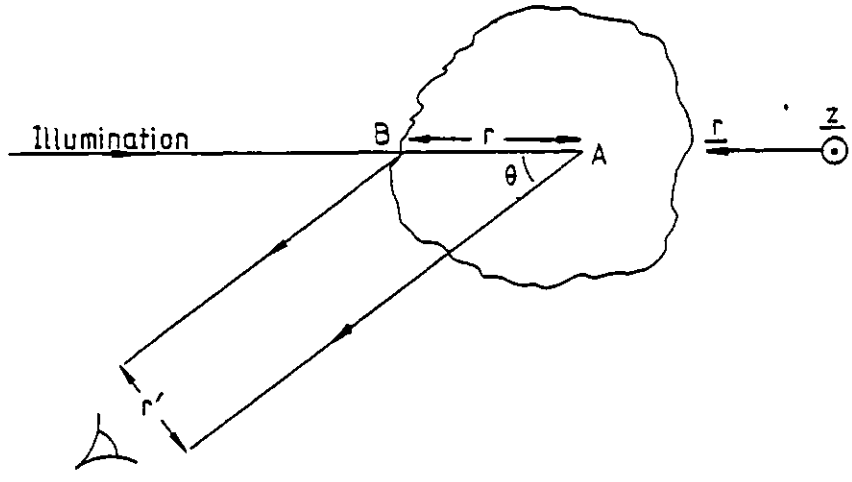

Figure 1. Principle of system

The degree to which data can be recorded will depend on whether every point on the object is illuminated; also the reflected light intensity in the viewing direction must be above a certain threshold. To increase the probability of a point being measured a three beam illuminating system was used as in Figure 2. All three beams are coplanar in the object space. The object is also coated with a matt reflecting substance and is

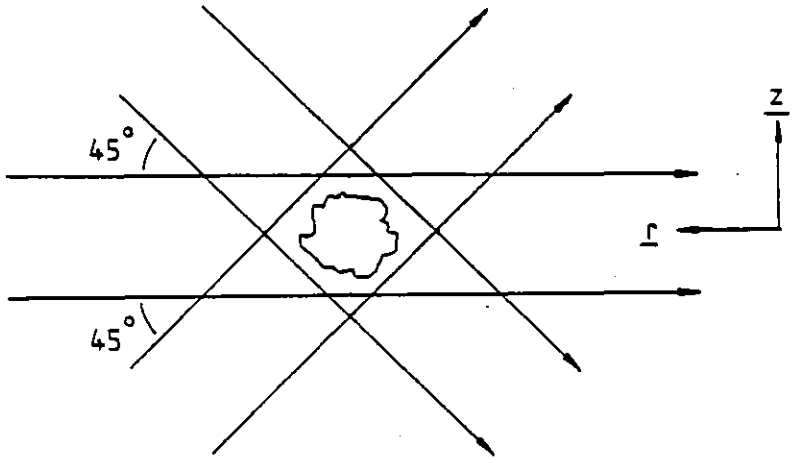

Figure 2. Three-beam illumination

viewed from two directions either side of the direction of illumination at angles θ. Even so a point B as in Figure 3 would not be visible.

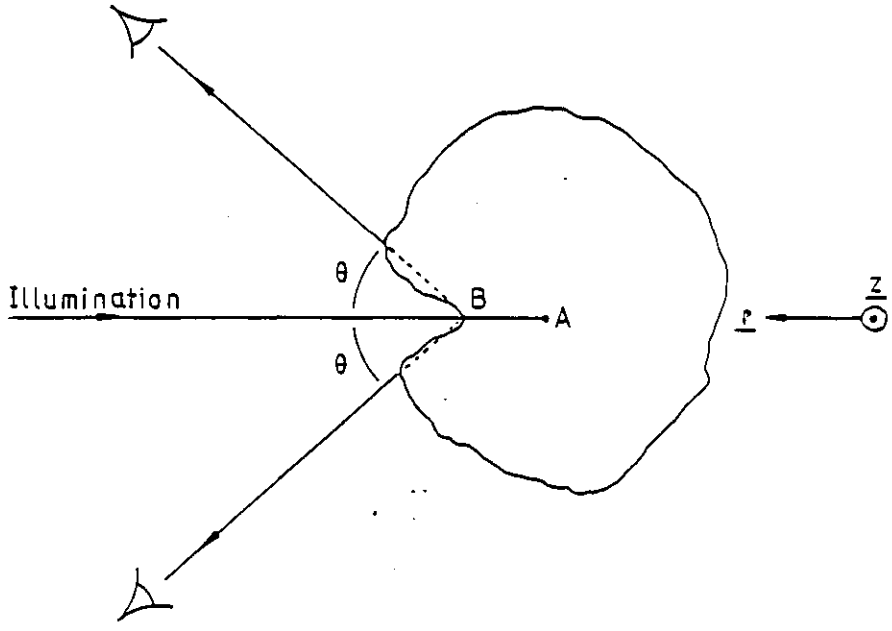

Figure 3. Hidden inclusions

There may also be areas at the poles of the object which would not provide data and therefore after the object has been rotated 360° about the z axis it must then be rotated by 90° about an axis orthogonal to the z axis and a second set of data obtained. These two sets would then be added after the second set was transferred to the coordinate system of the first set. The object would then be described in cylindrical coordinates.

Optical design

The system was designed to enable objects of up to 10 mm in size to be measured. For a depth of field of ±5 mm the optimum waist diameter for a Gaussian beam of wavelength 632 nm (i.e. a HeNe laser) is 60 μm giving a $1/e^2$ width at ±5 mm of 84 μm. The illuminating system consists of a 2 milliwatt laser, microscope objective, spatial filter and cylindrical lens, which forms a 60 μm image line. The three beam illuminating system is shown in Figure 4; it consists of a composite prism which divides the incoming wavefront into three. The two beams which travel via the aluminised 30° prisms are

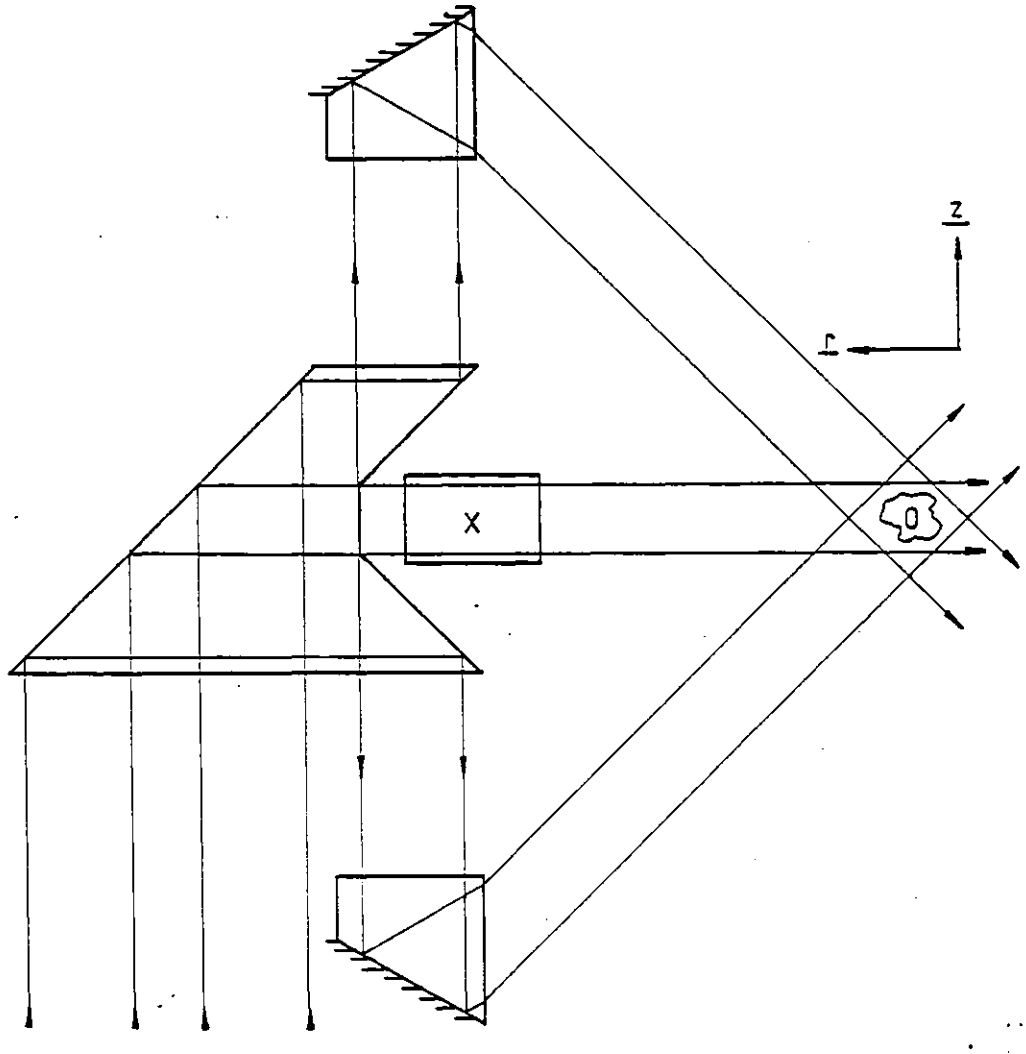

Figure 4. Three-beam producing system

brought to a line focii in the object space, O, whilst the central beam passes through a two lens refocusing system at x so as to refocus the beam into the object space whilst keeping the 60 μm image line width. Experimentally the three beams have been aligned so as to be coplanar to within ±5 μm over the total object field.

The imaging system is symmetrical and telecentric as in Figure 5.

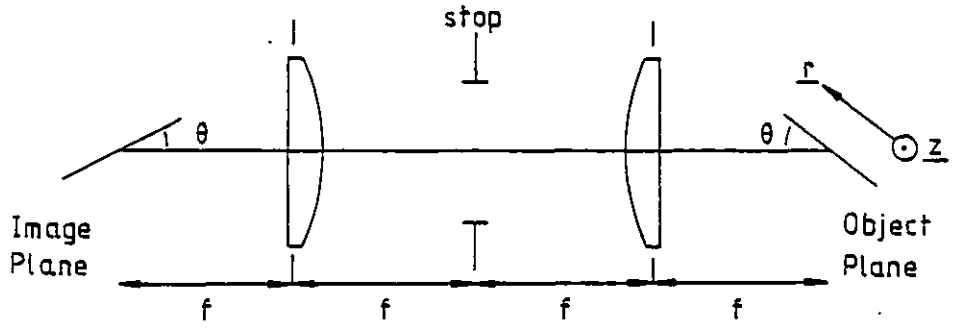

Figure 5. Viewing system

With unit magnification and an object plane at an angle θ to the optical axis, the image plane is also at an angle θ to the axis. The two lenses are cemented achromats which are nearly diffraction limited for an on axis focal plane object point. With the exit cone of rays from any object point, being symmetrical about the principal ray which is parallel to the optical axis the system will map faithfully from object to image planes. The maximum off-axis object distance is approximately 5 mm and with a value of the lenses' focal length of 180 mm the system is nearly aberration free.

Unit magnification is possible as the detectors used are 25 mm vidicon cameras which have been adjusted to give a 10.5 mm square image area.

Decision on viewing angle

Three factors must be taken into account in deciding the viewing angle θ. The camera tubes' physical support and electrical screening will impose a minimum angle whilst the ability to see into inclusions as in Figure 3 will cause an increased probability of an object point being undetected with increasing θ. The ratio of the imaged line width to the total image field is the third consideration and is shown in Figure 6 for an object orientation perpendicular to the illuminating beam, of width d.

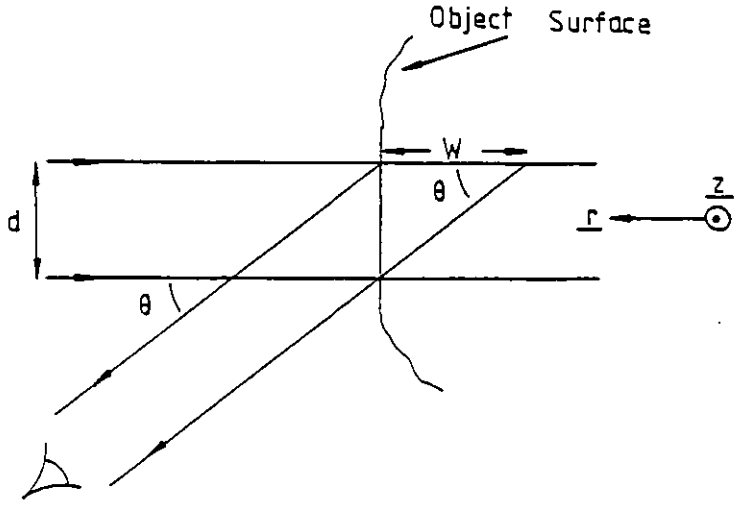

Figure 6. Image line width

The line width W will be given by

$$W = \frac{d}{\tan(\theta)}$$

The desired object surface coordinate will have to be extracted from a Gaussian profile of width W. In the system that was constructed the minimum angle possible due to the camera's construction was 32^{o} which with a value of d of 60 μm gives a value of W of approximately 110 μm. This profile width will be broadened by the point spread function of the imaging system and by the convolution of the image with the electron beam of the camera tube. Figure 7 shows the complete system as it is mounted on a 3 x 4 ft cast iron table.

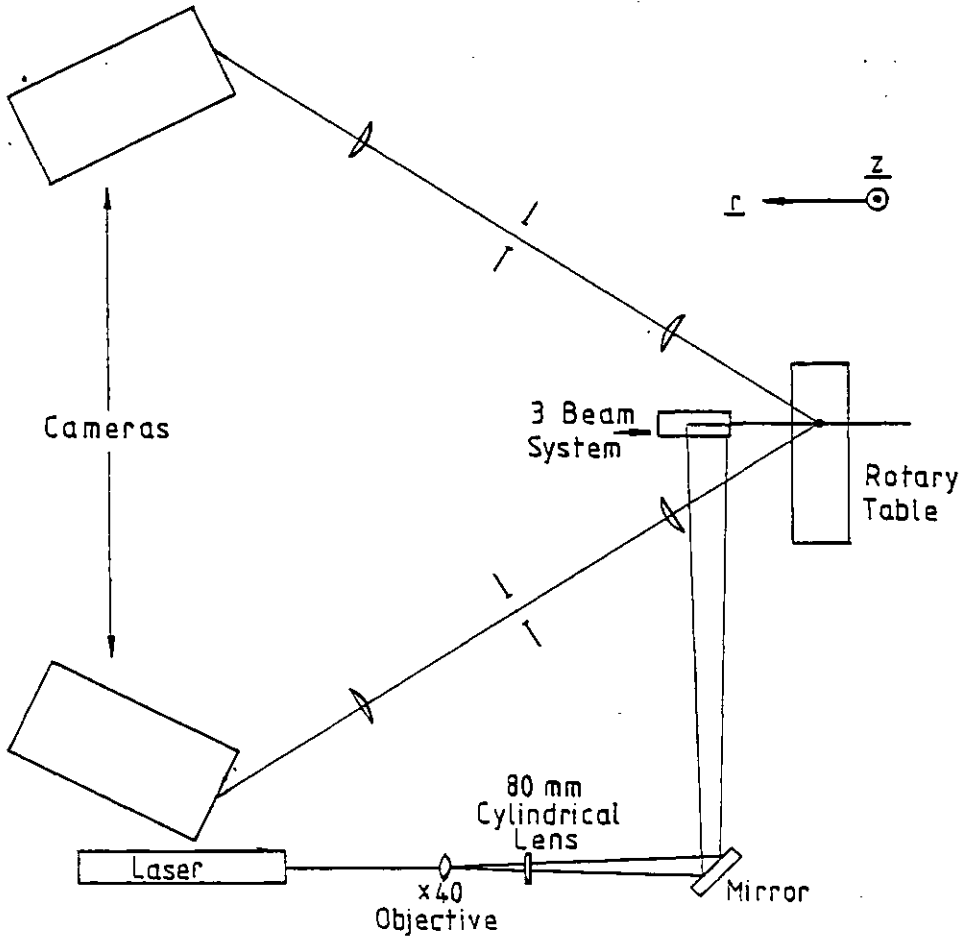

Figure 7. Overall layout

Reduction of speckle contrast

Due to the coherent illumination and to the rough nature of the object coating with respect to the light's wavelength, the image contains a random speckle component. It is well known (e.g.[1,2]) that for such a case the Autocorrelation of the speckle will be the point spread function of the system. With a pupil diameter of 28 mm and an image plane at 32^{o} to the optical axis, the average speckle size will be approximately 10 x 18 μm. The coating was found to depolarize the laser illumination and thus the image plane speckle in the incoherent addition of two unit contrast independent speckle patterns. To reduce the speckle contrast further so that the video signal from the cameras appeared as a

Gaussian it was necessary to defocus the camera tube electron beam to a diameter of approximately 60 μm. Introduction of a larger aperture system would enable the beam to have a smaller diameter.

Coordinate measurement

The two cameras are driven from the same raster generators but have opposite direction scans. This enables, with raster registration, the two video signals to be added. The cameras are linear in the z direction to within ±20 μm and though they have nonlinearities of up to 0.5% in the line scans these are identical for both cameras.

Figure 8 shows a block diagram of the analogue electronics. The mixer allows either camera 1 or 2 or their sum to be processed. The signal is then differentiated and if the input signal is above a preset level the zero crossing detector is enabled and when the differentiated signal passes through zero a 0.5 μsec pulse is passed to the timing electronics. Due to limited data storage space, coordinates are taken on alternate T.V. lines (i.e. every 32 μm) when a counter is reset by the line sync pulse and then counts from a 6 MHZ clock, which is synchronized to the camera's master's clock until receipt of the 0.5 μsec pulse. This count is then latched at the end of the line to the computer. The computer is a PDP11 with a twin floppy disc drive and a Direct Memory Access Board for data acquisition. The data is latched via the DMA board into core memory until a T.V. frame is finished. This data is then transferred to disc whilst the object is being rotated a predetermined angle. This process continues until the whole object has been covered. The coordinates have therefore been stored in sequential blocks, each defined by an angle of rotation, and in each block by alternate T.V. lines corresponding to the z axis coordinate. The resolution in the r direction is one count of the 6 MHZ clock which corresponds to approximately 32 μm.

The rotation of the object is accomplished via a stepping motor and a geared drive enabling object rotations of multiples of 0.45° to be used. With the present floppy disc storage medium, data can be acquired from up to 800 frames each comprising 256 16 bit words describing the object. The time for this is 2½ minutes of which over half is for the transfer of data from core memory to disc.

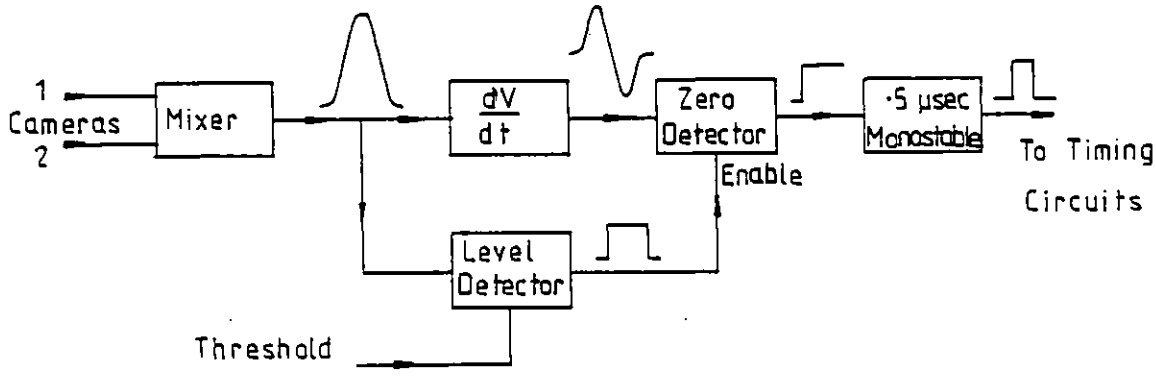

Figure 8. Analogue electronics

Results

The ability of the system to measure the coordinates of surfaces which are not perpendicular to the r axis is clearly important. The limiting angle of rotation of surfaces about the z axis is solely dependent upon the camera viewing angle θ. As θ increases the profile imaged in one camera will increase in width whilst the other image will decrease. As the method of ascertaining the centroid of the profile is by differentiation the decrease in width of one of the images ensures that the signal due to the sum of both provides a well defined coordinate. When the object plane is rotated by an angle (90-θ) only the broadened image will remain and it has been found that for an angle of θ of 32° the measurement of the centroid is dependent upon fluctuations in the signal due to noise. The amplitude of the two signals at large angles of θ was found to show reflected intensities from the object larger than those expected of a Lambertian reflector and the coating used (a Liquid Paper typing error corrector "SLICK")

exhibited retroreflecting properties.

For rotations of the object plane about an axis orthogonal to the z, r plane a measurable profile was obtained for angles of the surface to the r axis down to 20° for the three-beam illumination, and to 30° for the central beam only. The inclusion of a three-beam system therefore increases the probability of an object point being detected but increases the complexity of the optical system. For the system constructed with three beams and a viewing angle of 32° orientations of the object plane which can have their coordinates measured are defined by:

Rotation about the z axis $< 58^{\circ}$
Rotation about an axis $\perp$ to the z, r plane $< 70^{\circ}$

Using this system 4000 coordinate measurements were made on a ball bearing. A least square error fit was made for each frame of data to a circle and the theoretical and measured coordinates supplied the error. Figure 9 shows a histogram of these errors with a 4 μm bin size and also indicates a Gaussian with the same standard deviation as the data. As the coordinates are digitized every 32 μm it was expected that the histogram would be flat between ±16 μm but as these points on a ball bearing would mostly lie in the equatorial region of the ball then if the rotation of the ball is not reasonably eccentric there will not be a large enough variation in the equatorial coordinate to provide a statistical average. Nevertheless this would not affect the standard deviation of the data which is 14.2 μm, implying that over 95% of the data is within 30 μm.

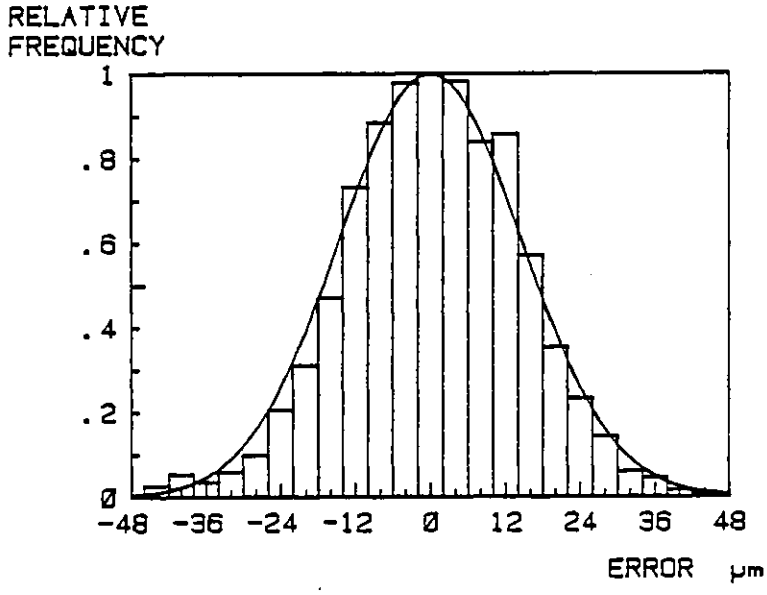

Figure 9. Ball bearing error histogram

Conclusions

It has been shown that a method of measuring the surface coordinates of an irregular object, quickly and accurately has been achieved. Further development of the prototype described in this paper should extend its capabilities and introduce a new method of mensuration.

Acknowledgements

I am grateful to W. T. Welford and F. Reavell for their help and advice and to Room 611 for their long suffering.

References

1. Lowenthal, S. and Arsenault, H., J. Opt. Soc. Am., Vol. 60, pp. 1478. 1970.
2. Goodman, J. W., Laser Speckle and Related Phenomena, Ed. Dainty, J. C., Springer 1975, pp. 9-75.